Desiccation-driven senescence in the resurrection plant *Xerophyta schlechteri* (Baker) N.L. Menezes

Astrid Lillie Radermacher

RDRAST001

Thesis presented for the degree of

DOCTOR OF PHILOSOPHY

In the Department of Molecular and Cell Biology

University of Cape Town

November 2019

Supervisors: Prof J.M. Farrant and Prof S.G. Mundree

I, Astrid Lillie Radermacher, hereby declare that the work on which this dissertation/thesis is based is my original work (except where acknowledgements indicate otherwise) and that neither the whole work nor any part of it has been, is being, or is to be submitted for another degree in this or any other university.

I empower the university to reproduce for the purpose of research either the whole or any portion of the contents in any manner whatsoever.

Signature: Signed by candidate

Date: 10/11/2019

Abstract

Drought-induced senescence is a degenerative process that involves the degradation of cellular metabolites and photosynthetic pigments and uncontrolled dismantling of cellular membranes and organelles. Angiosperm resurrection plants display vegetative desiccation tolerance and avoid drought-induced senescence in most of their tissues. Developmentally older tissues, however, fail to recover during rehydration and ultimately senesce. Comparison of the desiccation-associated responses of older senescent tissues (ST) with non-senescent tissues (NST) will allow for understanding of mechanisms promoting senescence in the former and prevention of senescence in the latter.

In the monocotyledonous resurrection plant *Xerophyta schlechteri* (Baker) N.L.Menezes, leaf tips senesce following desiccation, whereas the rest of the leaf blade survives. This study characterised structural, metabolic and transcriptional changes in ST and NST at varying water contents during desiccation and rehydration. Light and transmission electron microscopy was used to follow anatomical and subcellular responses, and metabolic differences were studied using gas chromatography-mass spectrometry and colorimetric metabolite assays. These results show that drying below 35% relative water content (0.7 gH_2O/g dry mass) in ST resulted in the initiation of age-related senescence hallmarks and that these tissues continue this process after rehydration. Analysis of the transcriptome was done using RNA-Seq, which was subject to differential expression analysis and network analysis to elucidate the potential mechanisms for senescence regulation in this species. Significantly increased transcription of senescence associated genes was observed in the air dry sampling point, indicating that initiation of cellular death occurred below 20% RWC. Network analysis based on Pearson correlation revealed a high degree of clustering of these genes, suggesting co-regulation. The majority of these genes had two enriched motifs in their upstream regions, identified as binding sites for WRKY and other transcription factors. A model integrating these observations is presented, with insights into how senescence is initiated in ST and repressed in NST.

Table of Contents

For Selina

Chapter 1

Positioning *Xerophyta schlechteri* as a model for studying desiccation-driven senescence: A literature review.

Introduction

Due to climate change, drought is emerging as one of the greatest dangers to food security in our time (Kogan *et al.,* 2019). As sessile organisms, plants are at the mercy of their environmental conditions. Water is essential for survival; thus, most plants have developed certain adaptations for surviving mild to moderate deficit. Resurrection plants (defined below) have been positioned in recent years as models for understanding how drought tolerant crops of the future may be engineered (Blum and Tuberosa, 2018; Hilhorst and Farrant, 2018; Zhang and Bartels, 2018). Understanding how resurrection plants prevent cellular death (senescence) during desiccation is a crucial piece of this puzzle. This review outlines how stresses are mitigated by resurrection plants, how senescence is brought about in response to water deficit in desiccation sensitive species and how the study of these processes in *Xerophyta schlechteri* could inform design of drought tolerant crops of the future.

Desiccation Tolerance

Desiccation tolerance (DT) is the ability of an organism to survive loss of virtually all subcellular water. Albeit rare, this phenomenon has been observed in several unicellular and multicellular life forms (select species of bacteria, lichens, mosses, ferns, angiosperms, tardigrades), as well as in some life-cycle stages of particular taxa (e.g. DT seeds, larvae of the worm *Caenorhabditis elegans* and the midge *Polypedilum vanderpankii*) (Berjak, 2006; Watanabe *et al.,* 2006; Guidetti *et al.,* 2012; Costa *et al.,* 2016). In vegetative tissues of angiosperms, it was first described by Gaff (1977), who coined the term “resurrection plants” for the ability of these plants to ‘resurrect’ from an apparent dead-like state after prolonged periods in the air-dry state. These plants exhibit total desiccation tolerance, i.e. the ability to survive loss of water until 0.1g H_2O/g dry mass. This represents water content in equilibrium with the air at 50% relative humidity and 20^{o}C, and water potential of -100 MPa (Gaff, 1997). In contrast, desiccation sensitive angiosperms are only able to survive up loss of 20-50% relative water content (RWC), corresponding to water potential of -10MPa (Proctor & Pence, 2002). When water is once again available, these plants regain full metabolic competence within hours of rehydration (Hoekstra *et al.,* 2001; Farrant *et al.,*2007; 2012). While this

phenomenon is common in the seeds of many angiosperm species, it is rare in their vegetative tissues, with only 135 species exhibiting this trait (Gaff and Oliver, 2013).

Stresses imposed by water deficit and resurrection plant strategies for mitigating them

Numerous mechanisms for mitigating the stresses imposed by total water loss have been described for several resurrection plants. Consistent responses amongst different species of resurrection plants include shutdown/limitation of photosynthesis, accumulation of anti-oxidant compounds and enzymes, accumulation of protective compounds (sugars, amino acids, etc.), accumulation of stress-responsive proteins and changes to cellular architecture. These changes result in the ability to enter a quiescent state, wherein plants arrest growth and reproductive functions in order to survive total water deficit for extended periods (Farrant *et al.,*2007; Challabathula and Bartels, 2013).

Redox stress

Photosynthesis is a dangerous process in the absence of water. As the soil surrounding a plant dries, signals are transmitted to leaves and stomata are closed to retain moisture. This prevents intake of carbon dioxide, limiting regeneration of NAD^+ through the Calvin cycle and over-reduction of the photosynthetic electron transport chain. This causes leakage of electrons to oxygen, leading to the formation of reactive oxygen species (ROS) (Cruz De Carvalho, 2008), highly reactive molecules that are able to oxidatively damage lipids, proteins and nucleic acids (Del Río, 2015). These molecules were previously considered only to be a toxic by-product of stress, needed to be dealt with through the deployment of anti-oxidants. However, the thinking has shifted towards ROS as oxidative signals, communicating the degree of stress experienced by cells within the cell and between cells and organs of the plant (Foyer, 2018). Nevertheless, as resurrection plants experience water deficit stress, anti-oxidant enzymes and compounds are deployed *en masse* to counter the ROS generated through drought (loss of <60% of subcellular water) and desiccation (loss of between 65 and 97% subcellular water) (Sherwin and Farrant, 1998; Kranner, *et al.,*2002; Farrant *et al.*, 2007; Moore *et al.,* 2009; Gechev *et al.,* 2012). This prevents damage to cellular constituents and the initiation of oxidative burst signaling, a trigger for programmed cell death (PCD) (Cruz De Carvalho, 2008). The importance of anti-oxidants cannot be understated – the viability of

resurrection plants after rehydration is highly associated with their anti-oxidant status in the dry state (Kranner *et al*., 2002).

To further mitigate redox stress as they lose water, resurrection plants limit the degree of photosynthesis they undertake. In fact, the feature that divides resurrection plants into two groups is their behavior in limiting photosynthesis. Homoiochlorophyllous resurrection plants, such as *Myrothamnus flabellifolia*, *Craterostigma wilmsii*, *Tripigon loliiformis* and *Boea Hygrometrica* maintain some level of chlorophyll in the dry state, relying on leaf curling and pigment accumulation on the adaxial surface to protect their photosynthetic apparatus (Sherwin and Farrant, 1998; Karbaschi *et al.,* 2015; Tan *et al.,* 2017). Poikilochlorophyllous resurrection plants, such as *Xerophyta scabrida, Xerophyta viscosa, Xerophyta schlechteri, Xerophyta humilis, Barbacenia purpurea, Sporobolus stapfianus* and *Eragrostis nindensis*, on the other hand, break down chlorophyll during drying and rapidly resynthesize the molecules upon rehydration (Tuba *et al.,*1996; Dace *et al.,*1998; van der Willigen *et al.,*2001; Ingle *et al.,*2007; Gaff *et al.,*2009; Suguiyama *et al.,*2014). Poikilochlorophyllous plants also dismantle thylakoid membranes during dehydration, which are reassembled on rehydration, and thus take longer to re-establish photosynthesis and carbon fixation upon rehydration than their homoiochlorophyllous counterparts (Challabathula, Zhang, and Bartels, 2018). In terms of their ecophysiology, the homoiochlorophyllous strategy is generally employed by those species that spend less time in the dry state, whereas the poikilochlorophyllous strategy is generally employed by those who spend longer periods in water scarcity (Tuba *et al.*,2002). Despite individual species' relationship with chlorophyll, regulated photosynthetic shutdown is a feature in all resurrection plants measured to date, as evidenced by thylakoid structural changes, rearrangement of photosystems, Calvin cycle limitation, decrease in photochemical activity and decrease in critical photosynthetic apparatus protein abundance (Challabathula, Puthur and Bartels, 2016; Challabathula, Zhang, and Bartels, 2018).

Mechanical Stress

As plant cells lose water, a great risk is presented by the loss of cell volume. Integrity of connections between cells via plasmodesmata is crucial for survival, as is integrity of the membrane which is generally thought to be inelastic (Bartels and Hussain, 2011). Changes to membrane fluidity have been proposed as a strategy to increase elasticity, particularly

through polyunsaturation of membrane lipids (Bartels and Hussain, 2011; Tshabuse *et al.,* 2018). Cell wall folding is employed by some species to mitigate mechanical stress and allow for rolling of the leaves (Moore *et al.,* 2013) and is enabled through the activity of wall-loosening enzymes, wall remodeling proteins and changes to the chemical composition of cell wall sugars (Moore *et al.,* 2013; Giarola *et al.,* 2016; Jung *et al.,* 2019). Vacuolation (splitting of the central vacuole into smaller subdivided vacuoles) is observed in several species (particularly those that undergo less cell wall folding) and is thought to maintain subcellular volume and prevent plasmalemma withdrawal. This enables maintenance of connections at the plasmodesmata, preventing lysis as the cell volume decreases (Farrant *et al*., 2007). Vitrification is another strategy employed wherein as water is lost, it is replaced by compatible solutes and sugars to maintain some volume within the cells (Farrant *et al*., 2007; Bartels and Hussain, 2011; Challabathula and Bartels, 2013; Zhang and Bartels, 2018). Taken together, these strategies enable maintenance of cellular structure and compartmentalisation during drought and desiccation.

Macromolecular stress

As the cells of resurrection plants lose water, they are vulnerable to a number of deleterious effects involving macromolecular structure and function. Protein structure is essential for function, and correct protein folding is typically reliant on being in aqueous solution. It has been proposed that as water is lost, resurrection plant cells have adapted mechanisms to prevent accumulation of misfolded proteins, be that through chaperone activity or protein degradation (Farrant, Brandt and Lindsey, 2007; Challabathula and Bartels, 2013; Griffiths, Gaff and Neale, 2014). A number of molecular chaperones have been implicated in serving a chaperone function in resurrection plants, including late embryogenesis abundant (LEA) proteins, small molecular weight proteins ubiquitous in desiccation tolerant seeds. These LEA proteins are intrinsically disordered and some only gain secondary structure in non-aqueous solution (Olvera-Carrillo, Reyes and Covarrubias, 2011). They have been implicated in molecular stabilization of several cellular constituents, including proteins and lipid membranes, and in prevention of protein aggregation (Artur *et al.,* 2019). Other molecular chaperones, such as heat shock proteins, have been proposed to serve similar functions in desiccating cells (Bartels and Hussain, 2011). A protein degradation mechanism that has been

proposed is triggering of the unfolded protein response (UPR) for removal of misfolded proteins generated during water deficit. A delicate balance is to be maintained, however, as the UPR has been implicated in triggering UPR-mediated cell death (Griffiths*, et al.*, 2014).

Senescence

An important unanswered question in the field of vegetative desiccation tolerance is how resurrection plants subvert senescence processes during desiccation. Senescence can be thought of as a developmental stage, wherein older tissues co-ordinate programmed cell death (PCD) processes to maximise redistribution of nutrients to younger tissues and reproductive organs. Senescence processes are also initiated in response to environmental stresses, such as water deficit stress, as an effective strategy to improve the likelihood of survival and reproduction. Senescence in desiccation sensitive species can be broadly divided into three phases: initiation, reorganisation and termination (Bresson *et al.,* 2018).

Initiation

Without application of external stress, leaf age and developmental stage are the main initiators of senescence, in a process also known as developmental PCD (dPCD) (Olvera-Carrillo *et al.,* 2015). Developmental PCD (dPCD) is employed for a number of reasons during plant growth, for example in tracheid formation, or during the final stages of fruit ripening or in the end of the organ/whole plant life cycle. Early onset of senescence can also be triggered by abiotic and biotic stressors, driven by hormones, sugars, and ROS generated by these processes, in a process also known as environmental PCD (ePCD) (Olvera-Carrillo *et al.,* 2015; Bresson *et al.,* 2018).

Reorganisation

The reorganisation phase is characterised by the breakdown of macromolecules and remobilisation of nutrients in small subunit form, wherein hydrolytic enzymes are extensively deployed (Bresson *et al.,* 2018). Basic metabolic activity during this phase is required to ensure remobilisation of breakdown products to the vasculature for incorporation in viable cells. Toxic intermediates are likely to form during this phase, and thus antioxidant enzymes

and compounds (particularly anthocyanins) are deployed to protect against oxidative stress in this state (Bresson *et al.,* 2018).

Termination

What happens during the termination phase depends upon what initiates PCD, i.e. whether it is auto-lytic or non-autolytic. During autolytic termination, vacuoles collapse, releasing nucleases and proteases into the cytoplasm, leading to acidification and contraction of the cytoplasm and uninhibited breakdown of DNA, RNA, proteins and membranes. At this point, the cell is effectively dead, leaving behind cell wall and debris (Van Doorn, 2011; Lim *et al.*, 2007; Bresson *et al.,* 2018). Non-autolytic PCD typically occurs in the context of a hypersensitive response or in the case of invasion by a necrotrophic pathogen, where the tonoplast is not completely ruptured and complete clearance of the cytoplasm does not occur (Van Doorn, 2011). In recent years, there is evidence of apoptosis-like PCD occurring in plants (Li and Dickman, 2004; Dickman *et al.,* 2017), characterised by cell shrinkage, membrane blebbing, DNA laddering, photosystem externalisation, cytochrome c release, protease activity, increases in ROS, decreased ATP production and the release of damage-associated molecular patterns (DAMPs).

PCD signalling during abiotic stress

Of interest in the context of senescence in a resurrection plant is PCD initiation in response to abiotic stress (particularly water deficit). In drought sensitive species, withholding of water (ie drought) and osmotic stress cause ROS accumulation (as described above) and are known to induce vacuolar cell death via vacuolar processing enzyme (VPE) (Hatsugai *et al.,* 2015). VPE is a player in apoptotic-like PCD, utilizing its caspase-1-like function to disrupt the vacuole and release vacuolar proteases into the cytoplasm that degrade cellular constituents (Dickman *et al.,* 2017). In the case of heat stress, intracellular calcium (a ubiquitous abiotic stress signal) increases with an increase in ROS, and binds to calmodulin, a second messenger. This calmodulin activates MAPK6, which increases expression of VPE (Petrov *et al.,* 2015). Another posited inducer of PCD via VPE is endoplasmic reticulum (ER) stress, caused by an accumulation of misfolded proteins. This stress triggers the unfolded protein response (UPR), which seeks to increase the protein folding capacity of the ER. However, if this stress is

prolonged and the ER maladaptive, apoptotic-like PCD is triggered via caspase-like activities (Hatsugai *et al.,* 2015). Thus, VPE induction is putatively controlled by signaling from the chloroplast, mitochondria (sites of ROS generation during abiotic stress) and ER (UPR pathway). Additionally, there is evidence that DNA damage during abiotic stress can be triggered by ROS. The first response is to deploy DNA damage repair mechanisms (Yoshiyama *et al.*,2013) However, if left unmitigated, ROS may tip the nuclear response from DNA repair to PCD via SUPPRESSOR OF GAMMA 1 (SOG1) signaling (Yoshiyama *et al.*,2013). A number of ROS homeostasis signaling factors in the nucleus have been described, including heat shock factors (HSF) and ethylene responsive (ERF/AP2), zinc finger (ZF), basic leucine zipper (bZIP), and NAC transcription factors, as well as several micro RNA species (Cimini *et al.,* 2019).

Hormonal control of Senescence

Ethylene is the canonical hormonal signal for the onset of leaf senescence (Graham *et al.,* 2012) but has varying degrees of effect based on leaf age. Studies on ethylene-insensitive mutants (*etr1–1, ein1* and *ein2*) in *Arabidopsis Thaliana* showed decreased sensitivity to exogenous ethylene and delayed senescence, however leaf yellowing eventually occurred (Bleecker *et al.,*1988; reviewed by Graham *et al.,* 2012). Further studies on *old* (onset of leaf death) mutants in *A. thaliana* provide insight into this age-related ethylene sensitivity, showing that the hormone does not induce senescence in young leaves (Jing *et al.,* 2002, 2005). Ethylene signal transduction is well-described in *A. thaliana* and involves binding of ethylene to receptors (ETR1 and ERS1), transduction of this signal (via CTR and EIN2) to the transcription factor EIN3, which activates expression of senescence associated genes (SAGs) and transcription factors. In the absence of ethylene, EIN3 is constitutively degraded by the proteasome (Graham *et al.,* 2012). EIN3 activates ORE1, which activates NAC transcription factors, which in turn drive expression of SAGs, such as SAG12 protease. EIN2 is also capable of activating WRKY transcription factors in *A.thaliana,* which have been implicated in senescence initiation signaling (Graham *et al.,* 2012). Jasmonic acid has also been implicated in bringing about senescence in *A.thaliana* via WRKY53, a driver of both SAG expression and WRKY6 expression (Miao and Zentgraf, 2007). WRKY6 has been implicated in senescence via MAPK6, a common abiotic stress signaling kinase (Chai *et al.,* 2014). It has also been proposed that ABA contributes to senescence signaling via modulation of the salicylic acid response,

employing EARLY RESPONSIVE TO DEHYDRATION 15 (ERD15) for upstream regulation of senescence associated NAC transcription factor expression (Griffiths*, et al.*, 2014; Woo *et al.,* 2019).

Studying senescence in the resurrection plant *Xerophyta schlechteri*

While most tissues in resurrection plants are able to suppress senescence, typically older tissues do succumb to senescence, which appears to be exacerbated by drying. While noted in some studies, e.g in *Craterostigma* spp (Christ *et al.*, 2014; Zhang and Bartels, 2016), this has not been thoroughly investigated. How resurrection plants are able to prevent cellular death has been hypothesized, based on molecular and physiological studies on non-senescent tissues during desiccation (Griffiths*, et al.*, 2014; Williams *et al*., 2015). However, no large-scale experimental comparisons between senescent and non-senescent tissue have been performed in the context of a desiccation event, and no work has been done to identify potential regulators of senescence processes in these species.

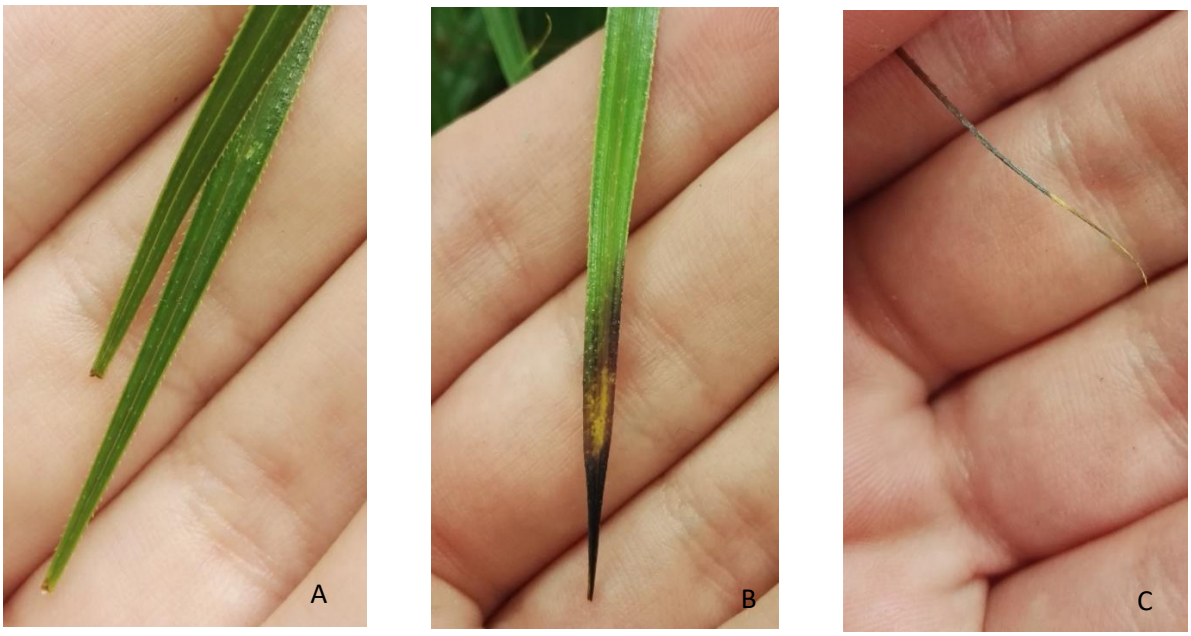

Figure 1: The same *X. schlechteri* leaf apex experiencing senescence during its first desiccation event. A; Full turgor and prior to desiccation; B at 60% RWC and C, desiccated, air dry state. A small area of the leaf apex is lost during desiccation (circled).

Xerophyta schlechteri[1] is uniquely poised to delve into some of these questions. This species is a poikilochlorophyllous monocotyledonous C3 resurrection plant, native to Southern Africa. It occurs on inselbergs and experiences a long dry winter period and intermittent rainfall during summer, as well as high light and extremes of temperatures (Farrant *et al.,* 2015). Several studies have been done to describe the protection mechanisms employed by this species during desiccation. It subverts mechanical stress through employing a high degree of vacuolation during drying, rather than cell wall folding (Moore *et al.,* 2013; Farrant *et al.,* 2015).In defense against redox stress, It degrades chlorophyll and enters the desiccated state with unstacked grana in the chloroplast (Sherwin and Farrant, 1998; Christ, *et al.,*2014), indicating complete shutdown of photosynthesis and limiting ROS accumulation. For the same reason, leaves are folded along the midrib during dehydration, and anthocyanins accumulated on the abaxial surface in order to limit light absorption (Sherwin and Farrant,

Figure 2: *X. schlechteri* leaves following multiple desiccation events. With each desiccation event, some tissue from the apex of leaves does not recover. This region is bordered by a purple zone, which is destined to succumb to the next desiccation event. This is observed regardless of the degree of leaf expansion; however, only fully expanded leaves that had never undergone a desiccation event were included in this study.

[1] In previous studies, plants collected from Buffelskloof Private Nature Reserve, Mpumulanga Province, South Africa, were classified at *Xerophyta viscosa* by Coetzee (1974). This population has been reclassified as *Xerophyta schlechteri* by Benhke *et al.,*(2013). All references supplied which worked from the Mpumulanga population, and thus on *X. schlechteri*, are asterisked in the reference section.

1998). Recently, the genome of *X.schlechteri* was published along with a desiccation-rehydration transcriptome (Costa *et al.,* 2017). Findings from this study revealed a biphasic mode of gene expression during imposed water deficit: an early response (changes in gene expression between 60% and 40% RWC) and late response (changes between 40% and 20% RWC). Accumulating transcripts included those to do with protein folding, protection and translational control, as well as nuclear import and gene expression. Diminishing transcripts included those to do with lipid metabolism, nucleotide metabolism, protection against oxidative stress, photosynthesis, energy metabolism, water transport and genetic information processing. Network analysis revealed that vegetative desiccation tolerance in *X. schlechteri* leaves is under control of both ABA-dependent and ABA-independent processes. The authors also found that a number of pro-apoptotic and senescence associated transcripts decreased in abundance during desiccation, and that transcripts associated with autophagy increased, reinforcing the hypothesis that autophagy is a pro-life strategy employed by resurrection plants (Williams *et al.,* 2015; Costa *et al.,* 2017). There is also late stage accumulation of UPR transcripts, indicating that this pathway is triggered during severely stressful conditions for mitigation of ER stress (Costa *et al.,* 2017).

While it is true that the bulk of *X.schlechteri* leaf tissue survives prolonged desiccation (Costa *et al.,* 2017), some tissue is lost with each desiccation event. It exhibits signs of “Tip burning”, coined by Brett Williams (personal communication), a process wherein leaf apex tissues become senescent with each desiccation event (**Figure 1 and 2**). Thus, desiccation-driven senescence processes can be studied in the context of a continuum in the leaves of *X. schlechteri.* This senescent tissue does not abscise but remains attached to the leaf until the full leaf blade is dead. Because growth occurs from a meristematic base, the apex is the oldest tissue on the leaf, indicating that there is interplay between age-related and stress-driven senescence. Identifying potential triggers for and regulators of senescence in *X. schlechteri* will provide insights into how these processes are prevented in viable tissues. Moreover, this work will provide insights into how mitigation of senescence processes may be bred or engineered in drought tolerant crops of the future. If potential repressors of senescence can be identified, they can theoretically be applied to engineering of crops that prevent senescence in response to prolonged drought.

Scope of this thesis

This thesis explores senescence processes during desiccation in mature leaves of *X. schlechteri,* from the whole plant level (physiology) to the cellular level (metabolomics and transcriptomics). In **Chapter 2**, fully expanded leaves from mature plants were dissected into apical and mid-leaf sections and subjected to water content determination, light and electron microscopy, pigment quantification, ABA quantification and primary metabolite quantification during desiccation and rehydration. Based on these observations, tissue was dissected for transcriptomic analysis in **Chapter 3**. In this chapter, transcripts were quantified via RNA-Seq (with qPCR validation) and subject to differential expression analysis and network analysis to elucidate the potential mechanisms for senescence regulation in this species. In **Chapter 4**, an overview of the findings is presented, with a proposed model for senescence regulation in this species. Future prospects for this research are also presented in this chapter.

Study Aims:

1. To determine the water content range wherein senescence processes are initiated in this species.
2. To determine how metabolism shifts during senescence.
3. To model how senescence is regulated in this species.

Chapter 2

Desiccation-driven senescence in *Xerophyta schlechteri*: anatomical, ultrastructural and metabolic responses*

*Aspects of this chapter have been published as Radermacher, AL, du Toit, SF and Farrant, JM (2019). Desiccation-Driven Senescence in the Resurrection Plant *Xerophyta schlechteri* (Baker) N.L. Menezes: Comparison of Anatomical, Ultrastructural, and Metabolic Responses Between Senescent and Non-Senescent Tissues. *Frontiers in Plant Science* doi: 10.3389/fpls.2019.01396

Introduction

Xerophyta schlechteri is one of the most widely studied poikilochlorophyllous monocotyledonous angiosperm resurrection plants. Like other poikilochlorophyllous resurrection plants, *X. schlechteri* minimizes photo-oxidative stress and reactive oxygen species (ROS) formation during drying by breaking down chlorophyll and thylakoid membranes (Sherwin and Farrant, 1998; Mundree and Farrant, 2000; Farrant *et al.*, 2015). Biochemically, it employs an early (prior to shut-down of photosynthetic activity) and late (below *ca.* 55% RWC) response to drying, differentially engaging molecular chaperones, translational machinery, signal transducers and gene regulators to alter metabolism, respiration, photosynthesis, and organelle structure to bring about quiescence (Farrant *et al.*, 2015).

In desiccation sensitive plants, including cereal crops, leaf senescence processes during drought are initiated to limit water loss through transpiration and to remobilise nutrients from older tissues towards younger tissues and reproductive organs, ultimately resulting in the death of the leaf (Woo *et al.*, 2019). This is characterised by breakdown of chloroplasts, loss of photosynthetic pigments, protein degradation, nutrient remobilisation (Munné-Bosch and Alegre, 2004; Watanbe *et al.*, 2013; Bresson *et al.*, 2018) and autophagy (Woo *et al.*, 2019). It has been proposed that resurrection plants are able to supress drought-induced senescence (Griffiths *et al.*, 2014; Williams *et al.*, 2016) in the bulk of their tissues by employing signal blocking mechanisms. The same would be true of *X. schlechteri,* although the exact mechanisms associated with this are not yet known.

“Tip burning”, whereby the apex of the leaf fails to recover following desiccation, was observed in *X. schlechteri* in the present study, as discussed in **Chapter 1**. This led to speculation that desiccation-driven senescence might be occurring in these tip tissues. To test this, we compared the anatomy, ultrastructure and primary metabolism of the non-senescent tissues (NST) and senescent tissues (ST) of *X. schlechteri* during dehydration and rehydration, aiming to elucidate both the process of drought-induced senescence in ST and the mitigating features of senescence in NST. The presence of senescent and non-senescent zones on the

same leaf allowed for changes in both tissue types to be studied in the context of a continuum. This is the first study to consecutively contrast the metabolic and physiological changes in NST and ST in this manner during the desiccation of a resurrection plant. Our findings provide insight into the mechanisms associated with the suppression of senescence in the bulk of the tissue in this species.

Questions to be answered:

1. **At what point in the dehydration-rehydration cycle do ST and NST deviate significantly in terms of their anatomical and metabolic response to water deficit?**
2. **What are the physiological hallmarks of desiccation-driven senescence?**

Materials and Methods

Experimental conditions and sampling procedures

Mature *X. schlechteri* plants were collected from Buffelskloof Private Nature Reserve (25°19'48.83"S, 30°29'40.83"E) in the Mpumulanga province of South Africa and maintained in a greenhouse conditions as described in Sherwin & Farrant (1996). For the current experimentation, 10 mature plants were transferred to controlled environment chambers (Conviron Adaptis A350 chamber, Canada) under the following conditions; 16 h light, 300 $\mu molm^{-2}\ s^{-1}$, 25°C; 8 h dark, 20°C. Plants were acclimated to these conditions for one week prior to induction of dehydration stress. Senesced leaf tips were removed from the plants two days into acclimation. Samples of fully hydrated (full turgor) plants were taken 8 h after artificial "dusk" on the last day of acclimation, therefore at artificial "dawn". These were processed as described below. Dehydration was induced by cessation of soil watering. Once the soil moisture of each individual pot approached <0.01g H_20/g, tissues were sampled at 1 h after artificial dawn. At each sampling point, three fully expanded leaves per plant were sampled and dissected to yield an apex region of 1 cm (the senescent tissue (ST) and a 1-cm-length section of tissue from the middle of the leaf blade (the non-senescent tissue (NST). These were used to determine tissue relative water content (RWC) and for the concomitant anatomical, ultrastructural and metabolite analyses. The sampling procedure is depicted in

Figure 1. Once the plants had reached an air-dry state (RWC of NST leaves being <5%), they were maintained in the dry state for 7 d, after which they were rehydrated by watering the plants and soils. Tissues were sampled as above at 12, 24, 48, 72 and 168 h post rehydration.

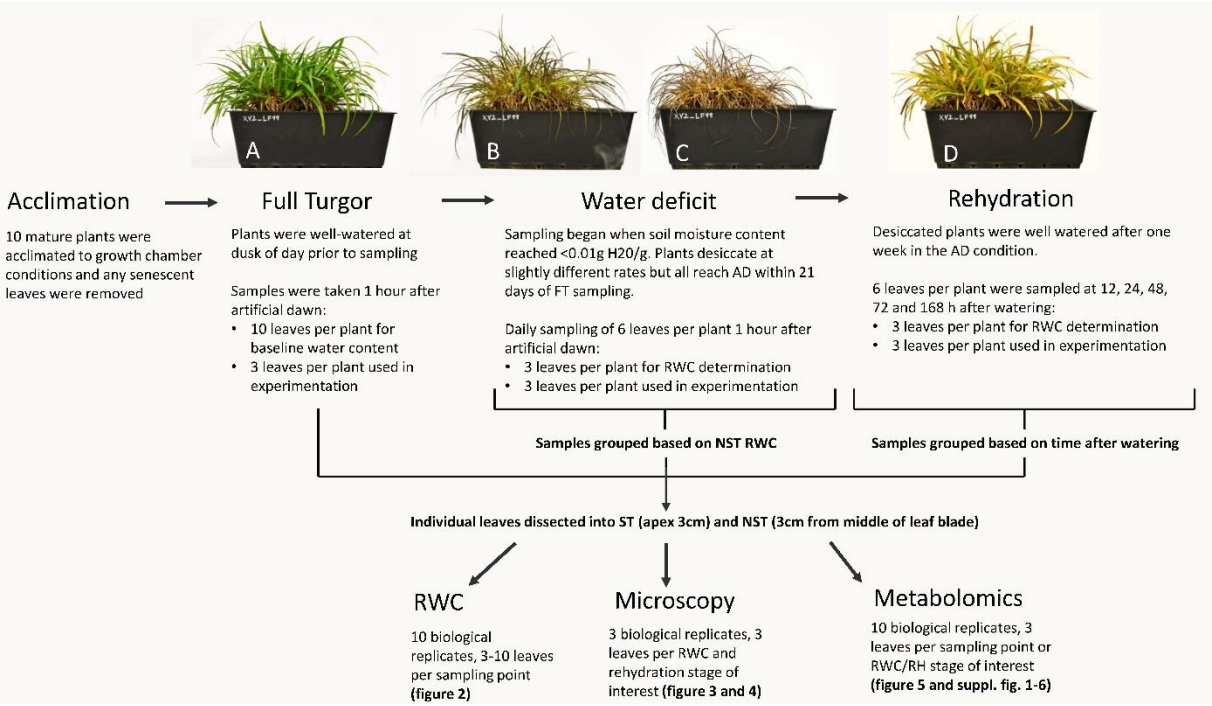

Figure 1: Sampling procedure for RWC, microscopy and metabolomics. Plants experiencing the same water deficit stress were sampled for multiple procedures. All ten plants were utilised for water content determination (3-10 leaves per plant per sampling point) and metabolomics (3 leaves per plant per RWC/RH stage of interest), while microscopy was performed on three plants (3 leaves per plant per RWC/RH stage of interest). A typical experimental *X. schlechteri* is shown before, during and after water deficit stress: FT (A), 60% RWC (B), AD (C) and 48h after rehydration (D).

RWC determination

The classic method of determination of plant RWC, as outlined by Barrs and Weatherley (1962), uses the formula:

RWC (%) = ((Fresh Weight - Dry Weight)/(Turgid Weight - Dry Weight)) x 100

Fresh and dry weights are determined before and after oven drying at 70°C for 48 h, and the absolute water content (AWC) is determined by subtraction of the former from the latter. The

turgid weight represents the full turgor weight obtained by immersing the leaves in water in the dark for 24 h at 4°C.

As the leaf tissues of *X. schlechteri* do not absorb water during the overnight incubation, the turgid weight cannot be easily and accurately calculated. Thus, the AWC of NST tissues from fully hydrated plants, sampled at artificial dawn, was calculated (AWC_{FTnst}) and used as the turgid weight in all subsequent water content determinations. Furthermore, preliminary assessment (data not shown) indicated that the AWC of the leaf tip tissue (ST) was lower than that of the mid-leaf tissues (NST). To monitor the water contents of NST and ST from the same leaf and at the same timepoints, we devised a modified formula for RWC determination.

Relative water content of NST at sampling point X:

$$\%RWC_{NST} = \frac{AWC_{Xnst}}{AWC_{FTnst}} \times 100$$

Relative water content of ST at sampling point X:

$$\%RWC_{ST} = \frac{AWC_{Xst}}{AWC_{FTnst}} \times 100$$

Thus, all RWC measures for ST are relative to FT NST. For comparative reasons, AWC are given in Figure 1 and in the text where relevant. Leaf water contents were determined on all 10 plants at each sampling point.

Light microscopy

NST and ST tissues, from 3 representative plants, at daily sampling points were cut into sections and fixed in FAA fixative (formalin : acetic acid : 95% ethanol, 10:5:50) for 24h. Samples were serially dehydrated in a Leica TP 1020 tissue processor with (50% (v/v) ethanol for 30 min, 70% (v/v) ethanol for 60 min, 95% (v/v) ethanol for 60 min; absolute ethanol for 60 min, three rounds of 6 h in absolute ethanol; and two rounds of 24 h paraffin wax infiltration at 60˚C) before being embedded in paraffin wax. Sample blocks were sectioned to 10 µm using a Leica RM2125RT microtome and mounted on glass slides. Slides were dewaxed in xylol and then rehydrated through serial immersion in 100% (v/v), 90% (v/v) and 70% (v/v) ethanol. Each immersion lasted for 1 min and was performed in duplicate. Replicate slides were stained with 0.1% (w/v) Procion yellow in aqueous (2.5:1) dimethylformamide (DMF)

for 60 min at 37˚C (allows for visualisation of chloroplasts and chloroplast aggregates) and then 0.1% (w/v) Alcian blue in 3% (v/v) acetic acid for 30 min at room temperature (allows for visualisation of complex carbohydrates), with three 10 min washes in dH2O included after each staining. Slide staining methods were taken from protocols in Ruzin (1999). Glass coverslips were mounted on the stained slides with Mowiol mounting medium and allowed to air-dry for a minimum of 24 h, before being stored in slide boxes. Slides were investigated for changes in total tissue structure associated with the dehydration and rehydration for both NST and ST using a Nikon® Eclipse Ti-E inverted microscope. Only select representative samples at specific RWCs are shown in Figure 2.

Transmission electron microscopy (TEM)

TEM was used to investigate the ultrastructural details of the mesophyll cells from NST and ST at various stages of dehydration and rehydration. At each sampling point (FT, 75%, 55%, 35% and 5% RWC as well as 12, 24, 48 and 72 h post rehydration), tissues from 3 plants were dissected into the respective tissue types (ST and NST), which were then fixed and processed for TEM in accordance with Cooper and Farrant (2002), with slight modifications. Briefly, small pieces of leaf tissue (approximately 2 mm^2) were fixed in 2.5% glutaraldehyde in 0.1 m phosphate buffer (pH 7.4) containing 0.5% caffeine and then post-fixed in 1% osmium in phosphate buffer. After dehydration in a graded ethanol series, the tissues were immersed in 100% acetone, which was aspirated and replaced twice. The samples were incubated overnight at 4^{o}C in one part acetone (500 µl) and one part Spurr's resin (500 µl). Half of the solution was then removed and replaced with 500 µl Spurr's resin to yield a 75% concentration of Spurr's resin to acetone and incubated overnight at 4^{o}C. This was repeated to yield an 87.5% solution. The solution was then removed and replaced with 100% Spurr's resin and incubated overnight at 4^{o}C. The samples were then placed into block moulds and allowed to harden at 60^{o}C for 16 h. Samples were sectioned using a Richart Ultracut S ultramicrotome. Sections (95 nm) were mounted on copper grids and stained with uranyl acetate (2% w/v) for 10 min and lead citrate (1% w/v, in NaOH chamber) for 10 min. Sections were viewed on a Tecnai T20 electron microscope.

*Metabolomics **s**ample preparation*

Leaves from 10 plants were immediately flash frozen, freeze dried and stored at -80^{o}C until further analysis. For this analysis, tissues (5–15 mg) from each plant were dissected into their respective tissue types (NST and ST) and homogenised to a fine powder with a pestle and mortar. The powder was transferred to 2 ml centrifuge tubes. Residual material in the mortar was collected through the addition of 1 ml 80% (v/v) ethanol, which was added to the respective tubes. Samples were dried using vacuum centrifugation, and the mass of the dry powder starting material was determined. Metabolites were extracted using a modified phase separation extraction method described by Bieleski & Turner (1966). Modifications included filtration of all removed extracts through three layers of Whatmann paper and concentration of the non-polar and polar fractions via lyophilisation. These were used for the assays described below and GC-MS analysis.

Colorimetric metabolite assays

Dried non-polar fractions were resuspended in 500 µl 100% (v/v) acetone, 100 µl of which was then pipetted, in duplicate, into wells on a 96-well plate. The absorbance (*A*) of the extracts was measured at 662 nm, 645 nm and 470 nm, using a Multiskan™ GO Microplate Spectrophotometer, and pigment concentrations were determined by using the equations of Lichtenthaler & Wellburn (1983). Metabolites were resuspended in 500 µl distilled water, and the sucrose, D-fructose and D-glucose content determined using a R-BIOPHARM® Sucrose/D-Glucose/D-Fructose kit with the following modifications to the manufacturer's protocol: absorbances were only taken at 340 nm (absorption maximum of NADPH) using a Multiskan™ GO Microplate Spectrophotometer.;Initial data consolidation and formatting was conducted in Microsoft® Excel Office 365. Subsequent data transformation and analysis were conducted in R version 3.3.3 using the packages "ggplot2" (Wickham, 2016) and "plotly" (Sievert, 2018). Metabolite data were normalized to the mass of the dry starting material. For statistical analysis, samples were divided into two datasets based on whether the starting material was collected during the dehydration or rehydration cycle. The points collected from the air-dry state (prior to rehydration) were used in both datasets to give continuity to the data. Points from the dehydration cycle had a negative value attributed to their %RWCs to give directionality, and both sets of data points were plotted on the same axis against %RWC. Independent log10 linear models were constructed for the two tissue types and these models

were used to predict exponential models fitted to the raw data and were plotted on the same axis. Modelling information can be viewed in suppl. Table 1.

Gas chromatography-mass spectrometry (GC-MS)

Freeze-dried polar fractions were derivatized derivatised in methoxyamine hydrochloride and MSTFA as described by (Lisec *et al.*, 2006). A library of standards was prepared in the same manner using a mixture of amino acids (75 nmol each: alanine, arginine, aspartic acid, asparagine, glutamic acid, glycine, histidine, isoleucine, leucine, lysine, methionine, phenylalanine, proline, serine, threonine, ornithine, tryptophan, tyrosine, valine, cystine and pyroglutamic acid). Sugar (10 ng xylose, arabinose, fucose, fructose, galactose, glucose, mannose, sucrose, cellobiose, maltose, myo-inositol, trehalose, raffinose), sugar alcohol (10 ng maltitol, sorbitol, galactitol, ribitol, xylitol, arabitol, erythritol) and TCA cycle intermediate (10 ng succinic acid, fumaric acid, malic acid and isocitric acid) standards were derivatised and run individually. Derivatised metabolite mixtures were analysed on an Agilent model 7890A gas chromatograph fitted with a 7693 Autosampler, interfaced with a 7000A Triple Quadrupole mass spectrometer (Agilent Technologies, Santa Clara, CA, USA). The helium flow was set to 1.39 mL/min. Samples of 1 µl were injected with a split ratio of 1:24 and resolved on a 30 m × 250 µm × 0.25 µm Agilent HP-5ms column. One technical repeat of each sample was run. A temperature programme optimized for separation of sugars and sugar alcohols was utilised (Bartolozzi *et al.*, 1997). Peak areas were calculated using OpenChrom® Community Edition, and compounds were identified by comparison to the National Institute of Standards and Technology (NIST) Library (filtered for TMS derivatives) using the PBM mass spectrum comparator with default parameters. Compound identification using the internal compound library was performed by aligning chromatograms to one another and this library using the GCAlignR package (Ottensmann *et al.*, 2018) in R (v3.6.0) with default parameters. Peak area was normalized to the internal standard (ribitol) peak area and lyophilized sample mass. Comparative statistics (ANOVA with Fisher's LSD method and t-test comparing relative abundance in tissue type) were performed in MetaboAnalyst 4.0 (Chong *et al.*, 2018) using all identified and unidentified peaks, and heatmaps were created in RStudio using the heatmap.2 function. Raw Data is provided in Supplementary Data Set 1.

ABA quantification by UHPLC–MS/MS

Freeze-dried samples of 1mg were ground and extracted as described (Floková *et al.*, 2014), with the following adjustments: only deuterated ABA was used as an internal standard and prior to injection, samples were filtered to remove particulates.

Results

Anatomical and ultrastructural changes during dehydration and rehydration

Under the conditions used in this work, the time taken for the leaf tissues of X. schlechteri to reach an air dry (desiccated) state after soil water depletion was 14 d (Fig. 2A&B). This is similar to that reported by Farrant *et al.,*(2015) to be typical of this species under such environmental conditions. The RWCs of the leaf tips, destined to become senescent (ST), were significantly lower (ca. 30–40%) than that of their matching mid-leaf NST counterparts throughout dehydration, until the desiccated state was reached in which both tissues stabilized at ≤3% RWC (Fig.2C). Upon rewatering, the RWC of the NST increased rapidly during the first 72 h, with tissues being fully hydrated by 1wk (Fig.2 D). ST absorbed little water after rehydration, with the maximum calculated RWC being 20% (0.4 gH_2O/g dry mass). High-resolution scans in Figure 2 depict changes in the last 30% of the leaf blade during the different stages of dehydration and rehydration. In the fully hydrated state, the leaves were bright green with slightly yellowing apical tips (Fig. 2A). During dehydration, the leaf blades folded along the midrib with the adaxial surfaces of the blades coming together, leaving only the abaxial surfaces exposed to the environment (Fig. 2B). These become purple in color, indicating anthocyanin production, which has previously been reported for this species (Sherwin and Farrant, 1998). This initiated from the apex, with the remainder of the NST becoming progressively purple during dehydration (Fig. 2C). Upon rehydration, the leaf blades of NST unfolded progressively as water moved from the base towards the apex. However, a large portion of the apical tip tissues did not unfold, this correlating with the low RWC of the ST (<20% RWC, Fig. 2D). NST were yellow in color during initial rehydration, regaining their green color by 72 h post watering, this correlating with a 30% increase in chlorophyll content (Supplementary Figure 1). Interestingly, the zone between NST and ST tissues became

demarcated by a purple band that remained permanently visible after rehydration, this tissue being designated for senescence on the next desiccation cycle (Fig. 2D inset).

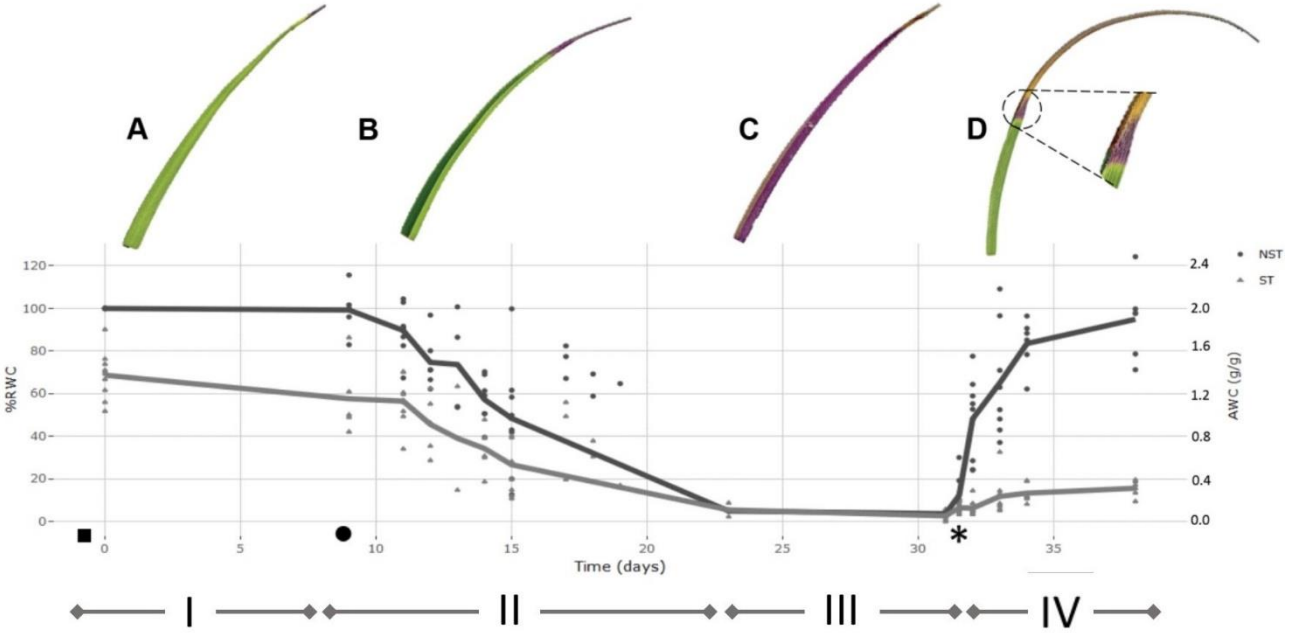

Figure 2: Desiccation-rehydration curve for the drying of *Xerophyta schlechteri*. The %RWC for 10 individuals was determined at daily intervals from the onset of water loss until the air-dry state was reached. The mean %RWC for each time point was used to plot the model dehydration curve. The model dehydration curve for both tissue types is shown (NST and ST). All calculated values were set relative to the AWC of the NST at day 0 (100% RWC). The curve is divided into four distinct phases: (i) fully hydrated; (ii) slow dehydration of all tissues; (iii) air-dry desiccated state; (iv) rehydration after addition of water. The initial watering took place at dusk before day 0 (indicated with a ■) and the first sampling at one hour after dawn on day 0. When the soil moisture content was recorded as <0.01g H_20/g (●), sampling for the desiccation phase was initiated. Plants were left in the dry state for one week, followed by rewatering at day 31 (*). High resolution scans of *X.schlechteri* leaves accompany each phase to illustrate physiological changes occurring in the leaf tissue, and to illustrate differential responses between the two tissue types. A represents FT, B represents 60% RWC in NST, C represents AD, D represents 72h following rehydration. Triangle points are representative of ST and closed circles represent NST.

The anatomical changes associated with dehydration and recovery of NST and ST of *X. schlechteri* are shown in Figure 3. Details of leaf anatomy and changes therein during desiccation of *X. schlechteri* have not been previously described. Transverse sections of fully hydrated leaves show a regular modular arrangement, each consisting of a central *Vellozia*-type vascular bundle (Behnke *et al.*, 2013), flanked by deep abaxial channels that extend through the majority of the spongy mesophyll (Fig. 3A & B). Most of the abaxial stomata occur within these channels, interspersed by epidermal cells (Fig. 2 G–J). Vascular bundles are

capped both ad- and abaxially by sclerenchyma, which extend into the adaxial palisade mesophyll (Fig. 3C). Three large bundles of sclerenchyma fibres are present, one at each lateral edge of the blade and one at the midrib (Fig. 3A & B). These run in parallel from the base of the blade to the apex and likely provide uncompressible points during desiccation.

Figure 3A depicts a cross section of fully hydrated NST. Upon dehydration of this tissue, the palisade mesophyll cells became increasingly compacted, causing infolding of the adaxial epidermis adjacent to the vascular bundle of each module (Figs 3D, E). These points of compaction possibly allow for the redirection of the mechanical forces associated with water loss (Iljin, 1957) and ultimately the folding of the leaf blade (Fig 3B). A model depicting these mechanical forces is given in Figure 3 O & P, with P depicting the proposed forces experienced by the leaf blade during desiccation and O representing the hypothesized means by which the points of compaction alter the direction of these forces, such that the resultant leaf folding is produced in the desiccated NST (Fig. 3). At the abaxial surface, a reduction in mesophyll cell size was observed as is typical of dehydrating tissue, but the most striking observation was the apparent subcuticular excretion from the epidermal cells of acid complex polysaccharides (as evidenced by Alcian blue staining; Parker & Diboll, 1966), this possibly being mucilage, into channels containing stomata (Fig. 3H). These subcuticular secretions increased on drying (Fig. 3I), and we postulate that the presence of mucilage might retard the rate of water loss from mesophyll cells and ultimately contribute to the timing of stomatal closure. Upon rehydration, the palisade cells expanded and epidermal infoldings were no longer evident by 48 h (>75%), this corresponding with observable unfolding of the leaf blade. At this stage, some secretions were still evident in the abaxial channels (Fig. 3J), but these had begun to resemble the FT tissue by 72 h post rehydration.

At full hydration, ST have a RWC of *ca.* 65%, and the appearance of the leaf tissues (Fig.3 K) was not entirely dissimilar to NST at similar water contents (Fig. 3 D, H). While there was little evidence of adaxial epidermal folding, abaxial stomatal-containing channels were positively stained by Alcian blue (asterisk in Fig. 3K). Further dehydration, however, appeared to result in less ordered structural changes than were evident in NST at similar water contents. Palisade cells appeared warped (Fig. 3L), and some stomatal channels appeared to have been forced open probably due to the strain associated with desiccation and incomplete plugging

of channels by mucilaginous substances (Fig. 3M). The ST did not recover structurally during rehydration and resembled the air-dry state at 48 h post rehydration (Fig. 3N).

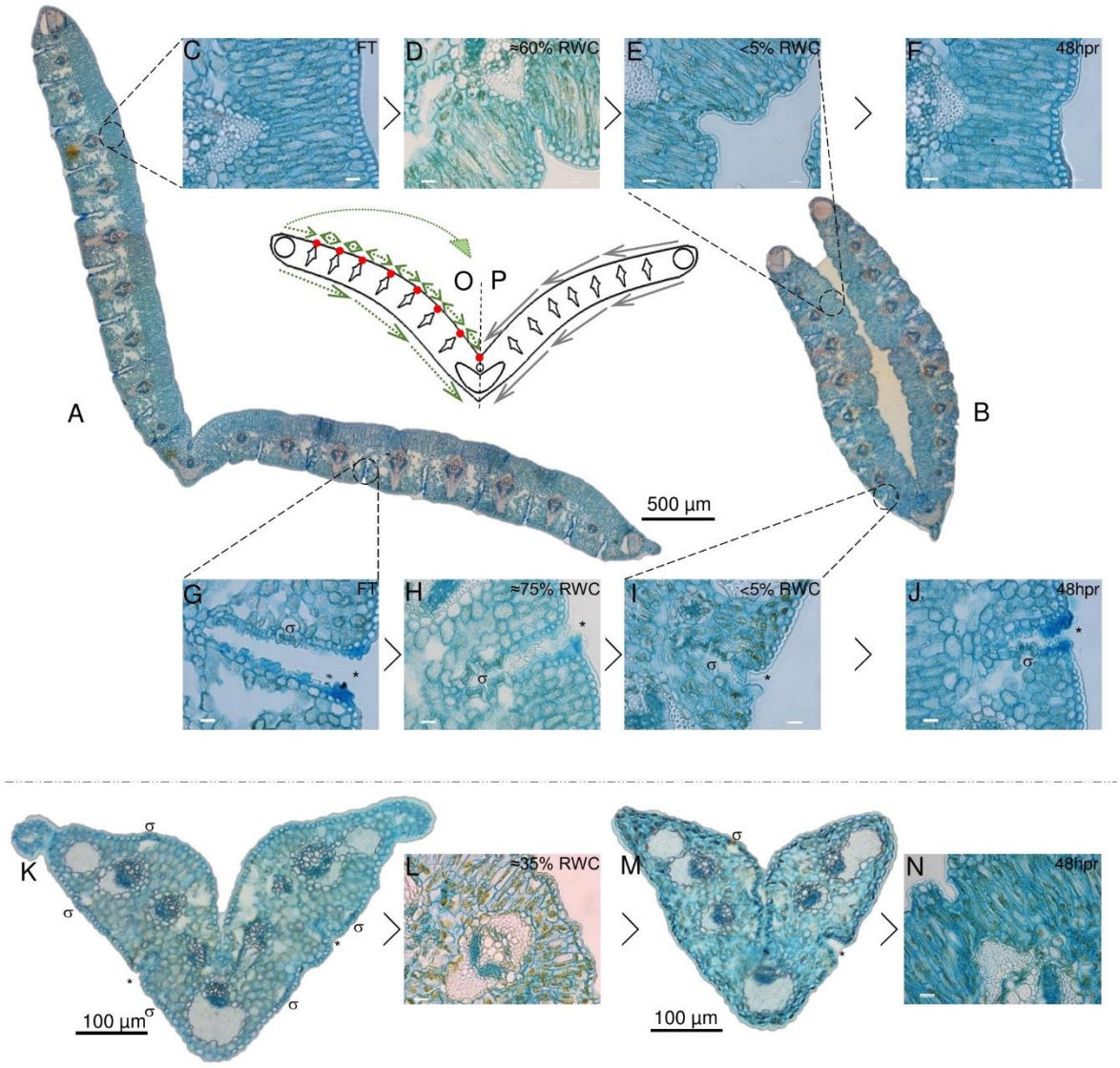

Figure 3: Desiccation associated tissue modifications in NST and ST. Typical cross section of a full turgor (≈100%RWC; FT) blade is shown in A with while a cross section at <5% RWC is shown in B. The abaxial surface in A is open to the environment, while this same surface becomes enclosed due to folding about the midrib in B. Modifications to the adaxial palisade mesophyll during desiccation and at 48hours post rehydration (48hpr) is shown in C – F with %RWC indicated. Modifications to abaxial stomatal channels is shown in G – J. Stomata (σ) lay in deep channels (*) (G-J) that become increasingly closed and mucilage-rich (H&I) with water deficit stress. ST is shown in K – N. Stomatal channels appear not to close as efficiently (M) and there appears to be a greater degree of Procion Yellow staining, indicating a higher degree of cellular constituent aggregation. O and P represent a simplified model of the typical leaf blade in cross section with all collections of sclerenchyma indicated. P displays the theoretical mechanical forces experienced by the tissues at water loss, while O displays a hypothesized means by which points of palisade compaction allow

The ultrastructural changes of the mesophyll cells of NST and ST during dehydration and recovery are shown in Figure 4. The changes in subcellular organization observed in NST were typical of that reported for this and other desiccation tolerant *Xerophyta* spp. (Sherwin and Farrant, 1998; Farrant, 2000; Farrant *et al.*, 2007), characterised by increased presence of smaller vacuoles, centralization of chloroplasts and progressive dismantling of thylakoid membranes, and increased presence of plastoglobuli during dehydration (Fig. 4 A–D). In resurrection plants, mechanical stabilization is achieved through a combination of cell wall flexibility and the presence of vacuoles containing non-aqueous metabolites, with species exhibiting less cell wall flexibility having a greater degree of vacuolation (Farrant *et al.*, 2007; 2012). The vacuolar content appeared to be uniformly electron dense during dehydration (Fig. 4D). In the present study, thylakoid organisation was still evident at 55% RWC, but starch was no longer present (Fig. 4B) and complete dismantling of the thylakoid membranes was evident by 35% RWC (Fig. 4C). In parallel with thylakoid dismantling, there was a significant decline in chlorophyll content, with losses of 80% by 55% RWC and near complete loss in the air dry state (Supplementary Figure 1), confirming the poikilochlorophyllous nature of *X. schlechteri.*

The STs exhibited a lower water content than their NST counterparts at any one time point, but interestingly, the general appearance of subcellular organization was initially not dissimilar to that of NST at similar water contents (compare G with A and H with C in Fig. 4). Photosynthetic pigments were also consistently lower in ST but were not dissimilar to those of NST at similar water contents (Supplementary Fig 1). This might suggest that the changes observed are associated with water content, rather than the engagement of different metabolic strategies between the two tissue types. At RWCs lower than 35%, however, the subcellular organization of ST differed from that of NST. Considerable plasmalemma withdrawal from the cell wall was evident and the extra cytoplasmic space between the wall and plasmalemma was electron dense, suggesting the presence of osmophyllic substances (Fig. 4 I, J). While some plasmalemma withdrawal might be an artifact of the method of chemical fixation used [this being evident also in NST (Fig. 4 D)], the extent of withdrawal might be related to insufficient contribution of vacuolar area to mechanical stabilization. In most cells, vacuole-like organelles containing uniformly electron-dense material were observed (see * in Fig 4 I, L), but the extent of vacuolation was not as great as in NST at similar

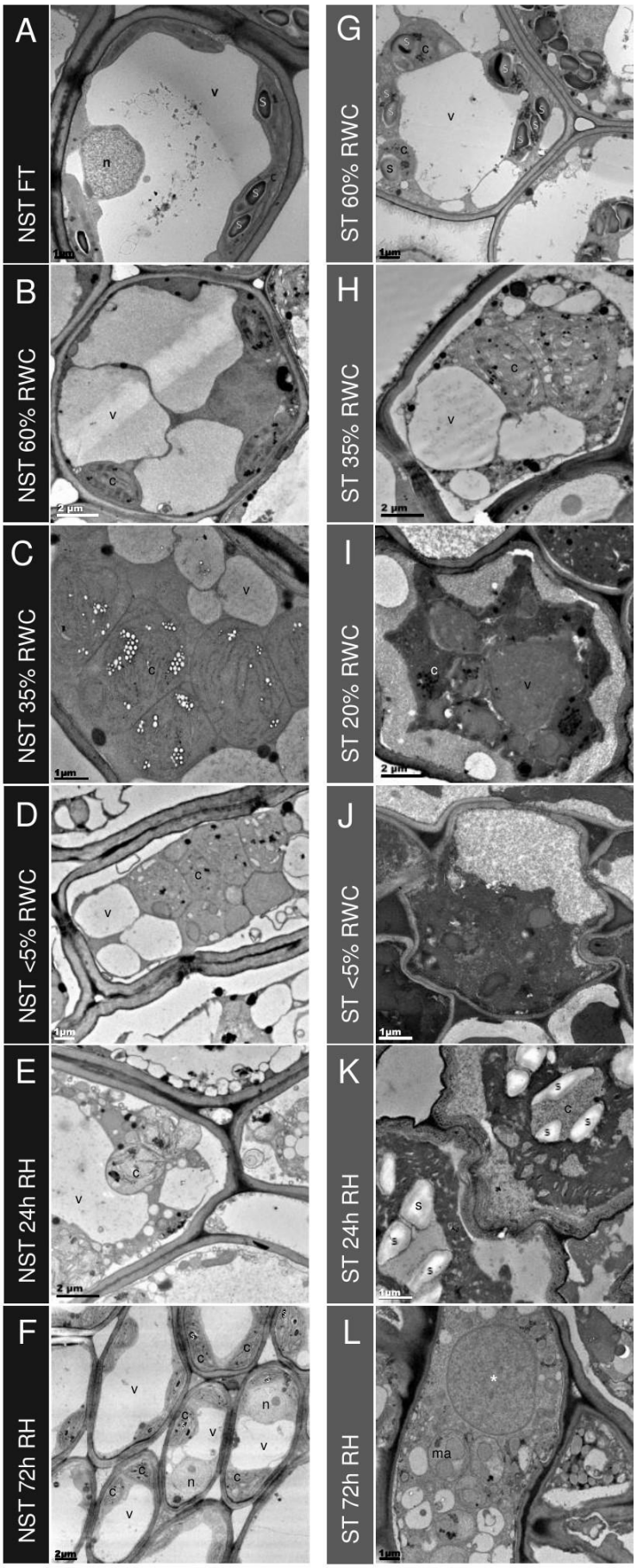

Fig 4: Ultrastructural changes during desiccation and rehydration. Transmission electron micrographs of mesophyll cells in NST (left column A-F) and ST (right column G-L) from the same leaves during desiccation and rehydration, with RWC for each on the left. When NST mesophyll cells are at FT (A), a central electron opaque vacuole is surrounded by active (indicated by the presence of starch) chloroplasts with good thylakoid organisation. As plants experience water deficit, the central vacuole splits into several smaller vacuoles (B-D) and the chloroplasts become swollen and lose thylakoid membrane organisation. Once rehydrated (E-F), NST mesophyll quickly regains the structure observed in the hydrated state, with reformation of the central vacuole observed at 24h (E) and thylakoid organisation regained by 72h (F). The presence of starch granules in peripheral chloroplasts indicates regaining of photosynthetic competence (F). Mesophyll cells of the ST (G-L) experience lower corresponding water contents during water deficit and this is evident on the ultrastructural level with mesophyll cells from fully hydrated plants (60% RWC in ST) resembling the organisation of drying NST (G compared to B). Drying below 35% in ST results in a different appearance of mesophyll in ST from that of NST – the cytoplasm becomes increasingly electron dense (I-L) and there appears to be contraction of the membrane from the cell wall (I-J), and cell wall folding (J-K). Of the cells that are not lysed in rehydrated mesophyll (L), there is evidence of macroautophagy and the appearance of a large electron dense vesicle (*). Symbols are used to indicate organelles: vacuoles (v), nuclei (n), chloroplasts (c), starch granules (s), electron dense vesicle (*) and macroautophagosomes (ma).

water contents. This suggests a completely different vacuolar content between the two tissue types. Chloroplasts were evidenced predominantly by the presence of plastoglobuli (Fig. 4 I,J).

Twenty-four hours after soil watering, the water content of NST was 60% RWC, while that of ST remained at < 5%. In NST, mesophyll cells had largely regained the central vacuole, and membranous strands resembling early thylakoids were present in the chloroplasts (Fig. 4 E). In contrast, ST remained similar in appearance to that of the desiccated state, with the exception of the presence of starch in what can be assumed to be ex-chloroplasts, as it is unlikely that any organelle biogenesis had occurred during the 24 h period since soil watering.

By 72 h post hydration, the mesophyll cells of NST (Fig. 4F) were similar to those of fully hydrated tissue prior to dehydration (Fig. 4A). Chloroplasts had well developed thylakoid membranes, chlorophyll content had increased (Supplementary Fig. 1) and starch was present, suggesting photosynthetic competence. In ST, now at 20% RWC, many mesophyll cells had lysed (Supplementary Fig. 7A), while some appeared to have limited organisation (Fig. 3L, Supplementary Fig.7B-F). Starch was no longer evident in plastids, indicating potential operation of amylases. Electron dense vacuole-like organelles were still evident (indicated by *), but several smaller macroautophagic-like vacuoles, containing remnants of organelles and cytoplasmic debris, were also discernible, suggesting that autolysis might be occurring in these tissues after rehydration.

Changes in primary metabolites with dehydration

Previous molecular physiological studies on *X. schlechteri* have demonstrated that key changes associated with desiccation tolerance are initiated at RWCs below 55%, this correlating with the shutdown of photosynthetic carbon gain (Mundree and Farrant, 2000; Farrant *et al.*, 2015). Dehydration below *ca.* 40% leads to further significant changes (both increased and decreased) in transcript abundance, with the tissues appearing to enter a quiescent state below 10% RWC (Costa *et al.*, 2017). Similar trends were observed in the suites of primary metabolites examined in the present study, in which changes in the concentrations of many metabolites were evident below 60% RWC, with further shifts being evident at 35% RWC and the air-dry state (Fig. 5A, Supplementary Figs. 2–6). If we assume

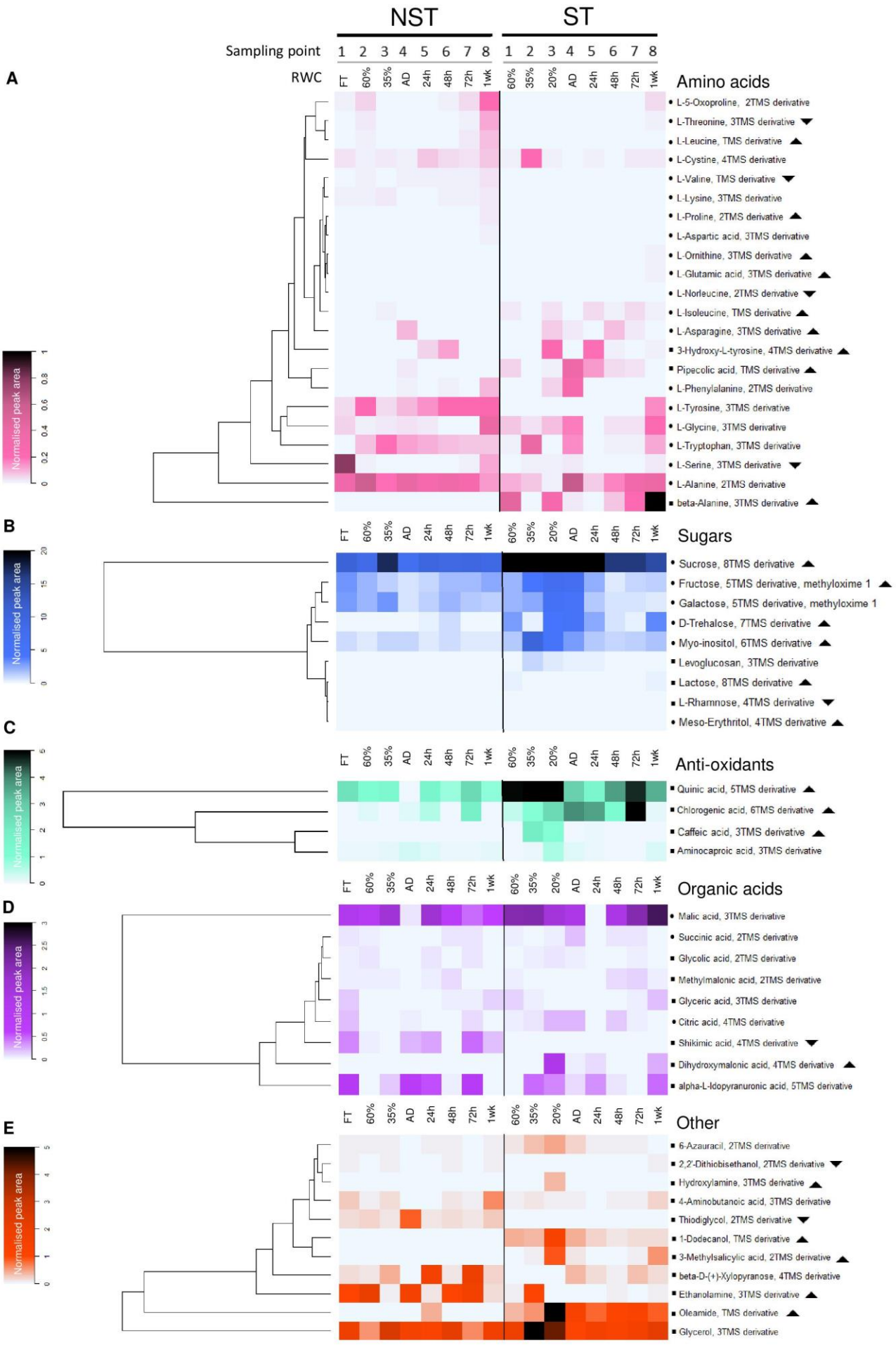
NST
ST
Sampling point
1 2 3 4 5 6 7 8 1 2 3 4 5 6 7 8
RWC
FT 60% 35% AD 24h 48h 72h 1wk 60% 35% 20% AD 24h 48h 72h 1wk
A
Amino acids
L-5-Oxoproline, 2TMS derivative
L-Threonine, 3TMS derivative
L-Leucine, TMS derivative
L-Cystine, 4TMS derivative
L-Valine, TMS derivative
L-Lysine, 3TMS derivative
L-Proline, 2TMS derivative
L-Aspartic acid, 3TMS derivative
L-Ornithine, 3TMS derivative
L-Glutamic acid, 3TMS derivative
L-Norleucine, 2TMS derivative
L-Isoleucine, TMS derivative
L-Asparagine, 3TMS derivative
3-Hydroxy-L-tyrosine, 4TMS derivative
Pipecolic acid, TMS derivative
L-Phenylalanine, 2TMS derivative
L-Tyrosine, 3TMS derivative
L-Glycine, 3TMS derivative
L-Tryptophan, 3TMS derivative
L-Serine, 3TMS derivative
L-Alanine, 2TMS derivative
beta-Alanine, 3TMS derivative
Normalised peak area
B
Sugars
Sucrose, 8TMS derivative
Fructose, 5TMS derivative, methyloxime 1
Galactose, 5TMS derivative, methyloxime 1
D-Trehalose, 7TMS derivative
Myo-inositol, 6TMS derivative
Levoglucosan, 3TMS derivative
Lactose, 8TMS derivative
L-Rhamnose, 4TMS derivative
Meso-Erythritol, 4TMS derivative
C
Anti-oxidants
Quinic acid, 5TMS derivative
Chlorogenic acid, 6TMS derivative
Caffeic acid, 3TMS derivative
Aminocaproic acid, 3TMS derivative
D
Organic acids
Malic acid, 3TMS derivative
Succinic acid, 2TMS derivative
Glycolic acid, 2TMS derivative
Methylmalonic acid, 2TMS derivative
Glyceric acid, 3TMS derivative
Citric acid, 4TMS derivative
Shikimic acid, 4TMS derivative
Dihydroxymalonic acid, 4TMS derivative
alpha-L-Idopyranuronic acid, 5TMS derivative
E
Other
6-Azauracil, 2TMS derivative
2,2'-Dithiobisethanol, 2TMS derivative
Hydroxylamine, 3TMS derivative
4-Aminobutanoic acid, 3TMS derivative
Thiodiglycol, 2TMS derivative
1-Dodecanol, TMS derivative
3-Methylsalicylic acid, 2TMS derivative
beta-D-(+)-Xylopyranose, 4TMS derivative
Ethanolamine, 3TMS derivative
Oleamide, TMS derivative
Glycerol, 3TMS derivative

Figure 5: Desiccation associated responses in the metabolome of NST and ST as determined by GCMS. Average peak area of compounds identified in this study, normalized to ribitol internal standard and sample dry masses. Note that for each sampling point (1-8), ST and NST from the same leaves differ in average RWC. In each of the compound classes is a dominant (highly accumulated) metabolite: alanine (A), sucrose (B), quinic acid (C), malic acid (D) and glycerol (E). Symbols: ● indicates compound identification was done using the NIST library and an internal library of standards; ■ indicates NIST library identification only; ▲ indicates significantly greater total accumulation in ST vs NST (Log_2 fold change ≥2, t-test p≤0.05, FDR≤0.1); ▼ indicates significantly lesser total accumulation in ST vs NST. AD refers to the airdry state.

corroborated by the ultrastructural observations in the present study (Fig. 4), then the nature of the metabolites present is likely to be reflective of the native metabolism in this species and shifts in concentrations during drying to 60% RWC are probably related to osmoprotection and the prevention of oxidative stress. The accumulation of amino acids, including threonine, alanine, tryptophan, 5-oxoproline, tyrosine, and leucine (Fig. 5, Supplementary fig. 2), was observed at this stage. Other amino acids remained similar or declined in abundance at this water content. Among the sugars and sugar alcohols examined, there was an increase in trehalose and rhamnose and a slight decline in myo-inositol, fructose, galactose, β-D-xylopyranose, lactose and glucose (for glucose, see Supplementary Fig. 1). Sucrose concentrations also diminished slightly, but were overall consistently high, being the dominant metabolite with a peak area 3 or 4 orders of magnitude greater than the other metabolites in all samples. The antioxidant chlorogenic acid, as well as organic acids, glycolic acid, and methylmalonic acid increased in concentration during dehydration to 60% RWC. Among the TCA cycle intermediates, all except succinic acid declined during drying to this water content, suggesting a slowing-down of respiration.

Dehydration to 35% RWC resulted in a shift from source tissue metabolism to protective metabolism in NST, as carbon assimilation could no longer take place. This shift resulted in the maintenance or decline in abundance of most metabolites tested, with the exception of glutamic acid, ornithine, lysine, tryptophan, fructose, galactose, levoglucosan, citric acid and 1-dodecanol, which increased in abundance (Fig 5, Supplementary Fig. 2-6). On further dehydration toward the air-dry state, there were increases in concentrations of the amino acids asparagine, aspartic acid, phenylalanine, ornithine, glutamic acid, alanine, tryptophan, tyrosine and pipecolic acid, the organic acids citric acid, methylmalonic acid and aminocaproic acid, and hydroxylamine.

As outlined above, ST was maintained at lower water contents than NST on the same leaves. However, metabolism did not resemble that of the NST tissues at similar RWCs, and the metabolite trends between 60% and AD were more pronounced than in the NST. Amino acid accumulation is predominantly where NST and ST deviated in terms of metabolic profile: ornithine, proline, β-alanine, norleucine, pipecolic acid, serine, 3-hydroxy-L-tyrosine, aspartic acid and glutamic acid were present in higher amounts in ST throughout DH. As observed in NST, ST significantly accumulated phenylalanine and asparagine in the dry state. Unlike in NST, serine, glycine, ornithine, β-alanine and pipecolic acid accumulated significantly (Fig 5, Supplementary Fig. 2–3). The sugars trehalose, sucrose, fructose, levoglucosan, lactose and myo-inositol remained consistently elevated in ST, while glucose followed similar declines to NST (Fig. 5, Supplementary Figs 1&4). Similarly, caffeic and quinic acid contents remained elevated in ST relative to NST throughout drying (Fig. 5, Supplementary Fig. 5). In the desiccated state, citric acid levels were elevated to the same degree as in NST, but unlike in NST, succinic acid was elevated rather than diminished. Most other organic acids were unchanged or diminished Fig 5, Supplementary Fig 5).

Changes in primary metabolites during rehydration

Most studies on resurrection plants have measured the metabolic changes occurring upon rehydration to full turgor and initiation of photosynthetic competence, with the longer-term metabolic changes being omitted. In such studies, early rehydration is characterised by an increase in TCA metabolites, correlating with rapid increases in respiration. Levels of protective sugars (sucrose, raffinose, stachyose and verbascose) decline, whereas antioxidants (superoxide dismutase, glutathione reductase, quinic acid), osmoprotectants and N storage metabolites (various amino and organic acids) tend to remain elevated (Moyankova *et al.*, 2014; Suguiyama *et al.*, 2014; Yobi *et al.*, 2017). In this study, while full photosynthetic competence is reported to occur by 72 h of rehydration (Farrant *et al.*, 2015), tissues were also sampled at 1-week post watering when the NST of all plants sampled had reached full turgor (Fig. 2).

After 24 h of rehydration (average tissue RWC of 50%), there was a return to basal (pre-dehydration) levels of citric acid and an increase in malic acid, as well as declines in sucrose, glucose and galactose in NST, which suggests the early resumption of respiration. Increased levels of quinic and chlorogenic acids imply that additional antioxidant protection was

required at this stage (Fig. 5C). There was also an increase in trehalose content, which remained elevated until 48 h after rehydration. By 72 h, except for the above-mentioned antioxidants and the amino acids tryptophan and tyrosine, which remained elevated relative to the hydrated state, other metabolites had returned to basal pre-dehydration levels. Increased levels of shikimic acid might imply that metabolism via the Shikimate pathway was occurring, corroborated by the elevation of tryptophan and phenylalanine at 1week post rehydration. At this stage, tyrosine remained elevated and there were increased levels of threonine, cysteine, glycine and serine relative to the pre-desiccated state.

Whereas the NST reached full turgor within 72 h, the ST was maintained at ~20% RWC. Despite this, there was evidence of metabolic activity in these tissues, with many of the metabolites indicating similar temporal trends as the NST (Fig. 5, Supp 2–3). After an initial decline at 24 h, the amino acids asparagine, glycine, serine, β-alanine and alanine accumulated towards the later stages of rehydration. Some amino acids followed similar trends to those in NST (5-oxoproline, leucine, phenylalanine, threonine) (Fig. 5, Supplementary Fig. 2–3). The sugars trehalose, levoglucosan, sucrose and myo-inositol were consistently elevated in ST but tended to follow a similar pattern to NST during rehydration (Fig 5, Supplementary Fig. 4). Citric and succinic acid very closely mimicked the accumulation patterns in their NST counterparts, except for accumulation peaking at 20% RWC. Shikimic acid peaked significantly at 72 h and remained high after 1 week of rehydration, corresponding with increases in tryptophan, tyrosine, 3-hydroxytyrosine and phenylalanine abundance, indicating that the shikimate pathway was active 1 week after rehydration (Fig. 5, Supplementary Fig. 2, 3, 5).

Changes in other compounds

The anoxic nitrate metabolite hydroxylamine (Sturms *et al.*, 2011), present in desiccated NST and at 24 h post rehydration, diminished significantly at 48 h (Fig. 5E), indicating a return to oxygenated conditions after anoxic quiescence. This compound remained elevated in ST throughout dehydration and rehydration, suggesting that the ST remains anoxic until 1 week following rehydration. The fatty acid derivative oleamide and fatty alcohol 1-dodecanol presumably appear in this dataset as they were sufficiently polar to be extracted in the methanol fraction. These compounds, after peaking in NST at 24 h post rehydration and the desiccated state respectively, returned to basal levels after 48 h rehydration. Both were

elevated in ST relative to NST at all times (Fig. 5, Supplementary Fig. 6). The sulphuric compounds thiodiglycol and 2'2-dithiobisethanol, while present in the NST, did not fluctuate much during dehydration and rehydration and were detected at very low levels in ST (Fig. 5, Supplementary Fig. 6).The cell wall components β-D-xylopyranose (Zhou *et al.*, 2018) and levoglucosan were elevated at 35% RWC in NST, corresponding with increases in other sugars at this stage. ABA content displayed an initial peak in both tissues early in water deficit (75%-60%) and then diminished in NST, remaining lowly accumulated throughout desiccation and rehydration. However, this hormone once again peaked in AD ST and remained highly accumulated during early rehydration.

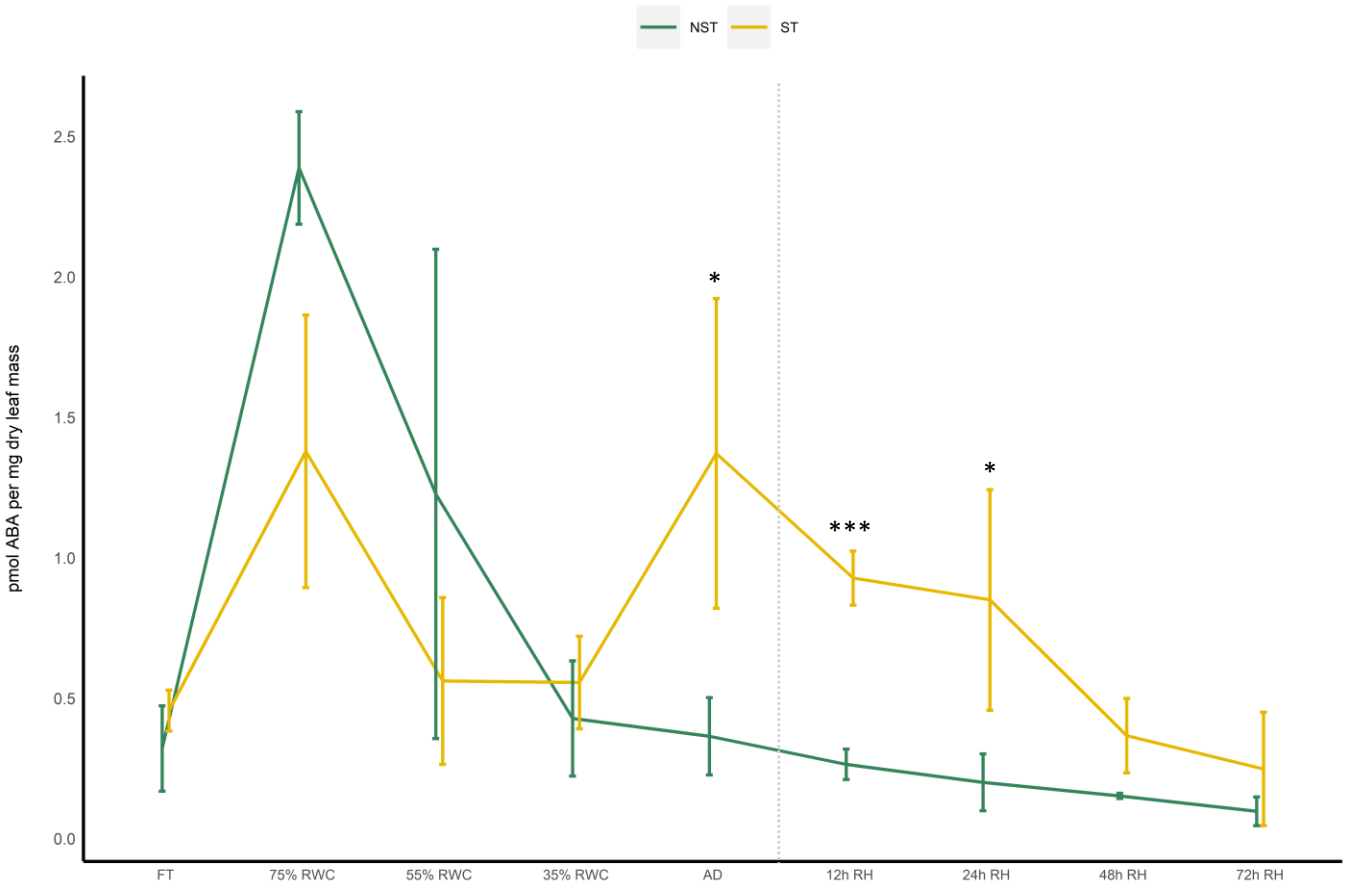

Figure 6: ABA content peaks in AD ST. ABA was quantified during dehydration (left of dotted line) and rehydration (right of dotted line) in NST and ST. RWC values are those of NST. The mean and standard deviation of each sample group is given, with the results of a t-test for comparison within the group. ABA content is only significantly increased in AD ST and in early rehydration (12h and 24h).

Discussion

Desiccation tolerance is a complex multigenic trait and is achieved via an intricate suite of molecular, biochemical and physiological mechanisms geared towards mechanical stabilisation, mitigation of photo-oxidative damage, stabilisation of key proteins and enzymes and repair upon rehydration (Farrant *et al.*,2007; Gechev *et al.*, 2012; Moore *et al.*, 2013; Karbaschi *et al.*, 2015; Challabathula *et al.*, 2016; Blomstedt *et al.*, 2018).While much work has been done on the molecular biology of this species (Costa *et al.*, 2017; Artur *et al.*, 2019), little work has been done on understanding its anatomical and metabolic adaptations for desiccation tolerance. Understanding these in surviving tissues, in comparison with metabolic changes in apical tissues which undergo senescence on desiccation, gives insight as to how senescence is repressed in the former yet proceeds in the latter, and provides a foundation for future work. Here we describe the drying and rehydration of NST, combining observations from this study and previous studies on whole leaves from *X. schlechteri* and other resurrection plants. We hypothesise on how senescence is initiated in response to aging and water deficit and describe the progression of this process during and following desiccation.

Mitigation of mechanical, osmotic and photo-oxidative stress during dehydration in NST

At full turgor, leaf anatomy and mesophyll ultrastructure are indicative of metabolically active tissues. Stomatal channels are open and free of mucilage, suggesting active photosynthesis and gas exchange. Sugars, organic acids and TCA cycle intermediates are highly accumulated. Sucrose, alanine, quinic acid and glycerol levels are high, and remain so during desiccation and rehydration, suggesting that they play a role as constitutive ameliorators of abiotic stressors associated with water deficit.

Dehydration to 60% RWC results in initiation of changes that mitigate against mechanical, osmotic and photo-oxidative stresses. Infolding of tissues adjacent to vascular bundles at this RWC allows for the redirection of mechanical forces associated with water loss (Iljin, 1957), likely alleviating much of the mechanical stress, while allowing for folding of the whole leaf at the midrib. The observed subcuticular excretion of mucilage by epidermal cells into abaxial stomatal channels serves to force the associated cuticle into close proximity, closing the stomatal channel aperture and limiting the rate of water loss while potentially still allowing

some gas exchange. At the subcellular level, mechanical stabilization is achieved by division of the central vacuole into several smaller vacuoles which collectively maintain subcellular volume, preventing plasmalemma detachment from the cell wall, as has been reported for resurrection plants which have less flexible cell walls (Farrant *et al.*, 2007; 2012). Metabolically, the accumulation of osmolytes such as sugars and amino acids have been proposed to slow water loss and maintain cell turgor (Fàbregas *et al.*, 2019). Oliver *et al.*, (2011b) have ascribed the accumulation of amino acids at 60% RWC in the resurrection grass *S. stapfianus* to affording such osmoprotection, and we propose that the increase in the amino acids threonine, alanine, tryptophan, 5-oxoproline, tyrosine, proline and β-alanine together with consistently elevated sucrose levels in *X. schlechteri* also serve this purpose. At this point, chloroplasts still have stacked grana, but there is little/no starch and chlorophyll content was a third of that in leaves at full turgor. These observations, coupled with the relative diminishment of fructose, glucose and TCA intermediates, indicate slowing of photosynthesis and carbon gain, corroborating previous studies on this species (Mundree and Farrant, 2000; Farrant *et al.*, 2015). Such studies have also shown increased activities of several antioxidant enzymes, proposed to play a role *inter alia* in protection against photo-oxidative stress during early dehydration. The present study demonstrates that the antioxidant quinic acid is constitutively high in NST and is accompanied by the accumulation of chlorogenic acid, these possibly adding to photo-protection required on drying to this water content. The increase in trehalose content at 60% RWC could explain maintained sucrose levels observed in this species. Sucrose regulation has been proposed to occur via the interaction of Trehalose-6-Phosphate (Tre6P) and Suc-non-fermenting-1-Related Kinase 1 (SnRK1), termed the Suc-Tre6P nexus, in which Tre6P acts as both a signal and a negative feedback regulator of sucrose levels in plants, maintaining optimal levels under all conditions (Zhang *et al.*, 2009; Yadav *et al.*, 2014; Oszvald *et al.*, 2018). Since Tre6P is essential to trehalose formation, it is possible that its presence did allow interaction with SnRK1, so enabling high levels of sucrose after cessation of photosynthesis. While operation of this regulatory pathway has been postulated in resurrection plants (Blomstedt *et al.*, 2018) this has not yet been clearly demonstrated.

Dehydration to 35% RWC results in complete shutdown of photosynthesis as evidenced by thylakoid dismantling and complete loss of chlorophyll. Declines in fructose, glucose and

shikimic, citric, and succinic acid indicate a decline in glycolysis and the TCA cycle and a potential carbon shift towards protection. At the cellular level, mechanical stabilisation is afforded by increased vacuolation and chloroplast swelling and is inextricably linked with metabolism. It has been proposed that in desiccation tolerant organisms water is progressively replaced with vitrifying sugar solutions (Hoekstra *et al.*, 2001; Buitink and Leprince 2004; Farrant *et al.*, 2012). In *X. schlechteri*, peak concentrations of sucrose, glycerol and malic acid are present at this water content. Sucrose content is constitutively high in this species, exhibiting only a 2-fold increase during drying, unlike most other resurrection plants reported on which sucrose content elevates more dramatically during desiccation (Bianchi *et al.*, 1991; Farrant *et al.*, 2007; Peters *et al.*, 2007; Oliver *et al.*, 2011; Mladenov *et al.*, 2015). It is likely that this sugar is the principal vitrifying agent in this species. However, it is also possible that it participates in the formation of Natural Deep Euctectic Solvents (NaDEs), which have been proposed to form a third liquid phase (other than water or lipid) in which cellular components can be effectively concentrated and proteins protected from denaturation (Choi *et al.*, 2011). Malic acid, sucrose and glycerol form a NaDES in a 1:1:2 ratio (Dai *et al.*, 2013) and could be contributing towards subcellular stabilization and potentially facilitate ongoing metabolism reported to occur at low water contents in this species (Mundree and Farrant, 2000; Farrant *et al.*, 2015; Costa *et al.*, 2017). Interestingly, β-D-xylopyranose and levoglucosan (a cell wall sugar) peak at 35% RWC. suggesting metabolic activity within cell walls. The reason for this accumulation is unclear but could reflect marginal changes in wall architecture (Moore *et al.*, 2013).

Upon further dehydration to the air-dry state, desiccation tolerant tissues are proposed to become quiescent and/or dormant (Farrant *et al.*, 2012; Gechev *et al.*, 2012; Costa *et al.*, 2016). In *X. schelchteri* metabolic quiescence is entered with a decline in malic acid and an accumulation of citrate, reflecting shut down of respiration, reported to occur at this stage (Mundree and Farrant, 2000). The accumulation of hydroxylamine, an anoxic nitrate metabolite (Sturms *et al.*, 2011), indicates that there is some degree of anoxia following repiratory shutdown. Interestingly, there was a notable accumulation of the amino acids asparagine (its only peak in accumulation), aspartic acid, phenylalanine, ornithine, glutamic acid, alanine, tryptophan and tyrosine in the dry state which we propose could serve as

nitrogen storage for rapid remobilisation and reincorporation into proteins upon rehydration, and/or as osmoprotectants (Djilianov *et al.*, 2005; Oliver *et al.*, 2011).

Recovery of NST

Recovery to full turgor occurs only after 72 hours, yet considerable structural and metabolic changes occur prior to this. By 48hr after receipt of water, infolding of palisade cells was relieved and both mesophyll and palisade cells take on the shape observed in fully hydrated tissues. At this stage, chloroplasts regain some thylakoid organization, but chlorophyll levels remain low and it is likely that they only gain photosynthetic competence at and after 72 h, where starch formation begins again. This correlates with previous reports on recovery of photosynthetic competence in this species (Sherwin and Farrant, 1996). Thus, the metabolites that were accumulated during desiccation are crucial for metabolic activity in the early stages of rehydration, where minimal photosynthetic activity drives the synthesis of ATP. We propose that sucrose acts as a major carbon source for the biosynthesis of cellular constituents and regeneration of ATP via glycolysis during early rehydration. Similarly, asparagine, which has been proposed to be the major nitrogen storage compound in *S. stapfianus* (Oliver *et al.*, 2011), diminishes considerably upon rehydration and thus, like sucrose, is probably utilised for the generation of other necessary metabolites. Poikolochlorophyllous resurrection plants are sensitive to photooxidative stress during restoration of photosynthetic competence (Sherwin and Farrant, 1996; Tuba *et al.*, 1998) and elevated levels of carotenoids and the antioxidants chlorogenic and quinic acid, which peak at 72 h RH are likely to contribute to photoprotection. By 72 h, recovery of shikimic acid and the biosynthetic end-points phenylalanine, tyrosine, and tryptophan is observed. The same is true for TCA intermediates, implying that energy production and biosynthesis proceeds via these pathways, fed partially by sucrose and asparagine and partially by photosynthesis. The significant increase in trehalose during the first 48h could again suggest operation of the Suc-Tre6P nexus, this possibly regulating sucrose content until photosynthetic competence is gained. Alternatively, it is possible that here trehalose is playing a role in autophagy, allowing clean up of subcellular damage or macromolecular aggregates that may have formed during desiccation and quiescence (Williams *et al.*, 2015; Asami *et al.*, 2019).

Understanding the fundamental mechanisms underlying desiccation tolerance in this species enables us to study senescence with a clearer lens. Is senescence simply a system failure in the oldest tissues, wherein they succumb to the stresses imposed by desiccation? Is it initiated and conducted in a controlled manner? Are age-related senescence processes exacerbated by drying?

Dissecting the lower RWC phenomenon and progression of senescence in ST: anatomical and metabolic arguments

There are three broad processes that characterise leaf senescence: initiation, reorganisation and termination (Bresson *et al.*, 2018). Without application of external stress, leaf age and developmental stage are the main initiators of senescence. Early onset of senescence can also be triggered by abiotic and biotic stressors, driven by hormones, sugars, and ROS generated by these processes. The reorganisation phase is characterised by the breakdown of macromolecules and remobilisation of nutrients in small subunit form, wherein hydrolytic enzymes are extensively deployed (Bresson *et al.*, 2018). Basic metabolic activity during this phase is required to ensure remobilisation of breakdown products to the vasculature for incorporation in viable cells. Toxic intermediates are likely to form during this phase, and thus antioxidant enzymes and compounds (particularly anthocyanins) are deployed to protect against oxidative stress in this state (Bresson *et al.*, 2018). During termination, vacuoles collapse, releasing nucleases and proteases into the cytoplasm, leading to acidification and contraction of the cytoplasm and uninhibited breakdown of DNA, RNA, proteins and membranes. At this point, the cell is effectively dead, leaving behind cell wall and debris (Lim *et al.*, 2007; Bresson *et al.*, 2018).

Tracking senescence is challenging in poikilochlorophyllous resurrection plants, which employ many of the “reorganisation” mechanisms as part of their desiccation tolerance programming (chlorophyll degradation, lipid changes, metabolic shifts, accumulation of compatible solutes, increased abundance of chaperones, antioxidant accumulation, etc.) (Oliver *et al.*, 2011; Gechev *et al.*, 2012; Christ *et al.*, 2014; Farrant *et al.*, 2015). Comparison of anatomy, ultrastructure and metabolism of ST to that of NST is the logical first port of call in the pursuit of understanding senescence processes in leaves. To begin with, under well-watered conditions, ST is maintained at a lower water content (1.8-2.2g/g dry mass) than NST (2.8-

3g/g dry mass). There are two potential explanations. Firstly, it is possible that these tissues have a lower osmotic potential and lack of active transpiration might slow the diving force of water, leaving the cells with a lower water status. Ultrastructural studies show limited thylakoid organization in the fully hydrated state, confirming limited photosynthetic activity driving water potential. A second likely explanation for this phenomenon is that the water content of cells within these tissues is not homogenous. The termination phase of senescence is associated with lysis of the vacuole and the consequent breakdown of cellular structure and plasmalemma rupture. When water content determination is performed, it is done so on a dry mass basis. Lysed cells are likely to hold less water as there are no intact membranes to contain it, but cell walls contribute towards total mass of the tissue. Thus, the impression could be made that tissues are held at an overall lower RWC, where this is true of only some cells. In the present study however, while subcellular organisation of most mesophyll cells of ST at RWC below 35% was compromised, there was little evidence of complete subcellular lysis until rehydration. Thus this hypothesis holds when considering the water contents of the ST mesophyll cells after 48 h and 72 h rehydration.

Ultrastructurally and metabolically, there is evidence that age-related senescence processes are ongoing in well watered plants and are exacerbated during desiccation. In fully hydrated plants, ST has an average RWC of ~60%. Chloroplasts contain significantly more starch than NST and less chlorophyll and carotenoids at similar water contents, typical of early stage age-related senescence in *Arabidopsis Thaliana* (Watanabe *et al.*, 2013). Other similarities to *A.thaliana* age-related senescence in ST at this water content are the relatively high levels of TCA intermediates, glycerol, trehalose, the antixodiants quinic and chlorogenic acid and persistent presence of anthocyanins in ST (Watanabe *et al.*, 2013). Furthermore, in terms of amino acids, β-alanine glycine, pipecolic acid and isoleucine are elevated in ST whereas threonine, alanine, tryptophan, 5-oxoproline, tyrosine and proline are not, suggesting the NST is geared towards osmoprotection and ST towards the initiation of senescence.

Upon dehydration to ~35% RWC, ST displays further evidence of ongoing senescence processes. Mesophyll and palisade cells exhibit a high degree of Procion yellow staining compared to NST at similar and lower RWCs, indicating stress and aggregation of cellular constituents. While ultrastructurally, most cells of ST appear similar to that of NST at 35%

RWC, metabolically these tissues have different signatures. In ST fructose, galactose and myo-inositol are elevated and additional antioxidant protection is provided in the form of elevated chlorogenic and quinic acid, and of caffeic acid, which appears to be exclusively elevated in ST. These responses closely resemble the "reprogramming" phase of senescence as described in *A. thaliana* (Watanabe *et al.*, 2013), with the exception of vacuolation, which is a desiccation tolerance phenomenon (Farrant *et al.*, 2015).

Dehydration to the air-dry state results in further significant differences. In the ST, the cytoplasm is electron-dense and the plasmalemma appears withdrawn from the cell wall, indicating severe osmotic stress. Chloroplasts are discernible only by the presence of plastoglobuli and appear shrunken. There is significant cell-wall folding, indicating either deliberate remodelling of cell walls in an attempt to mitigate the mechanical stress, or cell wall collapse and redistribution of non-structural sugars. Metabolically, this is corroborated by the elevation of levoglucosan exclusively in the ST during desiccation, starting at 35% RWC. Methyl-salicylic acid content also peaks at this point and has been shown to positively regulate leaf senescence in water-stressed plants (Abreu and Munné-Bosch, 2008) and protect against fungal infection (Dieryckx *et al.*, 2015), suggesting that a potential signalling role is played here. Abscisic acid increases at this water content, suggesting a regulatory role in bringing about cellular death, as observed in *A. thaliana* (Woo *et al.*, 2019). While there was some metabolic overlap with NST at low water contents, persistent differences were the higher accumulation of fructose, galactose, trehalose, alanine, glycine, pipecolic acid and phenylalanine, and a relative lack of asparagine and tyrosine.

Upon rewatering there is little increase in water content until 48h, when ST reach 10% RWC. Varying degrees of subcellular disorganization is evident with some cells being relatively intact and resembling the air-dry state, with others being entirely lysed. This pattern is maintained upon further rehydration to the ultimate maximum value of 20% RWC at 72h post watering and is typical of the termination phase of senescence (Bresson *et al.*, 2018). Interestingly, cells that maintain subcellular organisation have electron dense vacuole-like structures and there is evidence of macroautophagy. This differential pattern of cellular integrity suggests different levels of hydration could be occurring among cells in ST and supports the second hypothesis outlined above in accounting for differential water contents in NST and ST. There was also no

evidence of recovery of photosynthetic competence nor operation of the shikimic acid pathway observed in NST.

Conclusion

X. schlechteri undertakes a variety of anatomical, ultrastructural and metabolic responses to desiccation, responding to the unique requirements associated with each phase of water loss and recovery. Similarities between the reorganisation phase in senescence and desiccation-associated changes make studying senescence in resurrection plants difficult. The "tip-burning" phenomenon in this species enables the study of viable and senescent tissue from the same leaves, and so enabled comparison in this study. Both tissues executed their desiccation tolerance programming: both limited the rate of water loss through accumulation of mucilage in stomatal channels, both reorganised chloroplasts and formed numerous vacuoles, both accumulated protective metabolites. Drying below 35% RWC in ST resulted in exacerbation of age-related senescence processes already underway in these tissues, resulting in damage to and potential loss of many cells in these tissues on desiccation. This in turn is exacerbated on some hydration but prevents ultimate rehydration of these tissues to levels observed before water deficit stress.

Supplementary

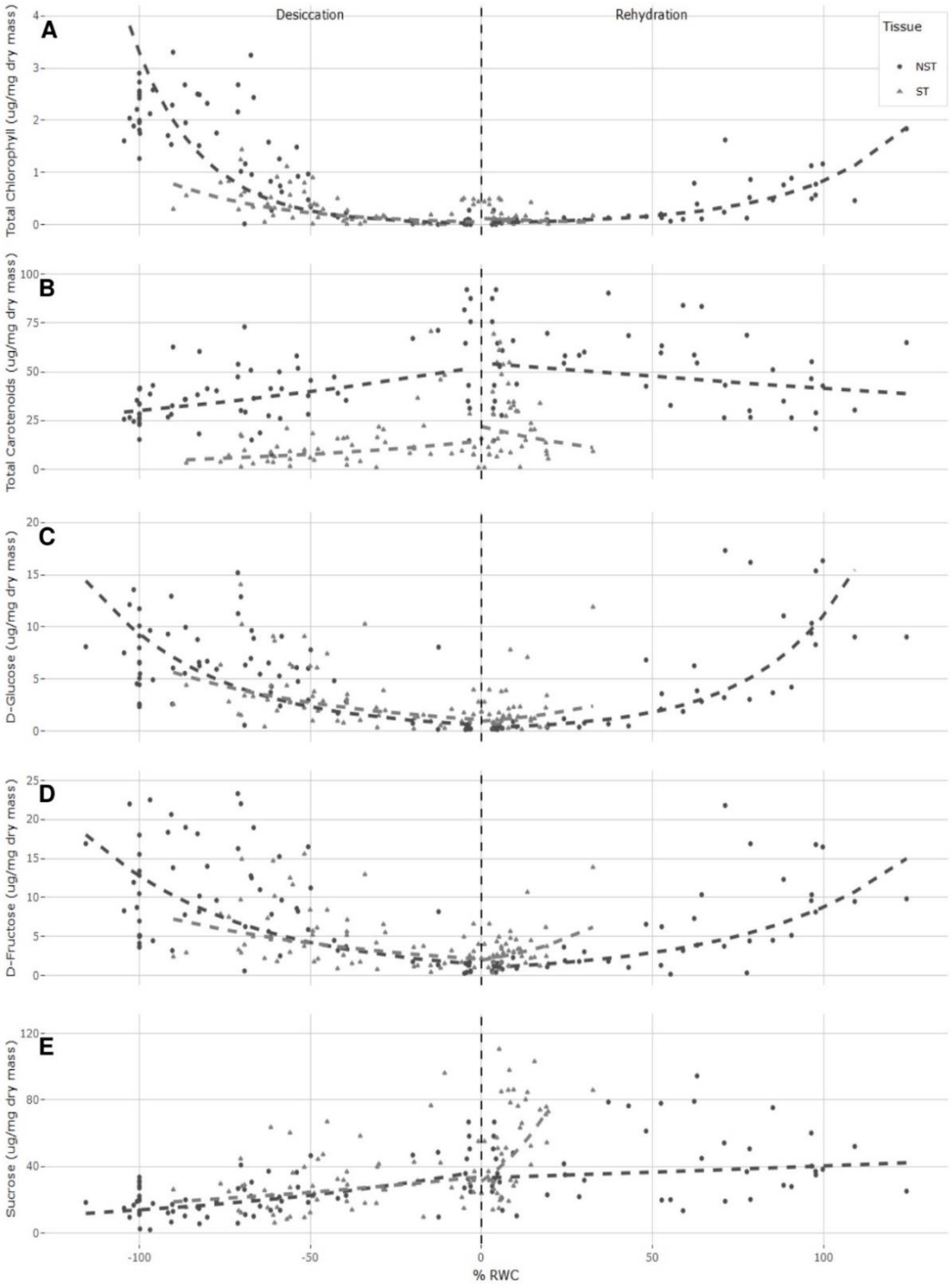

Supplementary Figure 1: **Metabolite changes observed during desiccation and rehydration in the leaf tissues of *Xerophyta schlechteri***. ST (triangles) and NST (closed circles) leaf tissues were sampled from 10 adult *X.schlechteri* plants over the course of one dehydration-rehydration cycle. The metabolite concentrations were determined using various colorimetric assays and normalized the mass of the lyophilized starting tissue. Individual measurements were plotted against the recorded %RWC for each sample. Linear models were constructed using log transformed data and fitted to the untransformed data to product exponential models of changes in metabolite concentration as %RWC changes for the two tissue types. Model summary statistics in **Supplementary Table 1**. Graphics for changing total chlorophyll (A), total carotenoid (B), D-glucose (C), D-fructose (D) and sucrose (E) are depicted.

Supplementary Table 1: statistical test results for models in Supplementary figure 1.
Significance codes: 0 '***' 0,001 '**' 0,01 '*' 0,05 '.' 0,1

A Metabolite	Tissue	Residual St. Error	Df	Adjusted R^2	F	p	
Total Chlorophyll	NST	1.212	61	0.66	119.5	<0.001	***
	ST	1.345	56	0.21	16.53	<0.005	***
Total Carotenoids	NST	0.4319	61	0.15	11.52	<0.005	***
	ST	0.9025	51	0.08	5.731	0.02	*
D-Glucose	NST	0.8356	62	0.55	77.79	<0.001	***
	ST	0.8395	56	0.2	15.34	<0.001	***
D-Fructose	NST	0.8036	63	0.46	55.72	<0.001	***
	ST	0.7462	59	0.16	12.46	<0.001	***
Sucrose	NST	0.5766	62	0.25	21.58	<0.001	***
	ST	0.5566	59	0.06	4.836	0.032	*

B Metabolite	Tissue	Residual St. Error	Df	Adjusted R^2	F	p	
Total Chlorophyll	NST	1.104	41	0.55	51.34	<0.001	***
	ST	1.137	33	<0.01	0.9089	0.347	
Total Carotenoids	NST	0.425	41	0.03	2.412	0.128	
	ST	0.9864	39	<0.01	0.7656	0.387	
D-Glucose	NST	0.6598	38	0.81	172.2	<0.001	***
	ST	0.9879	37	0.01	1.407	0.243	
D-Fructose	NST	0.8647	41	0.47	37.7	<0.001	***
	ST	0.647	40	0.09	5.167	0.028	*
Sucrose	NST	0.5315	41	<0.01	0.7738	0.384	
	ST	0.4849	41	0.25	14.99	<0.001	***

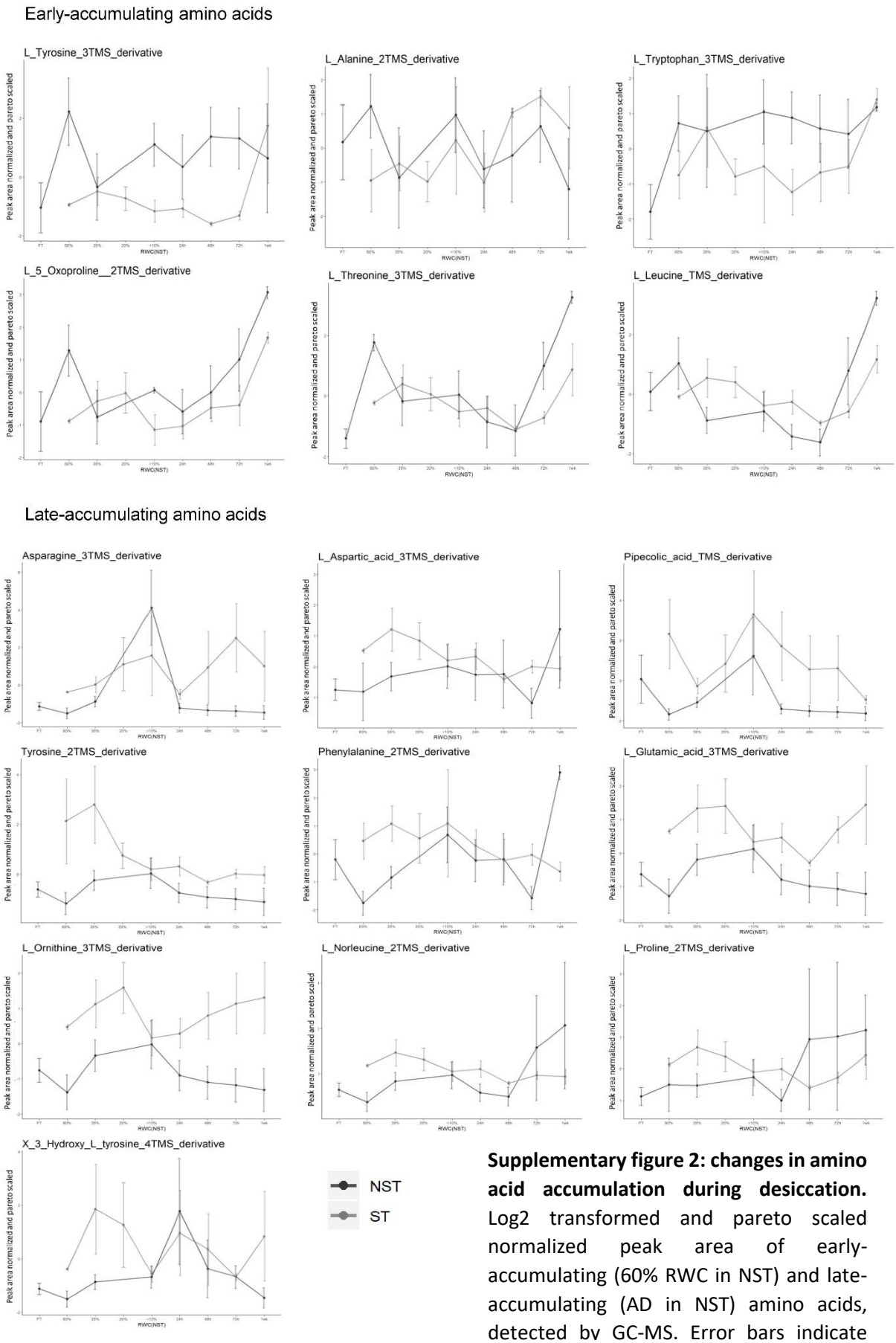

Supplementary figure 2: changes in amino acid accumulation during desiccation. Log2 transformed and pareto scaled normalized peak area of early-accumulating (60% RWC in NST) and late-accumulating (AD in NST) amino acids, detected by GC-MS. Error bars indicate

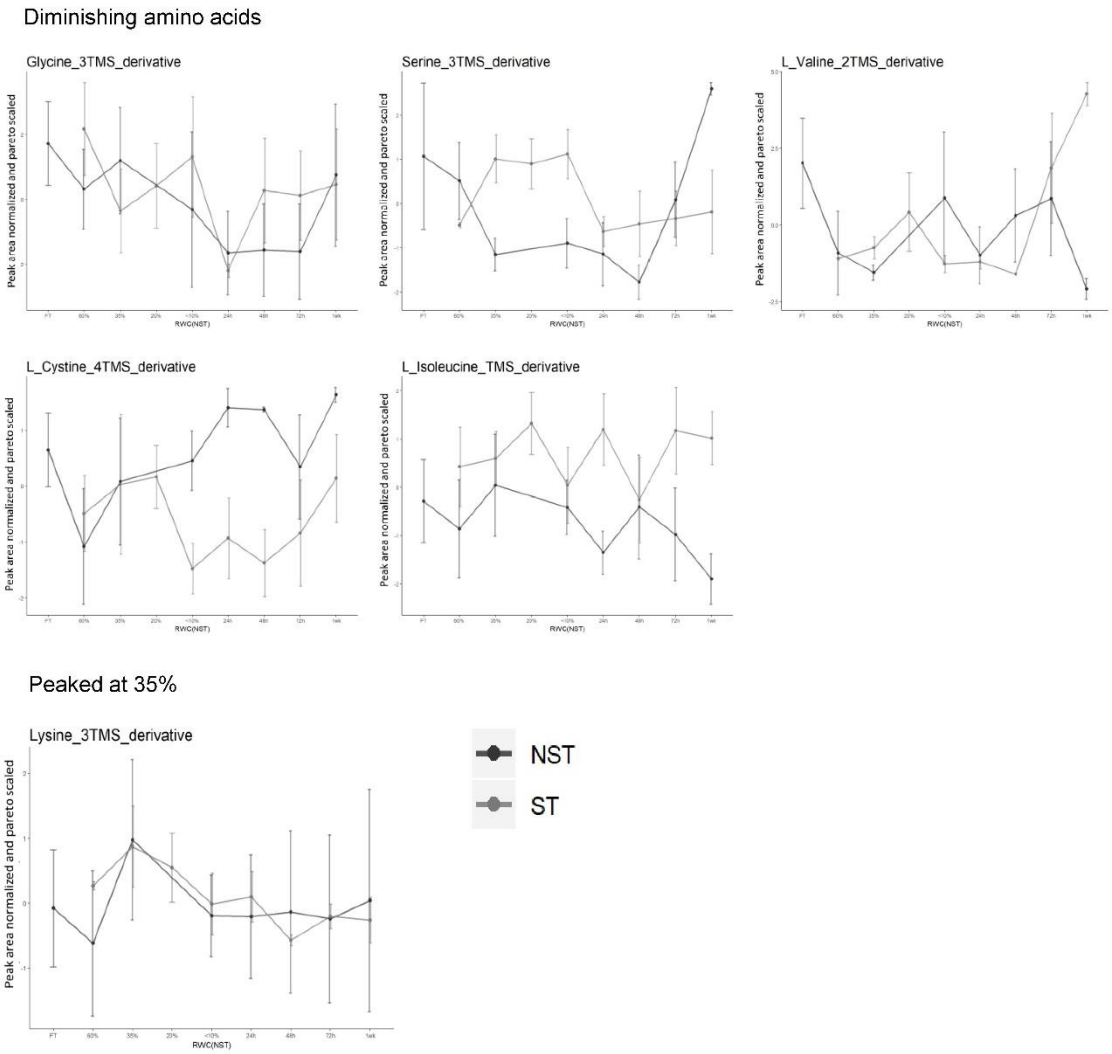

Supplementary figure 3: Changes in amino acid accumulation during desiccation (continued). Log2 transformed and pareto scaled normalized peak area of amino acids diminished in NST relative to FT NST and lysine (peaked at 35% RWC), detected by GC-MS. Error bars indicate standard deviation.

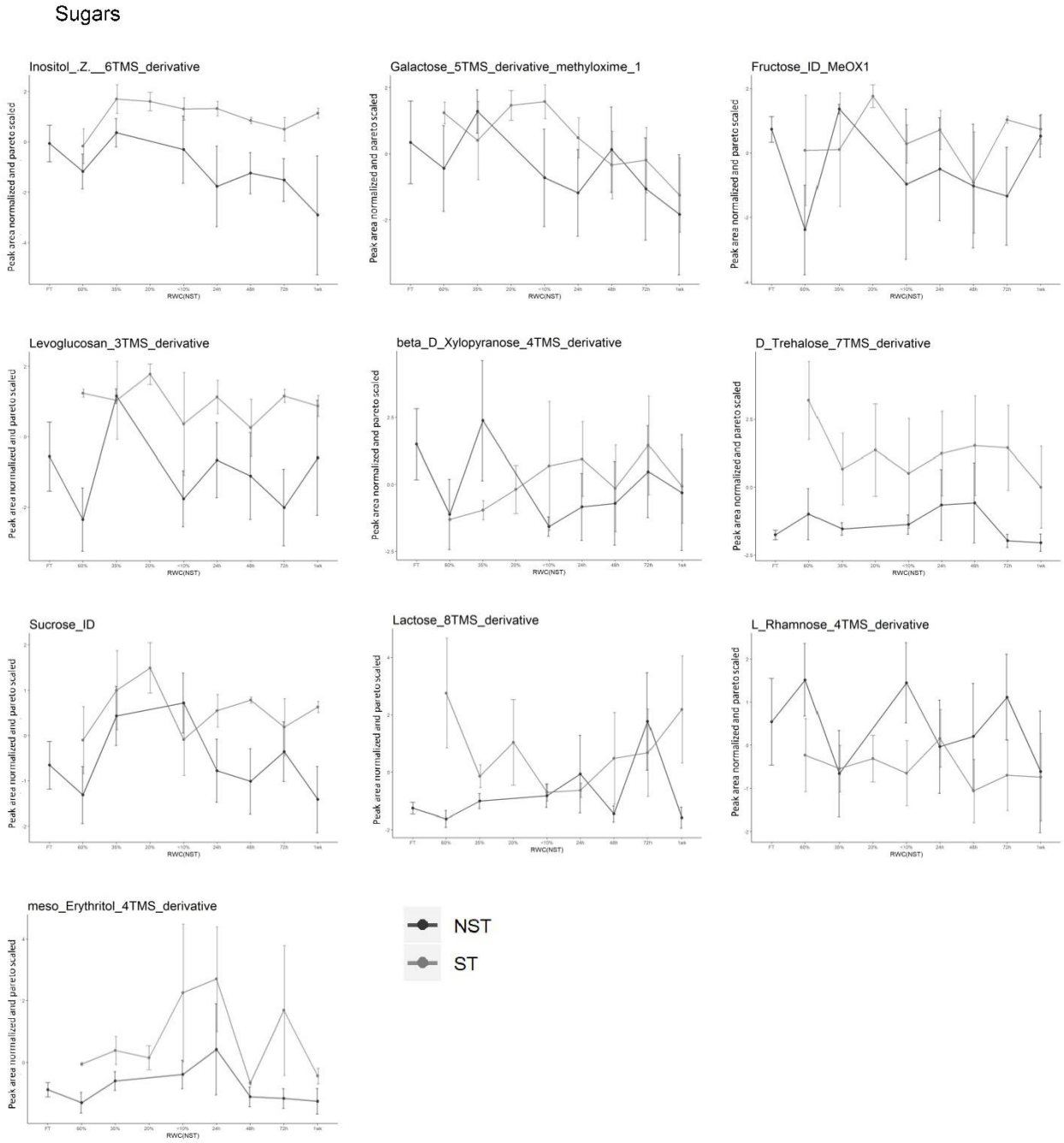

Supplementary figure 4: Changes in sugar accumulation during dehydration and rehydration. Log2 transformed and pareto scaled normalized peak area of sugars and sugar alcohols detected by GC-MS. Error bars indicate standard deviation.

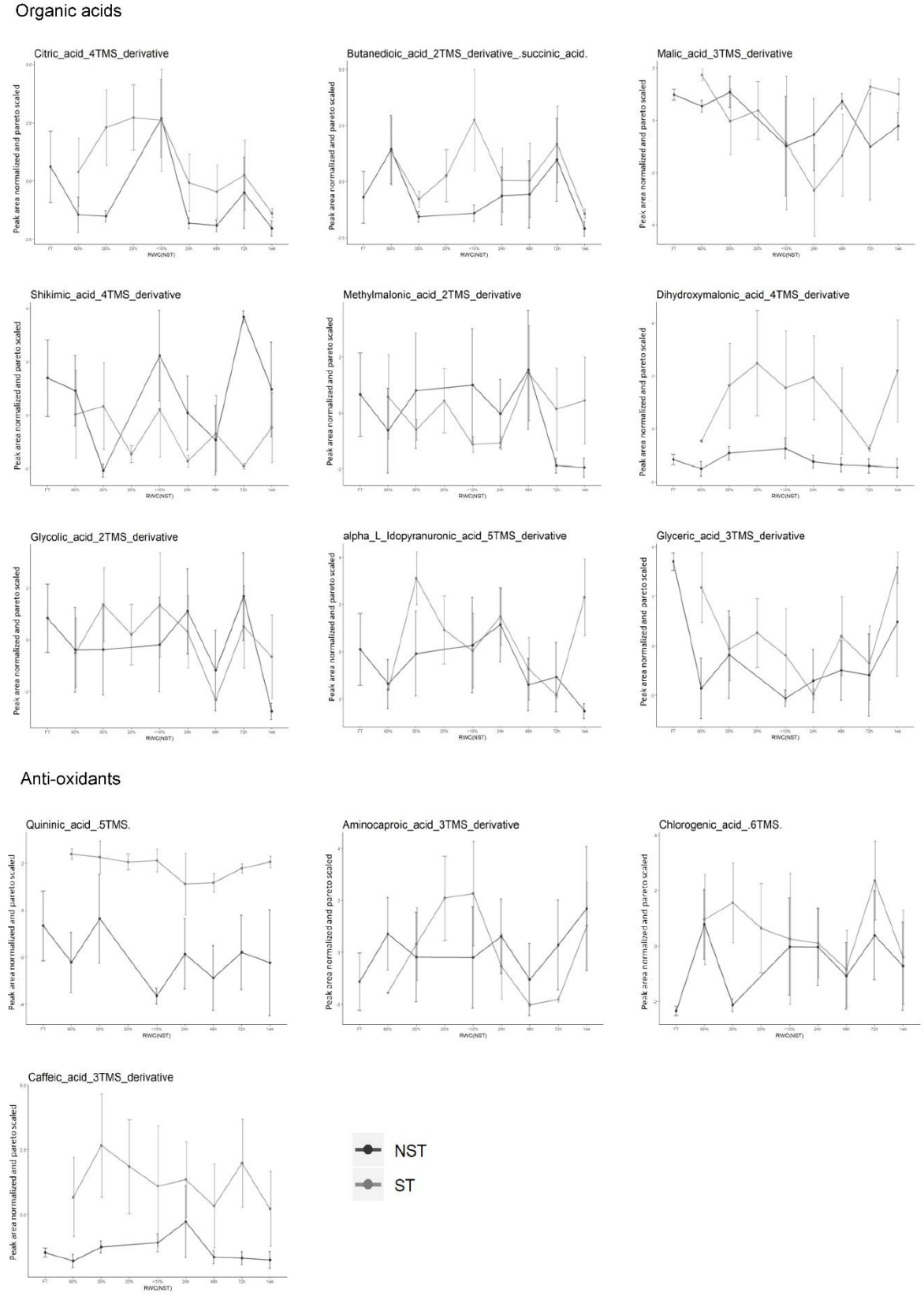

Supplementary figure 5: Changes in organic acid and anti-oxidant accumulation during dehydration and rehydration Log2 transformed and pareto scaled normalized peak area of organic acids and anti-oxidants detected by GC-MS. Error bars indicate standard deviation.

Other compounds

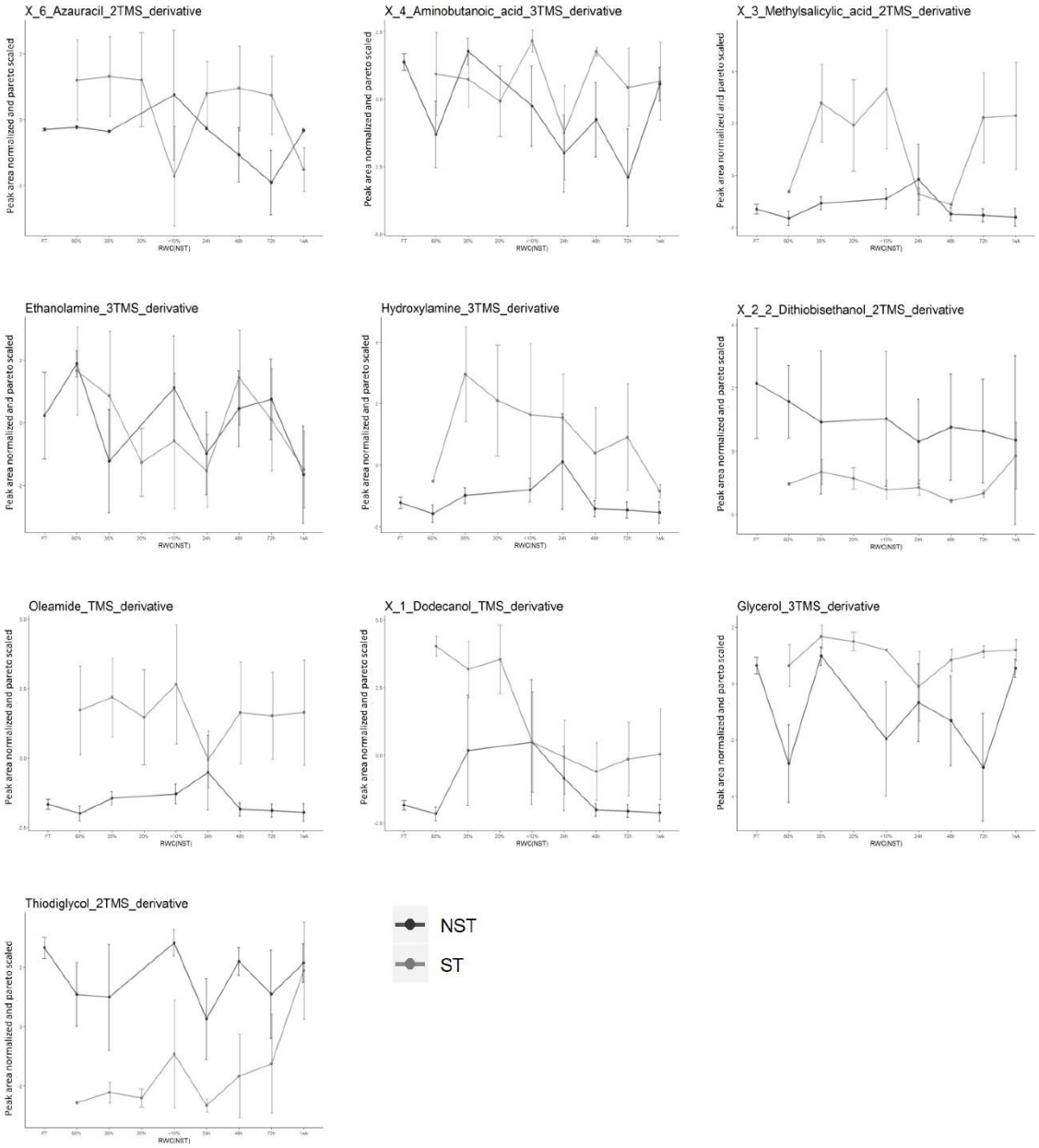

Supplementary figure 6: Changes in uncategorized compound accumulation during dehydration and rehydration. Log2 transformed and pareto scaled normalized peak area of uncategorised compounds detected by GC-MS. Error bars indicate standard deviation.

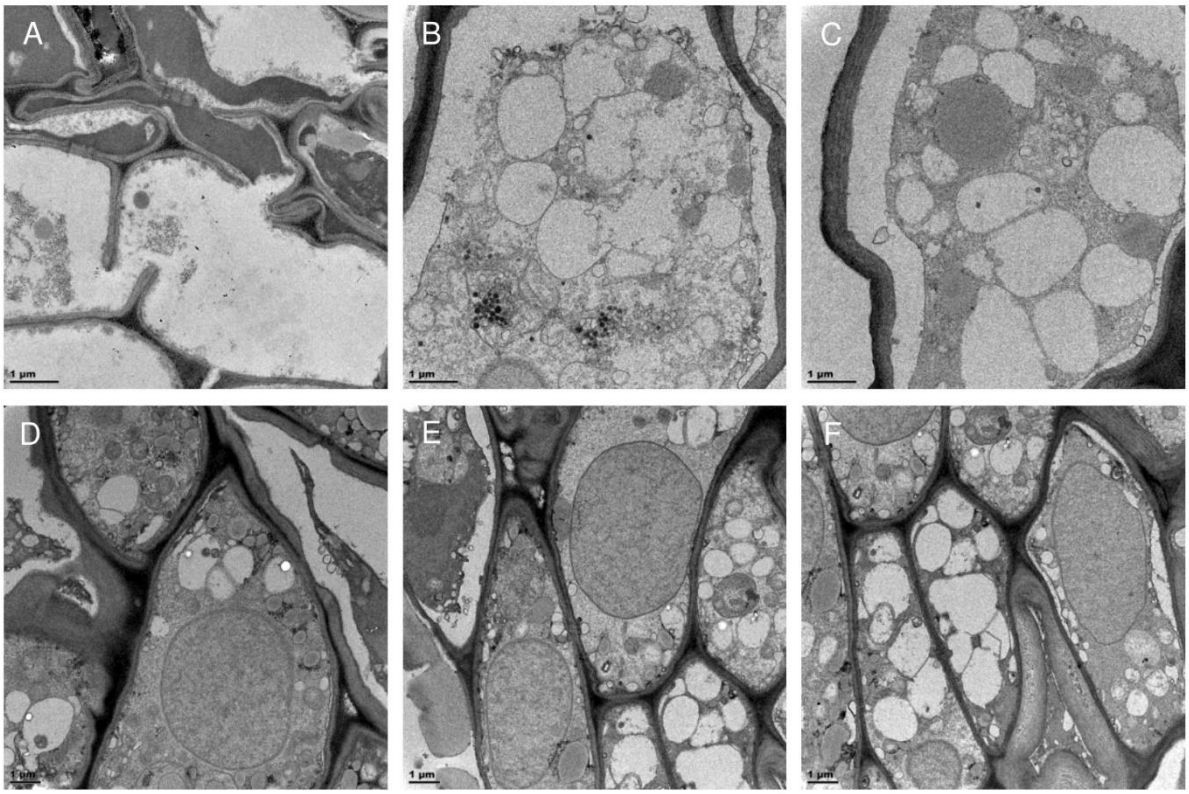

Supplementary figure 7: Transmission electron micrographs of mesophyll during rehydration in ST. 48h RH ST (A-C) and 72h RH ST (D-F).

Chapter 3

Regulation and progression of senescence in *Xerophyta schlechteri*: insights from the transcriptome

Introduction

The regulation of senescence in resurrection plants is largely under-studied. It has been postulated that resurrection plants are able to thwart cellular death processes during desiccation, through deployment of molecular protectants (anti-oxidants, LEAs, chaperones), clearing of debris (unfolded protein response and autophagy) as well as attenuation of cellular death regulators (e.g. Senescence-associated receptor kinase (SIRK) and the transcription factor WRKY53) (Griffiths*, et al.*, 2014), however no mechanism for transcriptional regulation of senescence has been directly studied in a resurrection plant. Study of senescent tissue (ST) gene expression enables elucidation of senescence prevention mechanisms in non-senescent tissue (NST), making transcriptional profiling in these tissues of great value.

Recent studies have increasingly shown the power of network analysis and how networks of genes and gene products interact affects plant survival outcomes to a larger degree than altered expression of single genes (Costa *et al.*, 2017; Woo *et al.*, 2019). This is particularly true in a species such as *X. schlechteri* where the genome is octoploid and many (often duplicated) homologous genes work in concert to bring about various cellular and whole-plant changes resulting in ultimate desiccation tolerance and quiescence (Costa *et al.,* 2017). Such analysis involves, *inter alia*, deployment of techniques such as K-Means clustering and co-expression network analysis, where the expression patterns of genes are grouped based on the similarity of their temporal expression. In this chapter, these analyses were utilised to understand aspects of desiccation tolerance in NST in comparison with transcriptional changes associated with desiccation induced senescence in *X. schlechteri*. In this regard, the following questions were posed.

1. **At what point during water deficit do the senescent and non-senescent tissues substantially deviate in terms of gene expression?**
2. **Which genes are differentially expressed in both tissue types, and what is their function in bringing about senescence?**
3. **How are these genes regulated?**

Material and methods

Sampling Procedure

Based on the outcomes of the physiological experiments in Chapter 2, total RNA was extracted from hydrated, dehydrating (75%, 55%, 35%) and desiccated (5% relative water content (RWC)) and rehydrated (48h – varying RWC values) tissue. Six plants were dehydrated in this experiment and all

were sampled continuously through the experiment as outlined below. Ten leaves per plant were utilised for absolute and RWC determination (see **Chapter 2**), this being determined on half of each sample for which the corresponding half was immediately frozen in liquid nitrogen for RNA-Seq analysis. On sampling, each leaf tissue was dissected into an apical region (3cm) designated as ST, a region of 1cm below this, termed pre-senescent tissue (PST: that which will survive a first dehydration but will senesce in a future desiccation event) and a section of 1cm, cut from the remaining NST. The meristem tissues were not included. At each sampling point, half of the leaf tissue was used for RWC determination. As plants, and leaves within a single plant, dehydrate at different rates, ultimately three biological replicates, each corresponding to a designated water content (outlined above) were used for RNA extraction. Tissue utilised from fully hydrated plants, prior to dehydration, included only the NST and ST samples. Thus, 51 samples were prepared for RNA extraction. The tissue was stored at -80^{o}C until extraction.

RNA extraction from *X. schlechteri*

A modified extraction method was used, using Tri-reagent (Sigma-Aldrich Corporation, St. Louis, MO, USA) and the RNEasy mini-kit (Qiagen, Hilden, Germany). Tissue was transferred from -80^{o}C storage to liquid Nitrogen prior to extraction. Tissue was transferred to liquid nitrogen filled 2mL Eppendorff tubes which contained three stainless steel bearings (pre-treated by soaking in chloroform and autoclaved twice along with the tubes). Before the tissue was allowed to thaw, 1mL cold Tri-reagent was pipetted into the tubes, ensuring that all tissue was completely submerged. The samples were maintained on ice until being transferred to an in-house homogenizer, where they were homogenised at room temperature for 12 minutes. The samples were placed on ice and 200µl chloroform was added to each tube. The samples were mixed by inversion and maintained on ice for 2 min. The tubes were then centrifuged at 13000g for 15 min at 4^{o}C. The upper aqueous phase of each sample was transferred to the RNEasy mini-kit Shredder column and the manufacturer's instructions for RNA extraction were followed with the following modifications: the RW1 buffer wash step was repeated with a volume of 200µl, the RPE buffer wash step was repeated twice and the RNA was eluted in RNase-free water pre-heated to 55^{o}C after incubating for 10 min at room temperature. RNA integrity and quality were verified using a Bioanalyzer (Agilent technologies, USA).

High-throughput sequencing and transcriptome annotation

Library preparation was conducted using the Illumina RNA-seq kit (San Diego, California) according to the manufacturer's instructions. The resulting cDNA libraries were sequenced using the Illumina MiSeq500 (San Diego, California) platform at Queensland University of Technology's Central Analytical Research Facility. The Tuxedo suite (Trapnell *et al.*, 2014) was used for annotation and mapping to the

reference genome for this species (Costa *et al.*, 2017). The genome indexing was built by bowtie2. The reference transcriptome indexing and the alignment of the RNA-seq reads to the reference genome were performed by tophat. The transcriptome assembly of samples was performed by cufflink and the assembled transcriptome of different samples were merged by cuffmerge (Trapnell *et al.*, 2014). Differential gene expression was performed using cuffdiff on FPKM (fragments per kilobase of exon per million mapped reads) gene expression data. Genes were considered differentially expressed if they exhibited a log2 fold change value greater than 2, compared to control and Exact test corrected pval <0.05. Two datasets are presented: the Desiccome (those genes which are significantly differentially expressed in all tissues during water deficit stress) and the Senescome (those genes differentially expressed in the airdry condition in ST, relative to AD NST). These data were plotted as a series of heatmaps in R (version 3.5.1; R Development Core Team, 2011) based on their Mercator Bins (Lohse *et al*., 2014) using the packages ggplot2 (Wickham, 2016) and wesanderson, and tabulated using the package dataTables (Jardine, 2019) and sparkline (Vaidyanathan, 2016). These plots and tables were rendered as interactive apps with the R package Shiny by RStudio (RStudio Team, 2015). The same method of analysis and data visualisation was followed for the Senescome, where genes significantly accumulated in AD ST relative to AD NST are visualised. The apps are available at astridite.shinyapps.io/XeroDesiccome and at astridite.shinyapps.io/XeroSenescome. The SwissProt, Gene Ontology and KEGG annotations were provided with the genome (Costa *et al.*, 2017). Additional annotation was performed by Mercator (Lohse *et al.*, 2014) to provide plant-specific "BIN" ontologies.

qPCR validation of transcriptome

Ten DEGs were selected from the transcriptomic analysis for validation using qPCR. The RNA extracted (1 µg per sample) for the transcriptomic analysis from all three tissues; 100%, 55% RWC and 48h RH, was converted to cDNA using Phusion HiFi Taq polymerase as per the manufacturer's instructions. qPCR was performed on 2µl of the resulting cDNA. The primers and the amplification efficiency of the ten DEGs were designed and optimised by assessing the relative transcript abundance of each GOI through RT-qPCR. Pipetting of the reaction mix (5µl SYBR green, 0.3µl forward and reverse primer, 2µl cDNA, 2.4µl nuclease-free water) was performed using an Eppendorf epMotion® 5075 automated pipetting machine. The amplification profile was as follows: 30 cycles of 15 sec at 95°C, followed by 60 sec at 60°C. Expression was normalised using PolyUbiquitin10 as the reference gene and log2FC values were calculated based on comparison to the FT NST condition. The resulting comparative plot (Supplementary fig. 1) was created in RStudio using the ggplot2 package.

Machine learning analysis

To explore and describe the temporal trends in the dataset, twelve K-means clusters were calculated in Genesis 1.8.1 from gene expression (Fragments per kilobase per million mapped reads - FPKM) data divided into the NST, PST and ST tissue types, which were clustered based on gene-level normalisation (Sturn, Quackenbush, and Trajanoski 2002). Further to this end, Pearson correlation coefficients were calculated between each gene pair to yield a correlation matrix in which each gene was compared to all genes in the dataset to determine co-expression (defined as $R^2 > 0.95$). Co-expressed genes were visualised in Cytoscape v3.7.1, where distances between nodes (edges) were representative of the level of co-expression over a threshold of 0.95; the higher the correlation, the closer the nodes. The network was displayed using the yGraph Organic layout and coloured based on the K-means cluster and the differential gene expression results.

Promoter motif enrichment analysis

Enriched promoter regions in the upstream regions (up to 1kb of sequence) of the senescence-specific subcluster of the gene expression network were identified using DREME from the MEME suite of promoter analysis tools (Bailey *et al.*, 2009; Bailey, 2011) with the upstream regions of the entire network as a control. Significantly enriched sequences were calculated using Fischer's exact test ($p < 0.05$). Transcription factors that bind to these enriched promoters were identified using TomTom (Jaspar Non-redundant 2018 plants database) (Gupta *et al.*, 2007) and annotated with *X. schlechteri* genomic identifiers in Microsoft Excel 365. Signalling pathway construction (**Fig. 10**) was performed using these annotations by incorporating transcription factor and signalling kinase nodes from the network as well as signalling information obtained from the cited literature.

Results and Discussion

RWC and differential gene expression

Samples for RNA extraction were grouped based on their RWC rather than time following water withholding (**Fig. 1**). As shown in **Chapter 2**, the RWC of ST is always lower than for NST. There were no significant differences in RWC between NST and PST tissues in rate and totality of dehydration, nor in the ability to fully rehydrate. The PST condition was introduced to determine whether there exists a spatial progression towards the senescent state (or not).

As discussed in **Chapter 2**, the RWC of ST observed was always lower than for NST. In terms of RWC, PST and NST were not significantly different to one another during water deficit. The ST RWC was significantly lower relative to both conditions throughout this process, except during the air-dry state. Forty-eight hours after rehydration, NST and PST reached average RWC of approximately 90%, whereas ST reached an average of 18% (approximately 90% of the total water content reached after 1 week as discussed in chapter 2).

In terms of gene expression at FT there was very little difference between NST and ST in that only 17 genes were differentially expressed (**Fig. 2**). As the plants experienced further water deficit stress and NST reached 75% RWC, differential gene expression among these tissue types showed significant changes in expression with over 1800 DEGs for each tissue type. The level of differential gene expression increased as the plant water content decreased. By 35% RWC in NST, there was very little difference in the number of DEGs that were expressed between tissue types, as shown in **Supplementary Figure 1.** When the plants desiccated towards the airdry state (<10% RWC), the difference in transcript abundance between tissues becomes evident, with 591 more DEGs upregulated in ST than its NST counterpart. Upon rehydration, the number of DEGs in NST and PST declined but the number of DEGs in ST remained elevated.

While comparison to the FT NST condition is useful as it highlighted when genes were differentially expressed during water deficit, it does not provide much information on how these genes act in concert to fulfil alternative functions of interest, 1) senescence inhibition or 2) enabling initiation of senescence. The present study will supply insights as to genes involved as well as putative regulators of these processes. This provides the opportunity for subjecting the data to alternative modes of analysis, such as machine learning.

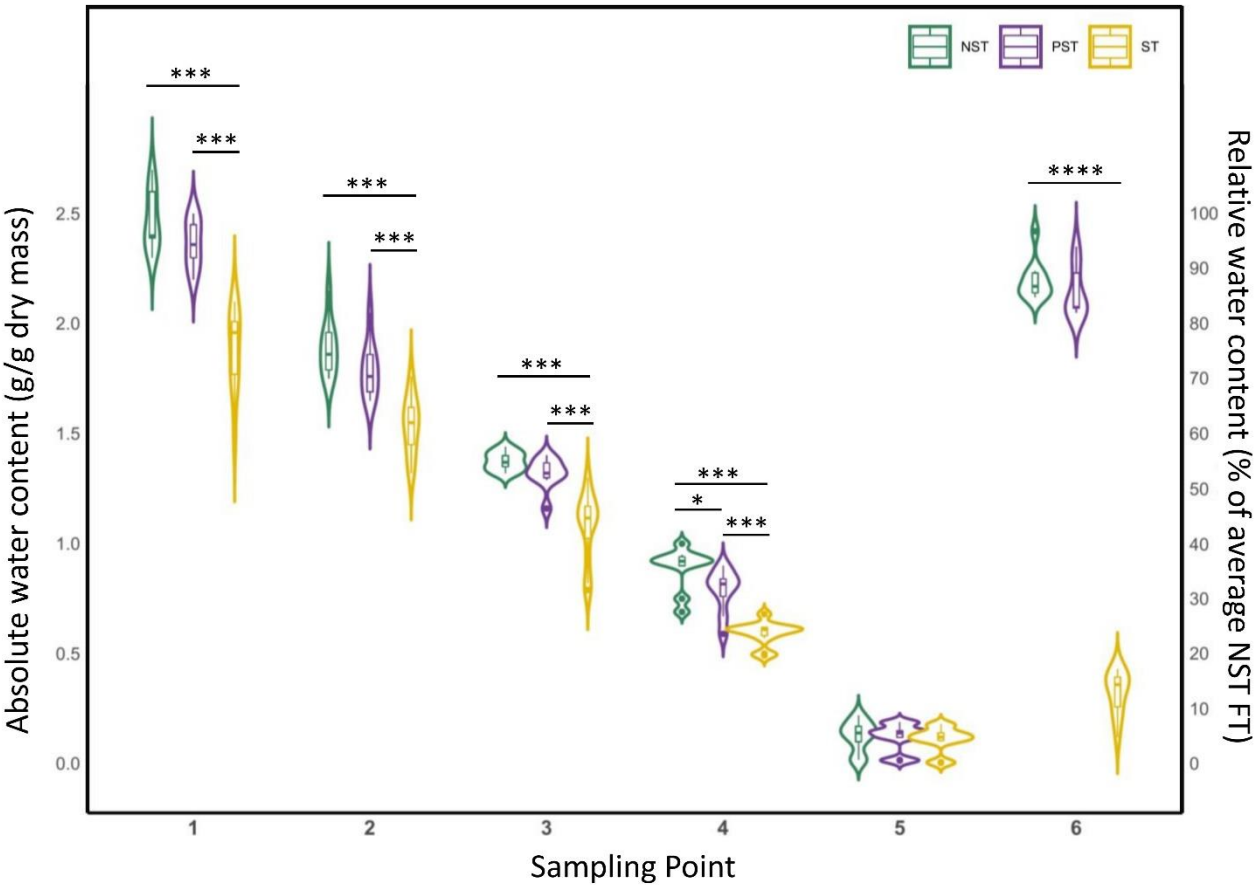

Figure 1: Relative water content differences between tissue utilized for transcriptomics. Leaf tissue was sampled daily one hour after dawn, half of the dissected leaf stored for RNA extraction and the other half used for RWC determination. Samples with a similar RWC value in NST (green) were chosen and grouped into sampling points for RNA extraction, utilizing the ST (yellow) and PST (purple) of the same leaves despite variability in RWC. Sampling point 1 represents the well-watered "full turgor" condition. Samples 2-4 represent drought stressed plants in descending order of severity (75%, 55% and 35% average RWC in NST). Sampling point 5, where the AWC content between tissues is not significantly different, represents the air-dry (AD) state. Sampling point 6 represents 48h post rehydration. The variability of RWC is shown here, with the results of a Wilcoxon test for each tissue type in the same sampling point given (only significantly differences are shown). Significance codes: "****" corrected pval < 0,0001; "***" corrected pval < 0,001; "**" corrected pval < 0,01; "*" corrected pval < 0,05.

K-Means Clusters

Means clustering is an unsupervised machine learning technique wherein K clusters are selected, and the data points iteratively assigned to each cluster based on the feature of interest. In the present study the level of gene expression, expressed as FPKM was used (**Fig. 3**). Mean FPKM values vs RWC were ordered sequentially based on tissue type. The K number determined to best describe the data was 12. **Figure 3** also shows the clusters organised into subcategories ("superclusters") based on their

response to desiccation. From here-on, descriptions of changes in select superclusters will be described.

Reduced and Recovered supercluster (RRS); clusters 8 and 12

Transcripts in these superclusters (represented in green in **Fig. 3**) diminished during water deficit and recovered to varying degrees within 48h post rehydration in NST and PST but not ST. These transcripts can thus be thought of as representing those genes required by the plant in the hydrated state, but require diminishment for survival of the desiccated state. In **cluster 8**, fundamental cellular processes which are significantly diminished during dehydration and desiccation included reproductive processes (pollen-pistil interaction, recognition of pollen), binding (DNA, polysaccharide and ATP), phosphorylation (protein amino acid and serine/threonine kinase activity). Similarly, in **cluster 10** so called fundamental processes were diminished during desiccation; these being protein formation (protein polymerisation), protein activity (hydrolases, endo-peptidases, kinases), cell cycle (regulation of cyclin-dependent protein kinase activity), nucleotide metabolism (purine, GTP, ribonucleotides), photosynthesis (photosynthetic process, photosynthetic membrane, thylakoid, photosystems I & II, oxygen evolving complex) and fatty acid biosynthesis. The only enriched process in **cluster 12** was glycine catabolism. Enrichment of non-redundant GO-terms can be found in **supplementary Table 2**.

Early response supercluster (ERS); clusters 1 and 9

The early response supercluster represents those genes that accumulated early in the water deficit cycle – at 75% or 55% RWC (**clusters 1 and 9**, represented in pink in **Fig. 3**). Significantly enriched gene ontologies in the early response super cluster are shown in **supplementary Table 3.** Those to do with photorespiration (ATP synthesis via proton pump, mitochondrial respiratory chain, bile acid symporter, cytochrome C), folate biosynthesis (dihydroneopterin aldoase) and gene expression (Ran GTPase binding, translation, ribosome, tRNA/rRNA binding) are significantly enriched in **cluster 1**. In **cluster 9**, significantly enriched responses are localised to the mitochondria and proteasome and involve cellular redox homeostasis (superoxide metabolic process, monovalent cation transport) and co-enzyme binding. Enrichment of non-redundant GO-terms can be found in **supplementary Table 3.**

Late response supercluster (LRS); clusters 4, 5 and 7

Genes in **cluster 7** peaked in expression later during desiccation (<35% RWC) in NST and PST. Interestingly, late stage increase in abundance in these tissues was accompanied by a sharp decline in their expression

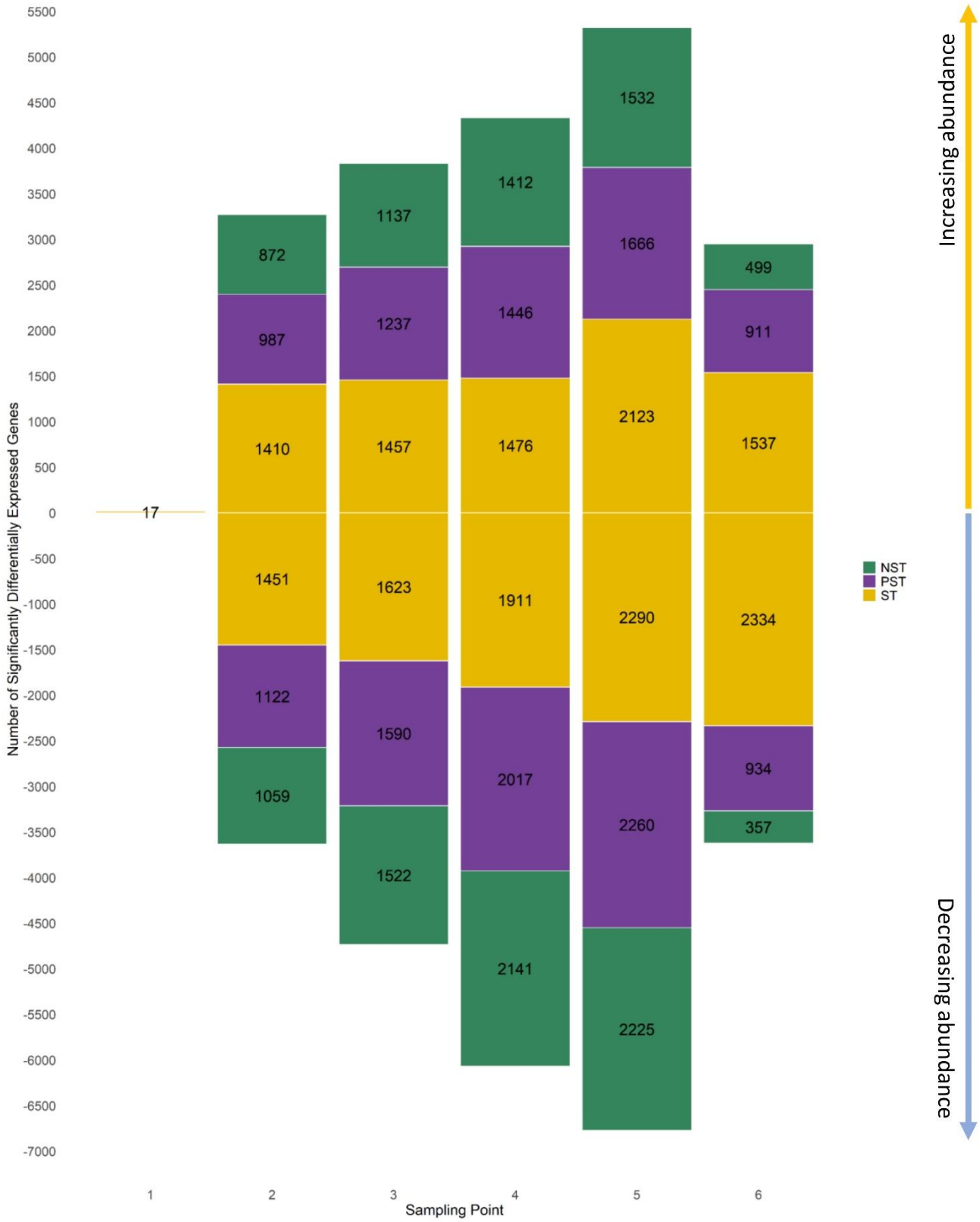

Figure 2: Significantly differentially expressed genes under well-watered conditions (sampling point 1), during water deficit (sampling point 2-5) and recovery (sampling point 6). The number of genes with a significant increase in expression is shown on the positive y axis, whereas the number of genes with a significant decrease in expression is shown on the negative y axis. Genes are considered significantly differentially expressed if they exhibit a log2 fold change value greater than 2 or less than -2, compared to control and an Exact test corrected pval <0.05.

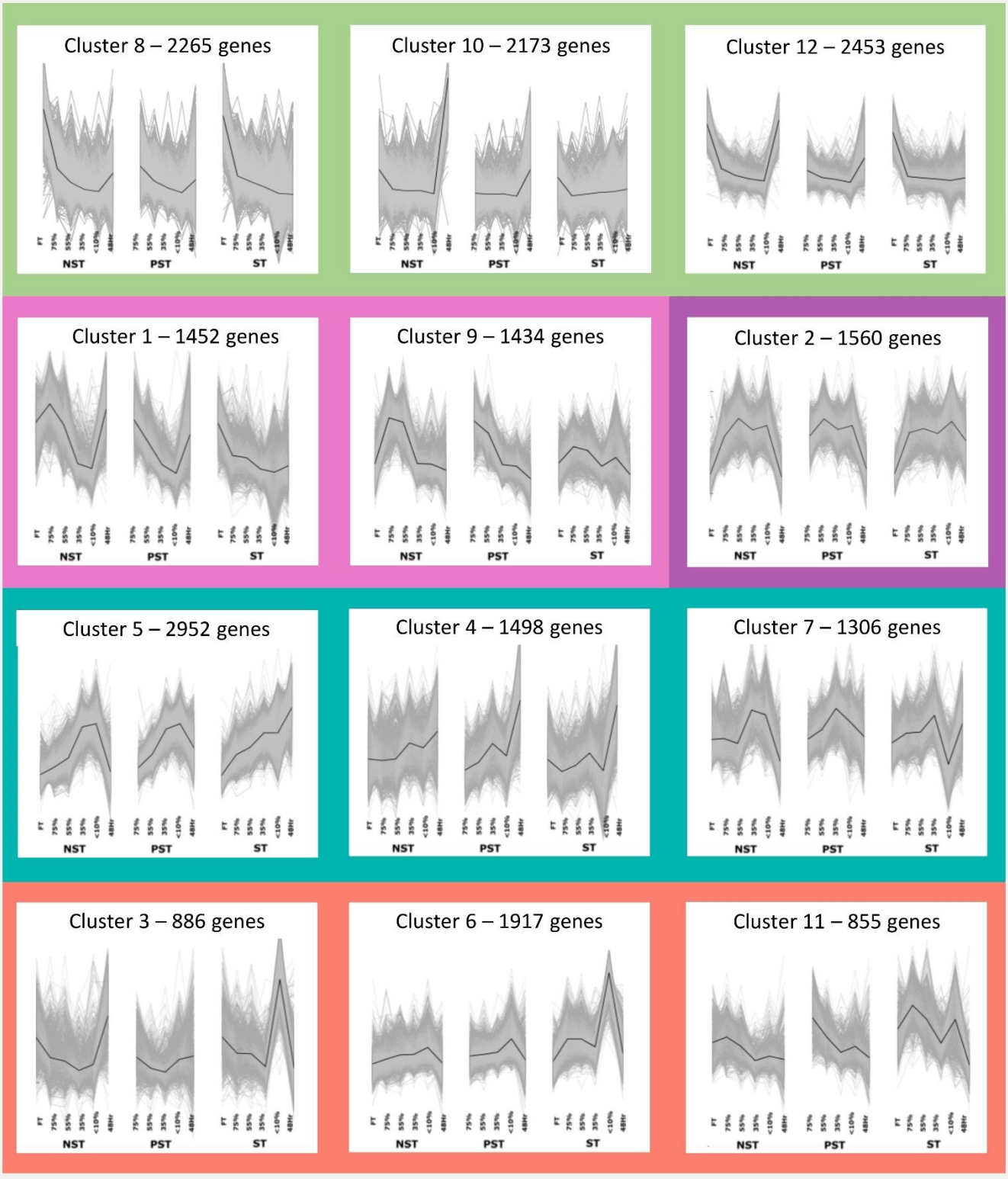

Superclusters:

- Reduced and Recovered
- Early Response
- Drought & Desiccation
- Late Response
- Late Response (ST)

Figure 3: K-Means clustered gene expression profiles. Transcript abundance (FPKM) assembled into 12 K-means clusters**.** The clusters are grouped into "superclusters" based on the response of to water deficit. Green represents those genes whose expression declines with water deficit and recovers upon rehydration. Pink represents those genes which peak in expression in NST and PST at 75% RWC. Purple represents those genes which are highly expressed in all three tissues from the onset of water stress until rehydration, when their expression declines. Genes in teal represent those who accumulate in the late stages of drying (<35% RWC) in NST and PST. Genes in orange represent those highly expressed in AD ST.

in ST (<10% RWC). Enriched gene ontologies in this cluster revealed enrichment in gene expression (ncRNA, ribosome biogenesis, transcription, translation, tRNA aminoacylation for protein translation, nuclear localisation) and transport (intracellular and golgi-to-plasmalemma) processes. **Cluster 5** contains enriched ontologies concerning proteolysis (ubiquitin-dependent protein catabolism), protein insertion into membrane, apoptosis (NAD+ ADP-ribosyltransferase activity) and spliceosomal activity. Enriched gene ontologies in **cluster 4** (expressed during desiccation in all tissue types, expression exacerbated upon RH in ST) include tetrapyrrole and porphyrin biosynthesis (porphobilinogen synthase, uroporphyrinogen decarboxylase, hydroxymethylbilane synthase and coproporphyrinogen oxidase activity), translation (tRNA aminoacylation, tRNA processing, ribosome biogenesis, tRNA guanylyltransferase activity, rRNA methyltransferase acivity) and photosynthesis (photosystem II). Enrichment of non-redundant GO-terms can be found in **supplementary Table 4.**

Drought/Desiccation elevation cluster (DEC); cluster 2

Genes in **cluster 2** are consistently elevated during dehydration and desiccation in all three tissue types and can be thought of as a consistent requirement for the DT response. Enriched gene ontologies in this cluster relate to rearrangement of cellular membranes (cytoplasmic vesicles, Golgi-associated vesicles and clathrin-coated pits), energy generation (ATP hydrolysis coupled proton transport), embryonic development and translation. Enrichment of non-redundant GO-terms can be found in **supplementary Table 5.**

ST Late response supercluster (ST-LRS); cluster 3, 6 and 11

Genes in these superclusters were highly expressed at <10% in ST in addition to being more elevated in this tissue compared to NST and PST during dehydration and desiccation. There are no significantly enriched gene ontologies in **cluster 3**. Significantly accumulated gene ontologies in **cluster 6** include breakdown of macromolecules (fatty acid oxidation, polysaccharide catabolism, coenzyme A), signalling, wounding response, transmembrane transport (amino acid transmembrane transporter activity), protein heterodimerisation and copper ion binding. Gene ontologies enriched in **cluster 11** include glycolysis (phosphopyruvate hydratase activity, phosphopyruvate hydratase complex), isoprenoid and phospholipid biosynthesis (dimethylallyl diphosphate and isopentenyl biosynthetic processes, 4-hydroxy-3-methylbut-2-en-1-yl diphosphate reductase activity, non-mevalonate pathway), pollen recognition, coenzyme metabolism, post-translational protein modification, oxidation/reduction, heme binding (iron ion and tetrapyrrole binding), ATP binding, redox (oxidoreductase activity, acting on paired donors, with incorporation or reduction of molecular oxygen), protein modification (transferase activity, transferring amino-acyl groups), protein kinase

activity and hedgehog receptor activity. Enrichment of non-redundant GO-terms can be found in **supplementary Table 5**.

Collectively, these superclusters can be thought of as encoding water-content and tissue-type specific functions within the desiccating and recovering cells. The DRS represents those genes whose expression is not required for the desiccation process, encoding such processes as photosynthesis, reproduction and progression through the cell cycle, and remains turned off in the ST upon rehydration. The ERS genes are initiated with the onset of water loss, where the plant has yet to commit to the desiccation tolerance process. As such, there is a spike in transcripts to do with energy generation and metabolism, as well as response to the stress-induced hormone ABA. The LRC is an intriguing cluster, where transcripts involved with DNA repair are accumulated in NST and PST, but supressed in ST. The DEC supercluster appears to represent those genes whose expression is integral to desiccation tolerance in all three tissues. Late responses to water deficit (ST-LRS) are experienced by all three tissue types, but are exacerbated in ST and encompass a wide range of stress responses.

Network Analysis

Network analysis is a powerful tool for identifying co-expressing hubs of genes. Each node in the network represents a gene, and each edge (line of connection) represents the level of correlated expression between individual genes. In this case, the edges are defined by the Pearson correlation coefficient, where connected nodes have a correlation coefficient of greater than 0.95. The closer the nodes, the more highly correlated their expression in this dataset. **Figure 4** shows the *X. schlechteri* transcriptome represented in this manner. Only a subset of 3206 nodes was correlated enough in terms of co-expression to yield representation in the network, nevertheless it gives a meaningful indication of the fundamental relationships between transcript expression in the different tissue types (**Fig. 4**). Colouring nodes as their corresponding K-Means cluster reveals the spatial separation between the central (**diminished** supercluster in green) as well as the peripheral (**early response** in shades of pink, **late response** in teal, **ST-late response** in orange) co-expression networks.

The colouring nodes with log2FC values relative to FT NST at 55% RWC as well as AD and RH shows how gene expression changes with RWC (**Fig. 4**). Most of the represented genes are downregulated or unchanged in their expression at 55% RWC in NST and PST, with the exception of the early response peripheral subnetwork that is upregulated. In ST at 55%, while early response genes are activated,

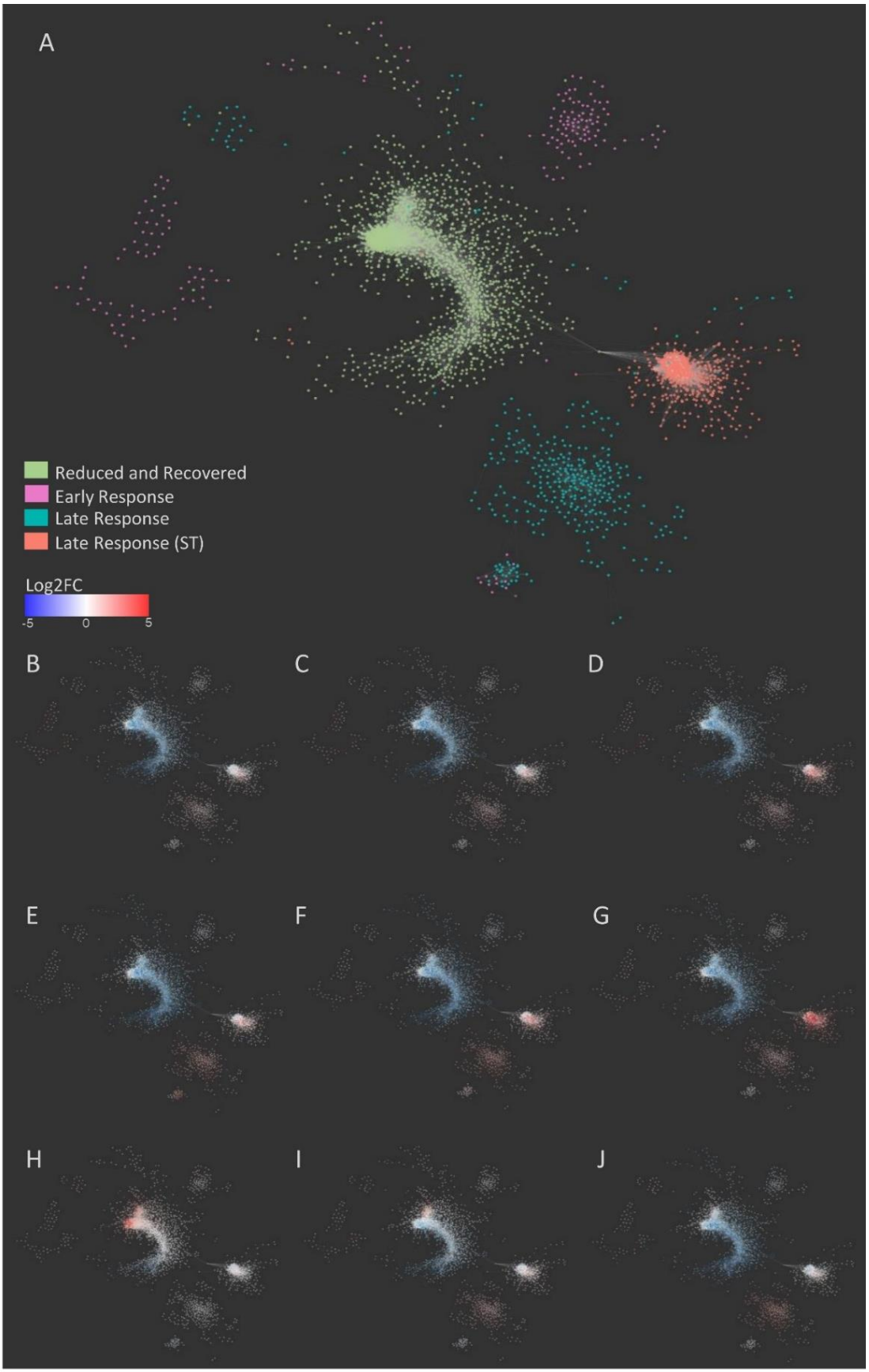

Figure 4: Subnetworks within the co-Expression network cluster according to tissue and water content. Transcripts with high degrees of correlated expression with other transcripts (Pearson correlation co-efficient ≥0.95) are represented in the network and coloured based on their corresponding K-means supercluster (A) and log2FC relative to NST FT (B-J). Panels B, C and D represent NST, PST and ST respectively at 55% RWC(NST) . Panels E, F and G represent represent NST, PST and ST respectively at AD. Panels H, I and J represent NST, PST and ST respectively at 48h post-rehydration.

expression of genes in the late response and ST-late response are also activated. As the tissues reach the air-dry state, all three tissue types show increased expression of the late response subnetwork. The ST-late response subnetwork reaches peak expression at air dry in ST and exhibits low levels of expression in NST and PST. In the early-mid stages of rehydration (48h), NST and PST have lifted the repression of formerly diminished (green in panel A) subnetwork genes and reduced expression of the late response genes. Conversely, the ST, while exhibiting diminished expression of ST-late response genes during RH, is as yet still in the desiccated state and the continued upregulation of late response genes and downregulation of diminished (green in panel A) genes reflects this.

Select transcripts associated with senescence and desiccation tolerance are emphasised in **Figure 5**. Enlarging nodes associated with photosynthesis ((▲) e.g. light harvesting complexes and electron carriers) show their clustering within the central subnetwork, indicating that their expression is mostly diminished during desiccation (**Figure 5A**). Interestingly, some photorespiration genes (◆) also cluster within the ST-late response subnetwork. Stress hormone biosynthesis genes (those to do with synthesis of ethylene, ABA, jasmonic acid and salicylic acid) are shown in **Figure 5B**. Ethylene (■) biosynthesis and jasmonic acid (▲) biosynthesis transcripts occur mostly within the ST-late response subnetwork, while ABA synthesis (◆) genes occur in this and the early and late response subnetworks. Several LEA protein genes occur in the peripheral subnetworks, with only two present in the central network indicating that their increased expression is reserved for the DT response (**Fig. 5C**). Cellular death genes are mostly confined to the ST-late response subnetwork (**Fig. 5D**), providing further evidence that this subnetwork represents the senescence response in *X. schlechteri.* Protein degradation via proteases, the proteasome and autophagy are shown in **Figure 5E**. Protein degradation seems to be divided based on hydration state with one subset of genes turned off during desiccation (green) and another most active in the late response and ST-late response subnetworks. Similarly, a subset of transcripts associated with macro- and micronutrient transport are distributed between the central and ST-late response subnetworks (**Fig. 5F**).

Desiccome

To determine whether ST deviates from NST in terms of its ability to initiate desiccation tolerance processes on the transcriptional level, and to provide cellular context for the upregulation of senescence-specific genes in the dry state, the genes displaying a significant increase in transcript abundance during desiccation in all three tissues were investigated (see **Desiccome app**). To do this, those genes in the DEC cluster were isolated, as well as those in the early (ERS) and late response (LRS) superclusters. Genes in the ERS with significant upregulation at 75% and 55% RWC relative to their expression at FT in NST were designated as **early responsive genes**.

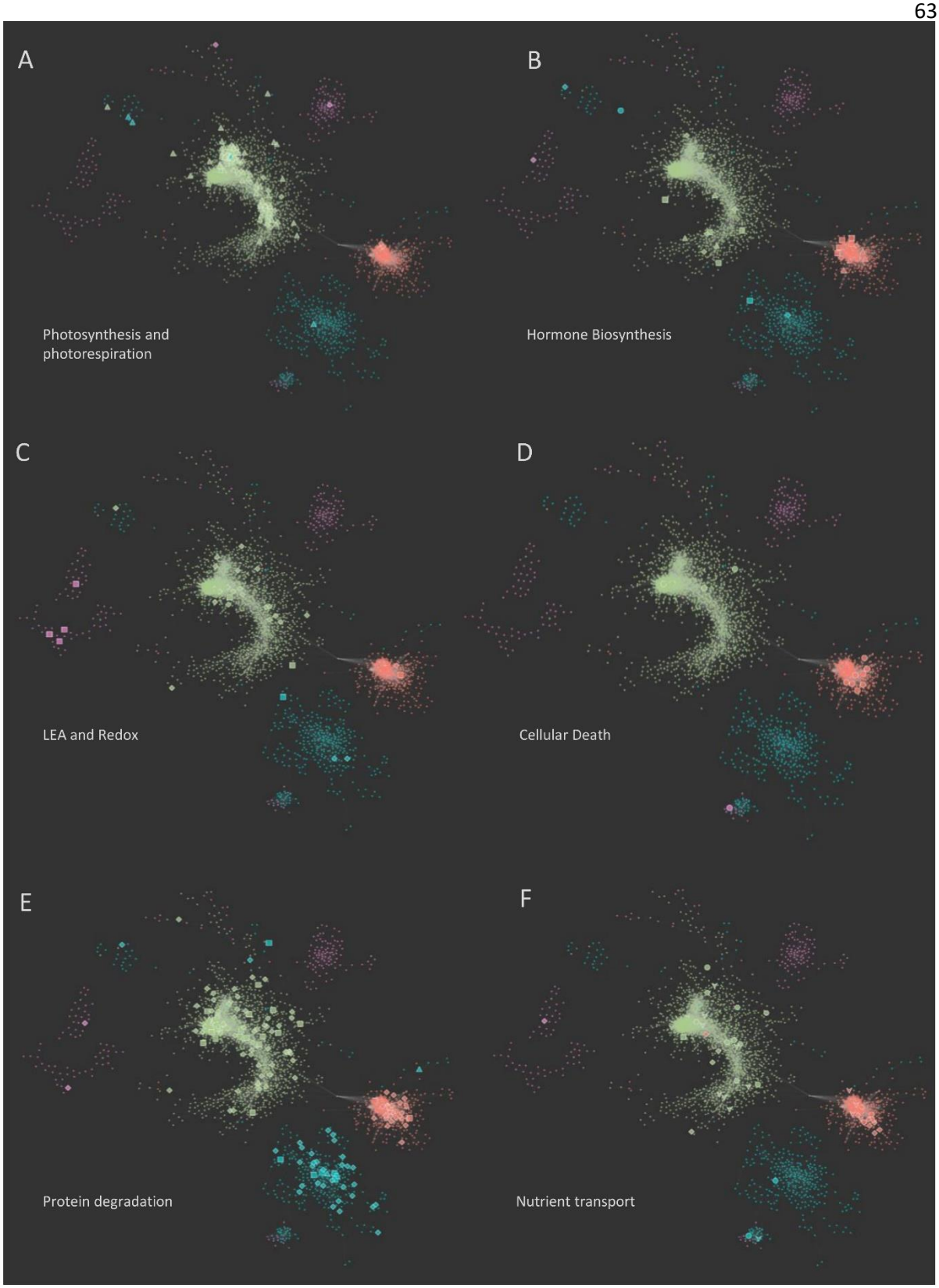

Figure 5: Fundamental processes are sub-network specific. Relevant Mercator-annotated process-specific nodes are resized for clarity. Photosynthesis (▲) and photorespiration (◆) transcripts are enlarged in panel A. Hormone biosynthesis transcripts for abscisic acid (◆) , ethylene (■), jasmonic acid (●) and salicylic acid (▲) are enlarged in panel B. Transcripts encoding LEA proteins (■) and redox homeostasis proteins (◆) are enlarged in panel C. Transcripts associated with cellular death (●) are enlarged in panel D. Transcripts associated with protein degradation (◆ general) via proteases (▲), autophagy (parallelogram ▰) and E3 ubiquitin ligase (■) are shown in panel E. Transcripts associated with transport of amino acids (◆), sugars (●), peptides (⬢) and micronutrients (nitrate, sulphate, potassium, phosphorus ▼) are shown in panel F.

Similarly, **late responsive genes** were those in the LRS with significant accumulation in 35% RWC and AD and **core responsive genes** were those significantly upregulated in the CEC with significant accumulation in 75%, 55% and 35% RWC and AD. Most of the genes identified in this manner accumulate similarly in NST, PST and ST during desiccation, with the exception of the rehydration sampling point where many genes remain elevated in ST, but not in NST or PST (see **Desiccome app**). The following text will focus on those processes considered important for desiccation tolerance (refer to **Chapter 1** for more context) in order to contextualise the senescence response in desiccated tissue.

Classical desiccation tolerance genes – LEAs, HSPs, anti-oxidants, molecular chaperones, aldose reductase

A common feature of desiccation tolerance in vegetative tissues is the increase in abundance of LEA proteins and chaperones. To determine whether ST employed the same protective mechanisms as NST on the transcriptional level, these transcripts are presented in **Figure 6**. Like NST, ST massively accumulated LEA protein transcripts during water deficit and desiccation (**Figure 6; LEA and Chaperones tab in Desiccome App**). This accumulation was evident at the first sampling point for ST – when the NST was at full turgor the ST already upregulates LEA transcript production, particularly that of the dehydrin Rab18. The same is true for those transcripts associated with redox homeostasis, such as the anti-oxidants PER1 and thioredoxin (**Anti-oxidants tab, Desiccome**). The same is also true for chaperones identified in the Desiccome, with the exception of genes encoding BAG family chaperone regulators 3 and 6, which decrease in abundance in AD ST. Two aldose reductase genes, the protein product of which has been shown to confer osmotic stress tolerance to *E.coli* (Mundree *et al.*, 2000), are highly upregulated in all three tissues (**Sugars tab, Desiccome**).

Sugar accumulation

Accumulation of stabilising and vitrifying sugars and decreasing starch is a shared response of several resurrection plants (Moyankova *et al.*, 2014; Yobi *et al.*, 2012; Farrant, Brandt, and Lindsey 2007). Transcripts encoding starch degrading alpha- and beta-amylases were increased in abundance in all three tissue types, as did sucrose synthase (**Sugars tab, Desiccome**), correlating with observed increases in sucrose in both NST and ST (**Chapter 2, fig. 5**). Genes associated with accumulation of raffinose family oligosaccharides, galactinol synthase 1, galactinol-sucrose galactosyltransferase and stachyose synthase (Yobi *et al.*, 2017) were upregulated here in all three tissues. All three components of trehalose synthesis regulation were upregulated as well: trehalose phosphate synthase (in the early phase), trehalase and trehalose phosphate phosphatase (in the late phase) (**Sugars tab, Desiccome**).

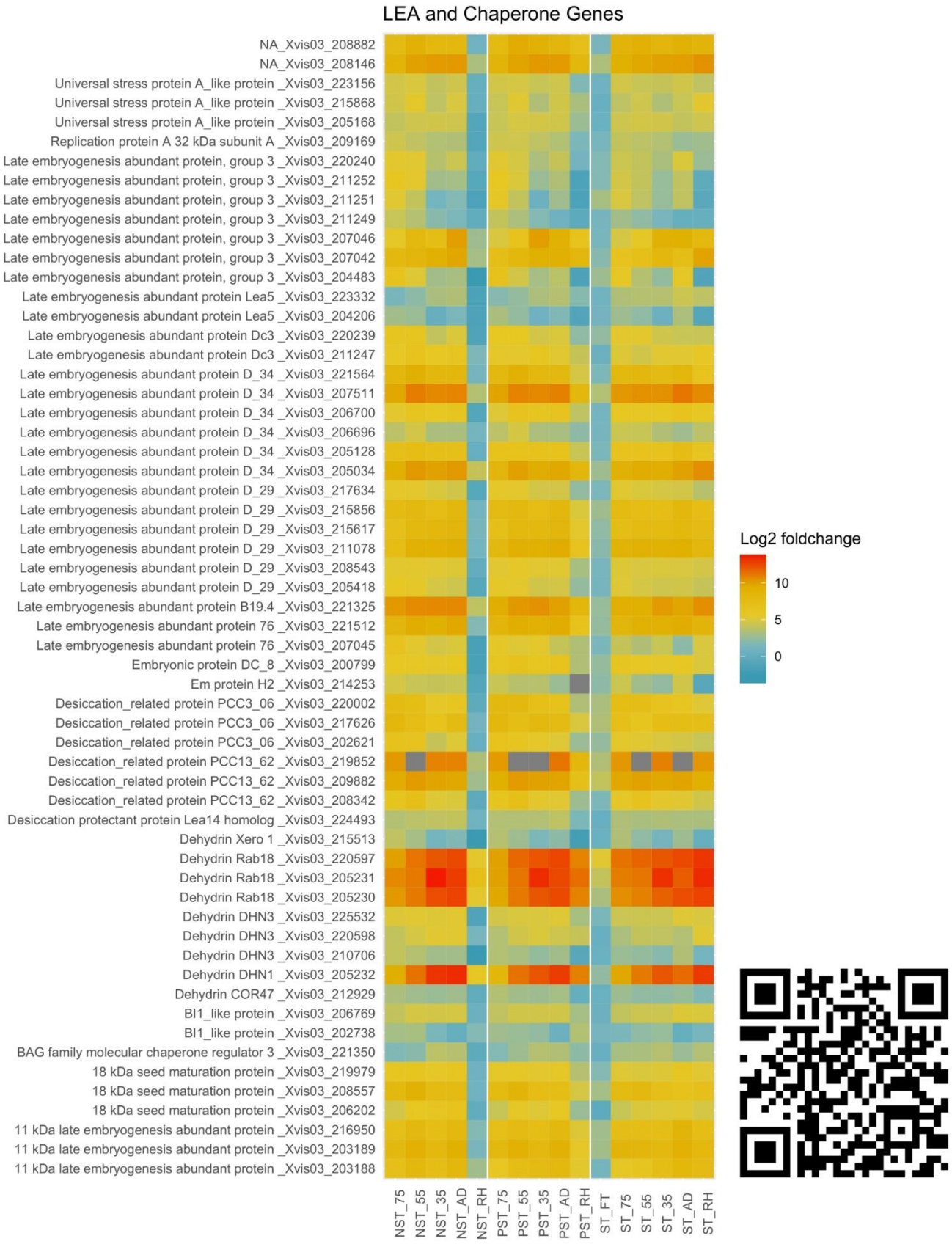

Figure 6: Desiccation-specific genes are highly accumulated in all leaf tissues of *X. schlechteri.*
Log2 fold change values relative to FT NST are shown in NST, PST and ST during water deficit and rehydration. Genes are annotated with their SwissProt annotation and genome ID. RWC values are representative of NST for easy comparison of tissues. White vertical lines separate tissue types. LEA and chaperone genes are shown here, but the full Desiccome dataset is available at the QR code or at https://astridite.shinyapps.io/XeroDesiccome/

Transcriptional Regulation and Signalling

Patterns of expression for signalling (ABA, calcium, light, G-proteins and receptor kinases) was consistent between NST and ST during desiccation (**Signalling tab, Desiccome**). ABA is a known regulator of abiotic stress and desiccation tolerance in this species (Costa *et al.*, 2017), and so the presence of ABA-responsive genes (ABI5, GEM-like protein 3 and several PP2Cs) is not unexpected. The same is true for the transcriptional regulators from a number of families including C2C2, C2H2, bZIP, AP2/EREBP, MYC, NAC, HB, HSF (**RNA-regulation of transcription tab, Desiccome**).

Energy generation

The question of energy generation during desiccation is an intriguing one, as in the absence of photosynthesis, resurrection plants still require energy (in the form of NADH and ATP) for the functioning of anti-oxidants and other considerable cellular changes undertaken to bring about quiescence. Transcriptionally, there is evidence for fermentation in the early response with an increase in Aldehyde dehydrogenase and pyruvate decarboxylase transcript abundance (**Primary metabolism tab, Desiccome**). Throughout the imposed water deficit, gluconeogenesis transcripts citrate synthase and Acetate/butyrate--CoA ligase AAE7 were upregulated, as were numerous glycolysis transcripts. Cytochrome c transcript abundance increased sharply in the early stages of water deficit and, while decreasing in the later stages, remained significantly elevated compared to FT NST. Two other electron transport protein transcripts (Putative arsenical pump-driving ATPase and ubiquinone) were also elevated during desiccation in all three tissues (**Primary metabolism tab, Desiccome**).

Altogether these transcripts appear to accumulate to similar degrees in NST, PST and ST with the exception of the rehydrated state, where they diminished in NST and to a lesser degree in PST and remained mostly unchanged in ST (with the exception of a sight accumulation at AD) (**Primary metabolism tab, Desiccome**).

Protein degradation

A number of serine, aspartate, cysteine and AAA-type protease genes were significantly upregulated during desiccation in all three tissues, as were 38 E3 family ubiquitin ligase encoding genes. The upregulation of these genes may indicate functioning of the unfolded protein response (UPR), and degradation of misfolded proteins produced during water deficit stress in the endoplasmic reticulum (Ye *et al.*, 2011; reviewed by Griffiths*, et al.*, 2014). Notably, two metacaspase 1 genes, encoding a caspase-like protein that is implicated in bringing about “superoxide-dependent cell death in a

reactive oxygen-sensitized state" (Coll *et al.*, 2017) are upregulated in the late stages of desiccation in all three tissue types (**Protein tab – Desiccome**).

Lipid metabolism

Like NST and PST, ST significantly upregulated a number of genes involved in lipid metabolism. A number of lipid-degrading enzymes, including lipases and phospholipases were significantly accumulated (**Lipids tab, Desiccome**). Lipid modifying desaturase enzyme genes are also upregulated in all three tissues, including Omega-3 fatty acid desaturase (chloroplastic), and have been proposed to play a role in drought and desiccation tolerance (reviewed in Tshabuse *et al.*, 2018). There is also a noteworthy increase in Oleosin transcript abundance in all three tissues, indicating that stabilisation of lipid bodies is a feature of DT in this species (**Lipids tab, Desiccome**).

Secondary metabolism

Transcripts associated with anthocyanin and carotenoid biosynthesis were highly differentially expressed in response to water deficit, accumulating in the early, late and core response to dehydration. Transcripts in all three tissues respond similarly, with the exception of those involved in anthocyanin biosynthesis, which remain elevated in PST and ST during rehydration, but not in NST (**Secondary metabolism tab, Desiccome**).

DNA repair

A number of DNA repair transcripts were upregulated in the late stages of desiccation in the NST and PST that are not upregulated to the same degree in ST: DNA repair protein UVH3, Deoxyribodipyrimidine photo-lyase and DNA-damage-repair/toleration protein DRT111. While these genes are upregulated in ST, they do not meet the threshold for "significance". The DNA-damage-repair/toleration protein DRT100 was, however, more highly accumulated in ST (**DNA-repair tab, Desiccome**).

Senescence Prevention

Two BI1-like (Bax inhibitor 1-like) genes were highly expressed in all three tissues during desiccation (see **Chaperones tab, Desiccome**). Bax1 has been proposed to attenuate PCD in *A.thaliana* roots (Duan *et al.*, 2010) and interact with ATG6 (autophagy-associated gene 6) to regulate autophagy and PCD (Xu *et al.*, 2017).

***X. schlechteri* Senescome**

Based on the differential expression analysis and K-means clustering result, the transcripts differentially accumulated at AD ST relative to AD NST are good candidates for illuminating the

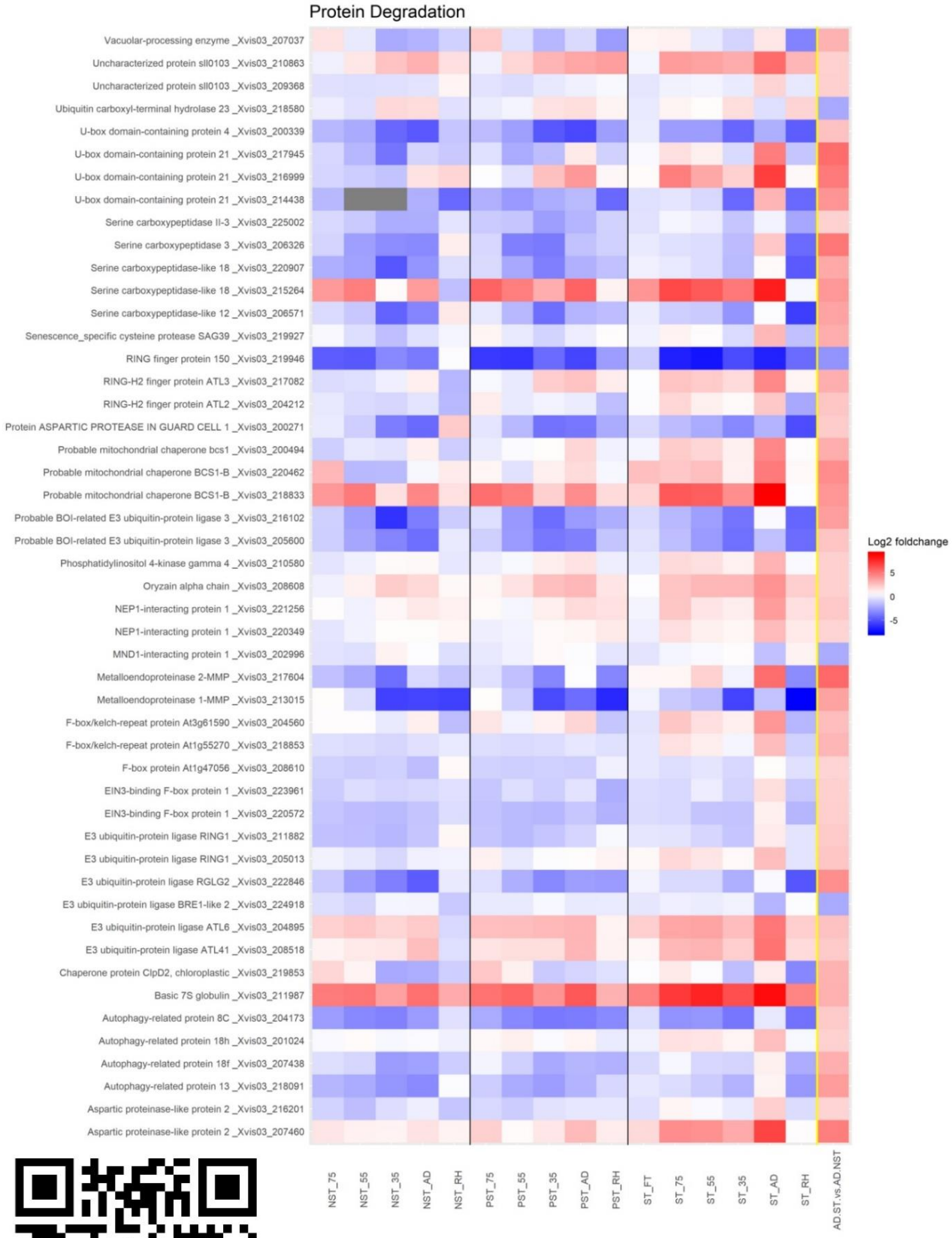

Figure 7: Desiccation-driven senescence occurs below 35% RWC in apical ST. Log2 fold change values relative to FT NST are shown in NST, PST and ST during water deficit and rehydration. Genes are annotated with their SwissProt annotation and genome ID. RWC values are representative of NST values. White vertical lines separate tissue types. The right-most column represents gene expression in AD ST relative to AD NST. The full Senescome dataset is available at https://astridite.shinyapps.io/XeroSenescome/

senescence phenomenon. Interestingly, in the air-dry (AD) state, where all tissues were at the same RWC, was where a considerable peak expression occurred in ST. **Figure 7** and the **Senescome App** report DEGs found to be significantly accumulated and diminished in AD ST relative to AD NST. Comparing within the AD sampling point enables dissection of senescence-related genes away from desiccation-related genes, which are presumably highly expressed in both tissues (based on the observation in **Fig. 3, cluster 2**), as opposed to a comparison to FT NST, which would conflate senescence and DT processes. Processes of interest to senescence are reported in the following text.

Cell death

The Mercator-identified cell death genes identified in this comparison fall exclusively within the DST supercluster, except for Apoptosis-inducing factor homolog B, which peaks in expression in NST at 75% RWC (**Fig. 3, cluster 9**). The remaining transcripts accumulate late in the desiccation timeline, and to a higher degree in ST. Transcripts encoding apoptosis-inducing factor homologues A and B, Yellow Leaf Specific (YLS9) proteins, accelerated cell death 11 (ACD11) and hypersensitive-induced response protein 1 are all highly expressed in response to desiccation in ST (**Cell tab, Senescome**).

Signalling: hormones

All major plant hormones are represented in the up- and down-regulated transcripts categorised under hormone metabolism (**Senescome**). One transcript involving the synthesis of ABA (9_cis_epoxycarotenoid dioxygenase 1) was upregulated in AD ST and two were down-regulated (Zeaxanthin epoxidase and Carotenoid cleavage dioxygenase 7). An ABA-induced cell-death mediator HVA22 (Guo and Ho, 2008) was also upregulated here. The auxin-responsive SAUR32, upregulated in senescing *Nicotiana tobacum* leaves (Zhao *et al.*, 2018), was upregulated in AD ST. As are two auxin-responsive probable aldo-keto reductases, theorised to play a role in detoxifying stress-induced formation of toxic aldehydes and ketones in *A. thaliana* (Simpson *et al.*, 2009). Expression of ethylene-responsive TF 4 was also significantly upregulated in AD ST and is a known repressor of GCC-box stress genes in *A.thaliana* (Fujimoto *et al.*, 2000). The ethylene-responsive N-acetyltransferase HLS1-like is also upregulated during senescence in *A.thaliana* (Buchanan-Wollaston *et al.*, 2005) and plays a role in mediating sugar and auxin signalling (Liao *et al.*, 2016). Three transcripts encoding 1-aminocyclopropane-1-carboxylate oxidase, an ethylene biosynthesis enzyme (Zhang *et al.*, 1995), were highly upregulated in AD ST. The transcript encoding a gibberellin deactivating enzyme Gibberellin 2-beta-dioxygenase is upregulated in AD ST, indicating that gibberellin-responsive gene expression is tempered (Thomas, Phillips, and Hedden, 1999). Jasmonate synthesis is encoded in AD ST by the transcripts 12-oxophytodienoate reductase 1 and Allene oxide synthase 1 and 2, role-players in oxylipin metabolism. The role of the upregulated lipoxygenases (Linoleate 9S-lipoxygenase 6 and

Putative lipoxygenase 5) is unclear, however they too participate in oxylipin metabolism (Bannenberg *et al.*, 2009), with the latter also upregulated during senescence in *A. thaliana* (Z. Li *et al.*, 2012). Two salicylic acid-binding protein transcripts were highly expressed in AD ST. *N. tabacum* homologues to these proteins have been shown to have lipase activity (Kumar and Klessig, 2003) (see **Signalling-Hormones tab, Senescome app**).

Signalling: kinases and phosphatases

A number of senescence-associated kinases and phosphatases (Buchanan-Wollaston *et al.*, 2005) are upregulated in the AD ST, including two PP2Cs (12 & 15), CBL-interacting protein kinase 6 and L-type lectin-domain containing receptor kinase S.5 (**Signalling-kinases tab, Senescome**). An additional two PP2Cs (9 & 75) were upregulated at AD and are implicated in abscisic acid metabolism (see **hormone metabolism – abscisic acid tab, Senescome**), the former also differentially expressed in *A. thaliana* during senescence (Buchanan-Wollaston *et al.*, 2005). The significant increase in expression of OXI1 (OXIDATIVE SIGNAL-INDUCIBLE 1) is notable – this serine/threonine receptor kinase is involved in oxidative burst signalling and various stress responses in *A. thaliana* (Rentel *et al.*, 2004). Except for the kinases and phosphatases described above, those found upregulated in AD ST were largely uncharacterised in desiccation sensitive species (**Signalling-kinases tab, Senscome**).

Signalling: transcription factors

A number of transcription factor (TF) families associated with senescence, namely ERF, MYB, NAC and WRKY (Balazadeh, Riaño-Pachón, and Mueller-Roeber, 2008), were significantly differentially expressed at <10% RWC (**RNA-regulation of transcription tab, Senescome**). The most highly represented TF family is WRKY, with 16 transcripts encoding WRKY TFs, including WRKY6 and WRKY42 which have been implicated in senescence processes (Buchanan-Wollaston *et al.*, 2005; Z. Li *et al.*, 2012). A large proportion of MYB and MYB-related protein genes are also represented here, with three transcripts shown to be transcribed during senescence in *A. thaliana* – MYB108, At1g4600 and Myb-related protein R (Buchanan-Wollaston *et al.*, 2005). Senescence-implicated ethylene-responsive TFs ERF and RAP2-4 (Buchanan-Wollaston *et al.*, 2005; Penfold and Buchanan-Wollaston, 2014) were upregulated as well – ERF053 plays an additional role in abiotic stress tolerance in *A.thaliana* (Hsieh, Cheng, and Lin, 2013). Zinc finger ZAT proteins, of which ZAT10 and ZAT12 have been shown to be responsive to abiotic stress (Mittler *et al.*, 2006; Davletova *et al.*, 2005) were highly differentially expressed in AD ST. The TF JUNGBRUNNEN1, highly accumulated in ST throughout DT (**Fig.3, cluster 11**), has been shown to be a stress-responsive promoter of phenylpropanoid biosynthesis and a longevity regulator in *A.thaliana* (Wu *et al.*, 2012). Similarly, Mediator of RNA polymerase II transcription subunit 33A was upregulated in the senescome and is a regulator of phenylpropanoid

biosynthesis (Bonawitz *et al.*, 2012). Transcription factors with diminished relative abundance in AD ST include members of the PHD finger, Homeobox (HB), heat shock factor, FHA and MYB families (**RNA-regulation of transcription tab, Senescome**).

Chromatin remodelling

A number of chromatin-remodelling factors and DNA methyltransferases (Zhao *et al.*, 2018) are also present in the data set, indicating that NST potentially conducts some epigenetic regulation in the dry state while ST does not (**Senescome – DNA synthesis/repair**). Chromatin remodelling complex protein SYD is responsible for chromatin remodelling during stress for easy access of stress-inducible genes (Walley *et al.*, 2008) and was down-regulated in AD ST. The same trend is true for three transcripts annotated as Protein DEK, a protein responsible for supercoiling DNA (Waidmann *et al.*, 2014) and Topoisomerase 1, the canonical DNA remodeller (**Senescome – DNA synthesis/repair**).

Macromolecular degradation: proteins

Protein degradation is favoured over protein synthesis in the ST at AD, with 40 transcripts indicating various protein degrading mechanisms significantly differentially accumulated (**Protein tab, Senescome**). Of these mechanisms, those involved with proteasomal degradation were most abundant. A number of aspartate, serine and metallo-proteases were significantly differentially accumulated in ST, these too being transcribed during senescence in Barley and *A. thaliana* (Parrott *et al.*, 2007; Golldack, Popova, and Dietz, 2002). A cysteine protease, vacuolar processing enzyme (VPE), has been shown to act during senescence (Hatsugai *et al.*, 2015). Hatsugai *et al.*(2015) proposed that VPE mediates activation of other vacuolar hydrolytic enzymes, leading to degradation of the vacuole and initiation of proteolysis and PCD. Of the protein degradation DEGs, four are members of the autophagosome complex: autophagy-related protein 8C, 13, 18f and 18h transcripts, indicating that the cells might be triggering autophagic cellular death (**Protein tab, Senescome**). This corresponds with the observation of macroautophagy in ST (**Chapter 2, fig. 4**), indicating that this process might be triggered near to or in the airdry state.

While numerous E3-RING proteasome transcripts were significantly differentially accumulated in ST, indicating that protein degradation via the proteasome may be occurring, three were relatively diminished. As the E3 family contains over 1400 members (Mazzucotelli *et al.*, 2006), it is reasonable to expect some conflicting differential expression of these transcripts.

Macromolecular degradation: nucleic acids

A number of DNA and RNA nucleases were upregulated in AD ST including an organelle-specific nuclease (DPD1) and ribonucleases (**DNA tab, Senescome**). Interestingly, AD ST highly accumulates

Endonuclease 1 transcripts, a senescence-specific nuclease that degrades both DNA and RNA in *A. thaliana* (Perez-Amador *et al.*, 2000) during the terminal stages of leaf senescence (Farage-Barhom *et al.*, 2008). It functions at low pH (5.5) and its DNA and RNA nuclease activity is increased with addition of calcium and zinc ions *in vitro* (Lesniewicz *et al.*, 2013). Additionally, structural maintenance of chromosomes proteins 1 and 3 (**cell- cell division tab, Senescome**) are diminished in AD ST, indicating that the structural integrity of chromatin is not prioritised in AD ST.

Metabolism: amino acids

Coinciding with the senescence-associated proteolysis is release of amino acids and peptides (Havé *et al*., 2017). The fate of these small molecules is thus of interest in the characterisation of senescence. The only DEGs to do with amino acid degradation were two upregulated methionine gamma-lyases (**Amino Acids tab, Senescome**). These enzymes catalyse the conversion of methionine to 2-oxobutyrate (an isoleucine or acetyl-CoA precursor), ammonium and methanethiol in the cytoplasm. An alternative fate for methionine is presented by the upregulation of four S-adenosylmethionine (SAM) synthase transcripts, which encode the enzyme responsible for catalysing the first step in ethylene biosynthesis: the conversion of methionine to SAM. Further evidence for the potential biosynthesis of ethylene from methionine comes from the upregulation of a 1-aminocyclopropane-1-carboxylate (ACC) synthase transcript (catalyses the conversion of SAM to ACC) and two ACC oxidase transcripts which catalyse the conversion of ACC to ethylene (Houben and Van de Poel, 2019). Aromatic amino acid synthesis transcripts, particularly those encoding phenylalanine biosynthesis (5-methyltetrahydropteroyl-triglutamate--homocysteine methyltransferase 2, Arogenate dehydratase/prephenate dehydratase 6 and Arogenate dehydratase 3) were upregulated in AD ST. Asparagine synthesis enzyme transcripts were upregulated in AD ST as well: Aspartate aminotransferase converts oxaloacetate into aspartate, and asparagine synthetase converts aspartate (and glutamine) into asparagine (Lea *et al.*, 2007). Bifunctional aspartate aminotransferase and glutamate/aspartate-prephenate aminotransferase, also upregulated in AD ST, catalyses the reversible conversion between 2-oxoglutarate and aspartate on one side of the equation and glutamate and oxaloacetate on the other (Graindorge *et al.*, 2010). There is additional upregulation of serine and glycine biosynthesis transcripts in AD ST (**Amino Acids tab, Senescome**), corresponding with elevation of these compounds (and asparagine) in AD ST (**Chapter 2, fig. 5**).

Metabolism: lipids

A number of lipid degrading enzymes were highly upregulated in the Senescome, including phospholipases A1, C1 and D (**Lipids tab, Senescome**), all of which have been shown to accumulate in senescent *A. thaliana* leaves (Schmid *et al.*, 2005; Van Der Graaff *et al.*, 2006; Breeze *et al.*, 2011).

Synthesis of phosphatidic acid, an important abiotic stress signalling lipid, is driven by the sequential action of phospholipases C or Dp1 and diacylglycerol kinase, all upregulated in AD ST. Degradation of lipids may also be used to drive central metabolism for generation of NADH and ATP (Troncoso-Ponce *et al.*, 2013) (**Lipids tab, Senescome**). The appearance of four transcripts binned under sphingolipid biosynthesis is also noteworthy, as this lipid family has been proposed as a regulator of apoptosis-like PCD in *A.thaliana* (Alden *et al.*, 2011) (**Lipids tab, Senescome**).

Metabolism: energy generation via alternate pathways and electron transport

The question of how a desiccating and senescent cell may be generating enough energy to undergo considerable molecular changes and possibly redistribute nutrients is an interesting one. For a start, transcripts encoding glycolysis (Phosphoenolpyruvate carboxykinase) and TCA cycle enzymes were upregulated in AD ST – these genes being expressed at FPKM values close to or higher than FT NST, representing the only peak in their expression during desiccation in ST (**Primary metabolism tab, Senescome**). This correlates with the observed increased accumulation of TCA cycle compounds malic, succinic and citric acid in AD ST relative to AD NST (**Chapter 2, fig.5**). There was also an increase in fermentation enzyme transcripts (L-lactate hydrogenase and aldehyde dehydrogenase) in all three tissues at AD, but particularly in AD ST, indicating that fermentation may be employed to generate NADH. Another potential source of NADH might be glutamate dehydrogenase 2, upregulated in AD ST, which catalyses the conversion of glutamate and NAD^+ to 2-oxoglutarate and NADH (The UniProt consortium, 2019). Similarly, another nitrogen assimilating enzyme with increased transcript abundance in AD ST, nitrate reductase, catalyses the conversion of nitrite and NAD^+ to NADH and nitrate in the cytoplasm. Alcohol dehydrogenase converts primary alcohols and NAD^+ to an aldehyde and NADPH. The enzyme 2-alkenal reductase converts alkanals into alk-2-enals with high specificity for $NADP^+$ and the release of NADPH (The UniProt consortium, 2019). This suggests that numerous sources for NAD(P)H generation exist despite the shutdown of photosynthesis and the Calvin cycle. The potential fate of this NAD(P)H is intriguing. The upregulation in AD ST of ubiquinol oxidase 1a (AOX), electron transfer flavoprotein subunit alpha and NADPH:quinone oxidoreductase transcripts suggests that mitochondrial electron transport is somewhat functional. If AOX is translated, the protein competes for electron flow, suggesting that some electrons may be terminating at this electron acceptor (after passing through complexes I and II and generating some proton flow into the inner mitochondrial space) rather than proceeding through complex III towards complex IV via cytochrome C. The termination of electron flow at AOX rather than complex IV dramatically reduces the ATP yield than if the entire pathway is functional (Vanlerberghe, 2013). There also seems to be some evidence that electron transport is still functioning in the desiccated state, as ATP synthase transcript abundance overall is not significantly different during desiccation to that at FT in NST

(**Primary metabolism tab, Desiccome**) and there appears to be an increase in cytochrome c abundance in all tissues during all stages of water deficit (**see Primary metabolism tab, Senescome**).

Secondary Metabolism

Phenylpropanoid biosynthesis transcripts were notably enriched in AD ST (**Secondary metabolism tab, Senescome**). Phenylalanine ammonia lyase (four homologues with increased transcript abundance) catalyses the conversion of phenylalanine to cinnamate, representing the first committed step in phenylpropanoid biosynthesis. Polyphenol oxidase, proposed to be a vital component of the desiccation-induced anti-oxidant menagerie (Jiang *et al.*, 2007; Veljovic-Jovanovic, Kukavica, and Navari-Izzo, 2008), was upregulated in AD NST and PST and extensively transcribed in AD ST. Polyphenol oxidase is responsible for the conversion of coumaric acid to quinic acid (Bibhuti Bhusan Mishra, 2016), a compound that is significantly differentially accumulated in ST during drying and desiccation (**Chapter 2, fig. 5**). Synthesis of phenylpropanoids, including chlorogenic acid (also highly accumulated in ST relative to NST), has been reported in senescent and drought-stressed tobacco (Torras-Claveria *et al.*, 2012). Caffeic acid, also highly accumulated in ST, is the substrate for Caffeic acid *O*-methyltransferase 1, (with increased transcript abundance in AD ST) and is responsible for the first step of lignin and flavonoid biosynthesis (Do *et al.*, 2007) (**Secondary metabolism tab, Senescome**).

A surprising enrichment of secondary metabolite genes to do with plant cell wall biosynthesis is present in the Senescome (**Cell wall tab, Senescome**). Four cellulose synthesis genes (Endoglucanase 9, Cellulose synthase-like protein E6, Probable cellulose synthase A catalytic subunit 3 [UDP-forming] and COBRA-like protein 7) are upregulated in AD ST relative to both AD NST and FT NST. The same is true for a number of hemicellulose synthesis and cell wall precursor synthesis genes, such as UDP-glucose. UDP-glucuronate:xylan alpha-glucuronosyltransferase 2 joins these precursors to form xylan (Mortimer *et al.*, 2010), but an alternative end-point for these precursors might be the synthesis of sucrose via sucrose synthase or raffinose family oligosaccharides (Yobi *et al.*, 2017).

Transport: nitrogen

Nutrient transporters are an important component of the senescence response, being responsible for distribution of the breakdown products of various metabolisms to viable (sink) tissues (Havé *et al*., 2017). Redistribution of nitrogen from source to sink tissues is crucial and is achieved by cleavage of proteins and nitrogenous compounds into amino acids, peptides and nitrate that are easily transportable. A tetra- and penta-peptide transporter, Oligopeptide transporter 7, was upregulated

in AD ST ST (**Transport-amino acids tab, Senescome**) and may play a role in transporting short peptides from senescing cells. Amino acid transporter cationic amino acid transporter 1 (CAT1) is responsible for transport of a broad range of amino acids into and out of cells in *A.thaliana* (Su, Frommer, and Ludewig 2004) and was highly expressed in AD ST. Proline transporter 2 is highly expressed in tissues with increased proline content and is responsible for amino acid retrieval from the apoplast (Lehmann *et al.*, 2011), hence, is a potential transporter of proline from ST to NST/PST. Interestingly, a cystinosin homologue is also upregulated in AD ST. Cystinosin is a transporter responsible for transporting cystine (cysteine-dimers) out of lysosomes after protein hydrolysis and has been described in mammalian cell lines and yeast, but not in plants (Kalatzis *et al.*, 2001). How released amino acids are accepted by sink cells is an important question to ask. The transcript encoding amino acid permease 1 (a permease involved with amino acid transport **into** cells) was highly accumulated in NST in the late stages of water deficit (see **Transport tab - Desiccome**), to a lesser degree in PST and not differentially in ST. Thus, uptake via this transporter could be a mechanism for apoplastic and phloem-loaded transport of amino acids from ST into NST as proposed by Dinkeloo *et al.* (2018). Nitrate transport is another mechanism for mobilisation of nitrogen. A transporter responsible for export of nitrate into xylem, Protein NRT1/ PTR FAMILY 7.3 (Lin *et al.*, 2008), was highly expressed in AD ST, but not in PST nor NST. Protein NRT1/ PTR FAMILY 4.6, a nitrate bidirectional transporter, was also highly expressed in ST relative to the other tissues and has been shown to also transport ABA (Corratgé-Faillie and Lacombe, 2017). A potential mechanism for nitrate uptake in NST and PST is via Protein NRT1/ PTR FAMILY 6.2, a nitrate transporter (Corratgé-Faillie and Lacombe, 2017) highly expressed in AD NST and PST (see **Transport tab** - **Desiccome**), but not in ST. Another potential mechanism comes from the upregulation of Urea-proton symporter DUR3 in AD ST, which has been shown to regulate transport of urea from the apoplast to phloem in *A. thaliana* (Bohner *et al.*, 2015) (see **Transport-amino acids/misc tab, Senescome**)

Transport: carbon

A number of transcripts associated with sugar transport significantly accumulated in AD ST. Sugar transport proteins 7 and 13 are sugar/proton symporters that are involved in the uptake of apoplastic hexoses in response to biotic stress (Lemonnier *et al.*, 2014). Two UDP-galactose transporters were also upregulated in ST and might be implicated in transport of cell wall precursors, which may be utilised to drive RFO synthesis (Yobi *et al.*, 2017) in surviving tissues. Two probable sugar phosphate translocators (At3g11320 and At5g25400) also significantly accumulated in all three tissue types, indicating that sugars may also be transported in their phosphorylated form for delivery of both carbon and phosphate to sink tissues. A fatty acid export protein 4 (Li *et al.*, 2015), highly upregulated

in ST during rehydration (see **Transport - Desiccome**), might be utilised to transport fatty acids to viable tissues during recovery (**Transport-sugars/lipids/misc tab, Senescome**).

Transport: phosphorous

Mobilised phosphate comes from phospholipids, nucleotides, phosphorylated molecules and specifically phosphorylated ribosomal RNA (reviewed in Shane *et al.*, 2014). Phospholipids are targeted by phospholipase C and D, both of which increased in expression in AD ST (**Transport-phosphorus tab, Senescome**), potentially releasing phosphates for redistribution. Shane *et al.* (2014) proposed that extracellular ribonucleases may facilitate phosphate remobilisation during senescence by cleaving leaked RNA in the apoplast, releasing free phosphorylated nucleotides suitable for uptake by surrounding cells and sink tissues. In *X. schlechteri*, extracellular ribonuclease LE was accumulated in all three tissue types during desiccation and remained elevated in all three upon rehydration (a significant rarity for this dataset – see **Desiccome app**). The nucleotide transporter purine-uracil permease, which was expressed to a greater degree in NST and PST than ST during desiccation, indicating that nucleotide transport may occur apoplastically from ST to surviving tissues via this mechanism. Cells of the ST also exhibit greater expression of purple acid phosphatases, which have been implicated in cleaving phosphates from phosphorylated molecules for the purposes of storage and/or redistribution (Shane *et al.*, 2014) (**Transport-phosphorus/misc tab, Senescome**).

Transport: other

Transcripts encoding four potassium transporters (Potassium transporter 5, Probable potassium transporter 17, two-pore potassium channel 5 and potassium channel AKT2) were significantly accumulated in AD ST, as were two sulphate transporters (Sulfate transporter 3.1 and Probable sulfate transporter 3.5) (**Transport-potassium/misc/metals tab, Senescome**). A senescence associated zinc transporter 5 was also upregulated in AD ST, as reported in senescent *A. thaliana* (Buchanan-Wollaston *et al.*, 2005). Molybdate transporter 2, a senescence-specific molybdate transporter, was highly expressed in ST and not NST or PST and is implicated in high efficiency molybdate transport (Gasber *et al.*, 2011). Conversely, expression of cadmium/zinc-transporting ATPase HMA2, a root-to-shoot zinc transporter was down-regulated in AD ST, indicating its transition from sink to source of this metal.

Intercellular communication

Two transcripts encoding lysine/histidine transporter 1 were greatly upregulated in ST at AD. This gene encodes a broad specificity amino acid transporter, which also functions as an apoplastic ACC

(aqueous ethylene precursor) transporter in *A.thaliana* (Shin *et al.*, 2015). Signalling via ACC might be a way for NST and PST to communicate the need for sacrifice and redistribution of nutrients from ST. Alternatively, it could be a way for the cells of ST to communicate with one another and coordinate their demise. Similarly, GABA transporter 1 was highly expressed in AD ST (and was also increased in abundance in AD NST and PST relative to FT NST). It is an important GABA uptake protein that was shown to have high expression in senescent *A. thaliana*, which coincided with increased levels of GABA in the leaf tissues (Meyer *et al.*, 2006) (**Transport-amino acids tab, Senescome**).

Regulation of the senescence co-expression subnetwork

The AD Senescome co-expression subnetwork was interrogated to identify putative regulators of senescence. Upstream regions of up to 1kb were obtained for this subset of genes (565 nodes) and subjected to DREME analysis to discover enriched transcription factor binding motifs in these sequences relative to the full network (3206 nodes). Two regions were significantly enriched, a GTCAAHS site and a CRCGTW site (**Fig. 8**). The upstream regions either contained the GTCAAHS site or both, but never the CRGTW site only. It is important to note that none of the other network superclusters contained significant differentially enriched motifs through this method – this is the only subnetwork that displayed significant motif enrichment. TomTom was utilised to identify potential motif-binding transcription factors in a plant transcription factor database (Jaspar plants 2018 non-redundant sites), the results of which are available in **supplementary Tables 6 and 7**. The majority of homologues for these genes are in the **ST-LRS** supercluster. Of the GTCAAHS motif-binding TFs, 15 are significantly upregulated in the Senescome: four WRKY23, one WRKY57, one WRKY6, one WRKY70, two WRKY71 and three WRKY75 homologues (**Fig. 8**). Of the CRCGTW motif binding TF homologues, 9 were present in the ST-late response supercluster, but only one was significantly upregulated in the Senescome: a BHLH13 homologue (**supplementary Table 7**). Coloured genes, based on the presence of these motifs in their upstream regions, show how prolific their presence was (**Fig. 8 inset**) and thus how many genes in the senescence subnetwork are potentially under WRKY transcription factor control. All WRKY TFs present in the network contain one or both domains, indicating that their expression is self-regulated (**Fig. 8**). **Figure 9** illustrates how most of the transcription factors in the senescence subnetwork contain these motifs in their upstream region, suggesting that expression of closely clustered senescence genes is directly and/or indirectly modulated by WRKY TFs.

A potential mechanism for the control of the senescence-specific subnetwork is detailed in **Figure 10**. After it was identified that a great number of TFs in the subnetwork are potentially under control of the WRKY transcription factors (**Fig. 8 and 9**), the upstream regions of WRKY TFs in the network were investigated to a higher degree. It was found that all seven WRKY TFs in the network possessed an

ERF096 and/or ERF1B binding site in their upstream region. This ERF096 binding site was also found upstream of the ACC oxidase and ACC synthase (ethylene biosynthesis) genes and upstream of ERF096 itself. ERF096 contained an additional upstream motif that is a binding site for MYB3, which was also highly upregulated within the subnetwork. The ACC oxidase, MYB3 and all seven WRKYs genes all contained a WRKY binding motif in their upstream regions, indicating a potential cyclical regulatory nature within this tightly associated subnetwork. Additionally, the ABA synthesis enzyme 9-cis-epoxycarotenoid dioxygenase NCED3 (chloroplastic) contained both motifs in its upstream region, indicating that ABA synthesis in late stages of drying may be driven by the action of this transcriptional regulatory network.

The activation of MYB3 and WRKY6 might occur via action of MAPK6, a known regulator of abiotic stress responses and actor in senescence (Chai *et al.*, 2014). The activity of signalling kinases is not necessarily reliant on the abundance of transcript encoding them, as their regulation occurs on the protein level. Thus, speculating on potential mechanisms without protein information should be performed with caution. The combination of osmotic, drought and oxidative stress on the AD leaf could imply cross-talk between signalling pathways and potential amplification of specific mechanisms. In *A. thaliana*, these stressors result in the accumulation of calcium ions within the cell, ROS and phosphatidic acid accumulation (Reviewed in detail by Smékalová *et al.*, 2014). The upregulation of anti-oxidant and calcium binding protein genes, as well as the upregulation of phosphatidic acid synthesis genes (**Signalling-calcium and Lipids tab, Senescome**) indicate that similar stimuli and responses are at play in *X. schlechteri.* A number of calcium signalling transcripts were found in the senescence subnetwork including calmodulin-like (CML) proteins (CML27, 30, 31, and 35), calcium dependent protein kinases and a receptor-like kinase (RLPK At5g7070) (**Fig. 10C**). Calmodulin1 has been shown to signal ROS production in response to ABA in *A.thaliana,* as well as function in receptor-like kinase 1 (RLK1) mediated senescence (Dai *et al.*, 2018).

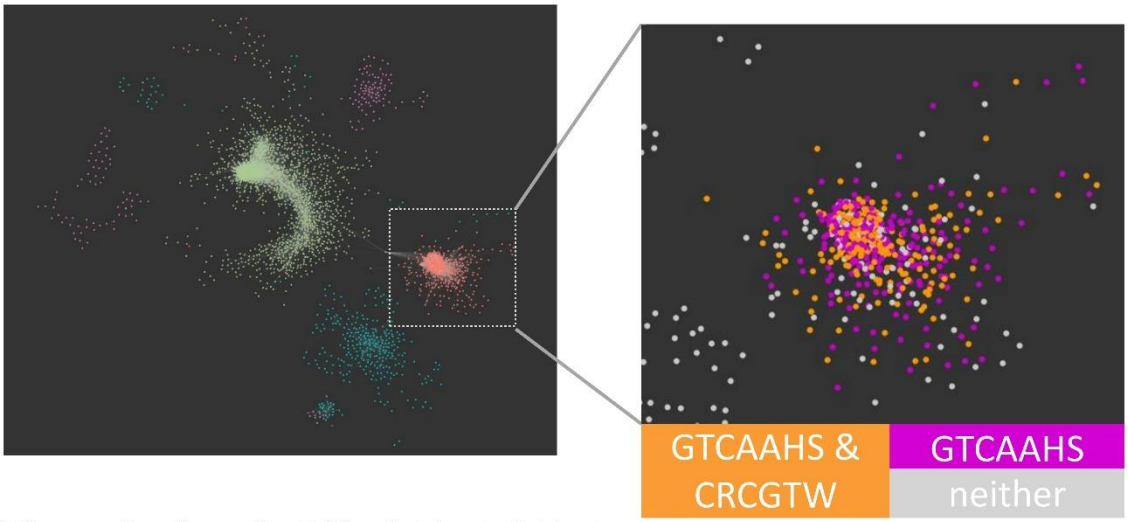

Motif	Present in subnetwork (565 nodes)	Absent in full network (of 3206)	Fischer's exact test p-value	Enrichment value
GTCAAHS	**291**	**1200**	**2.80E-10**	**1.20E-05**
GTCAAAG	87	311	6.60E-05	2.90E+00
GTCAAAC	91	358	7.70E-04	3.40E+01
GTCAACG	45	156	2.60E-03	1.10E+02
GTCAATG	62	242	4.80E-03	2.10E+02
GTCAACC	54	206	5.70E-03	2.50E+02
GTCAATC	56	218	7.00E-03	3.10E+02
CRCGTW	**337**	**1519**	**4.60E-08**	**2.00E-03**
CACGTT	178	686	2.00E-04	8.80E-03
CGCGTA	70	252	4.40E-04	1.90E+01
CGCGTT	86	365	6.90E-03	3.00E+02
CACGTA	148	689	8.30E-03	3.60E+02

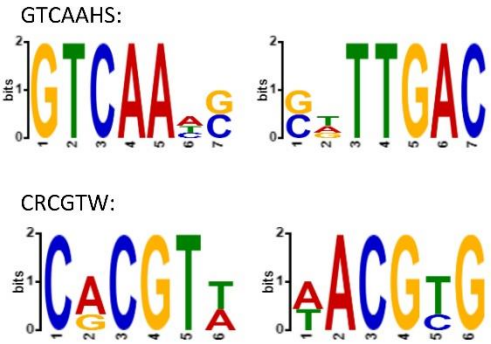

Figure 8: The senescence subnetwork is potentially under WRKY transcription factor control. Upstream regions (1kb) of the senescence subnetwork genes were subjected to differential motif enrichment analysis using DREME. The upstream regions of the full network served as control sequences for comparison. Two enriched motifs were discovered in the senescence subnetwork: GTCAAHS and CRCGTW. In those genes with enriched motifs present, they either contained GTCAAHS or a combination of both motifs. TomTom identified a number of putative GTCAAHS and CRCGTW, including a number of WRKY and bHLH transcription factors present in the Senescome.

,

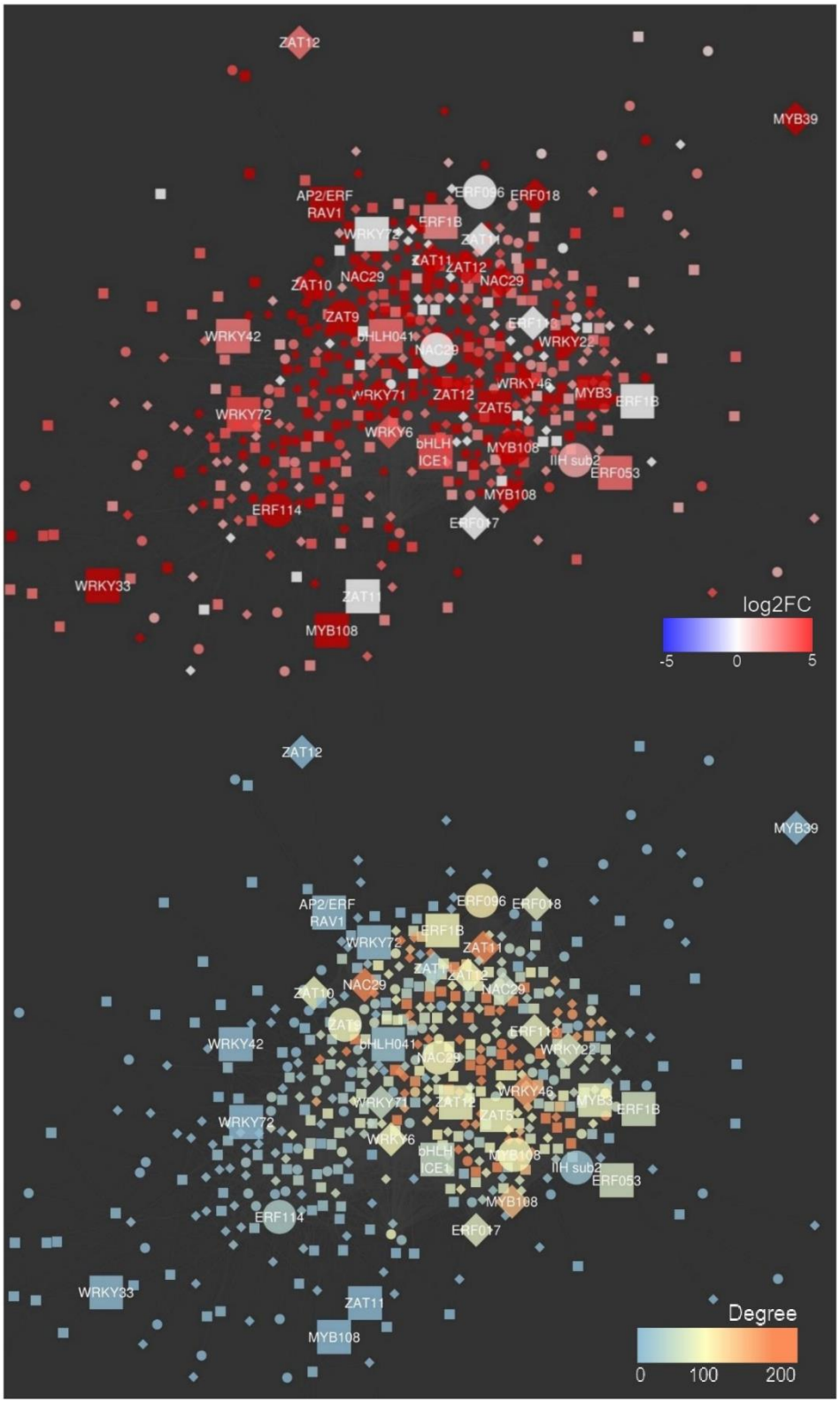

Figure 9: Transcriptional control of the senescence subnetwork. The senescence-specific subnetwork was isolated from the main network and re-organized with the yFiles Organic layout to prevent node overlap. The shape of nodes denotes whether they contain the GTCAAHS motif (squares) or both the GTCAAHS and CRCGTW motifs (diamonds) or neither (circles). Transcription factor nodes are increased in size for greater clarity and labelled with their abbreviated SwissProt gene description. The nodes in panels A-C are coloured for their log2FC relative to FT NST in AD NST (A), AD PST (B) and AD ST (C). The nodes in panel D are coloured for their degree (number of connections to other nodes in the subnetwork). The majority of transcription factors contain putative WRKY binding sites in their upstream regions.

In *A.thaliana*, intracellular calcium ions, ROS, PA and ABA all activate the serine/threonine receptor kinase OXI1 (highly transcriptionally upregulated in AD ST), which triggers MAPK6 activation (Rentel *et al.*, 2004; Shumbe *et al.*, 2016). Activation of various transcription factors, including MYB3, are carried out by MAPK6 (Smékalová *et al.*, 2014). It is proposed here that a similar mechanism for ethylene production and WRKY TF synthesis is at play in ST of *X. schlechteri*. WRKY6 is additionally activated directly by MAPK6 (Kim *et al.*, 2018). MAPK6 also has been shown to directly phosphorylates ACC-synthase, driving production of ethylene in *A.thaliana* in response to stress (Liu and Zhang, 2004). The activation of WRKY6 has been shown to drive a number of senescence-associated genes in *A.thaliana* including calmodulins, peroxidases, pectin esterase, lipase, MAP kinases, serine/threonine kinases, ABC transporters and others (Robatzek and Somssich, 2002). This is consistent with the classes of gene expression we report in the Senescome, which strongly indicates that a parallel process is at play in *X. schlechteri,* but at remarkably low water contents.

Another fascinating component to regulation of this subnetwork is presented by the enrichment of the CRCGTW motif in the upstream region of a substantial number of nodes, all of which also contain the GTCAAHS site. As annotated through TomTom analysis, this CRCGTW motif is a potential binding site for a number of transcription factors including bHLH13 and MYC2/3/4. Group IIId bHLH TFs (including bHLH13) have been shown to repress expression of senescence associated protease SAG29, whereas MYC3/4/5 TFs have been shown to bind to the same site and activate expression of this gene in the presence of jasmonic acid (Qi *et al.*, 2015). Thus, repressed expression of these genes in NST and PST may be facilitated by bHLH TFs. Indeed, there is a transcript annotated as MYC4 that displays increased expression in AD ST (albeit not to a great enough degree to be included in the Senescome data set). Collectively, these observations indicate that repression of senescence in NST and PST might be facilitated by binding of repressors to the CRCGTW site.

Conclusions

Stabilisation, mitigation of stress and senescence initiation

The dramatic increase in gene expression in AD ST represents a mixed population of cells at different phases of senescence: genes representing the initiation (transcriptional control), reorganisation (molecular degradation and transport) and termination (cellular death genes and nucleases) phases of senescence that are present in the same sample. The AD sampling point is, therefore, a snapshot of these processes and does not mean that these genes are necessarily transcribed in the air-dry state

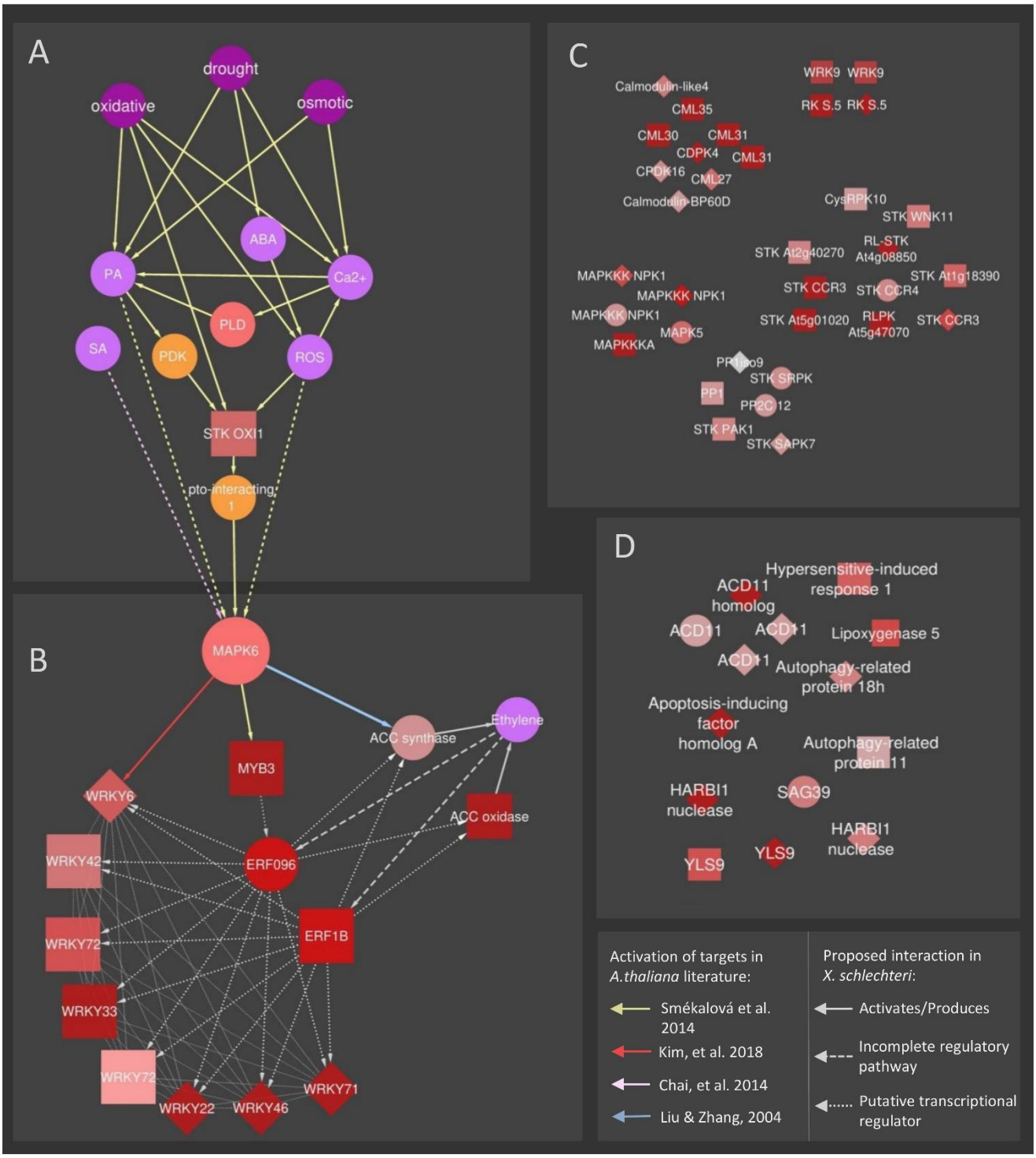

Figure 10: Proposed model for regulation of the senescence subnetwork based on homology in *A.thaliana*. Nodes in shades of red are a subset of nodes from the senescence subnetwork proposed to play a role in signaling during senescence in *X. schlechteri*. Nodes are shaped based on the presence of GTCAAHS (■), both GCTAAHS/CRCGTW (◆) or neither (●) motif in their upstream regions. Severe abiotic stresses (dark purple nodes) result in widely-reported elevations in stress signals (light purple) phosphatidic acid (PA), intercellular calcium (Ca2+), abscisic acid (ABA), salicylic acid (SA) and reactive oxygen species (ROS) (panel A). There are many targets of these signals (un-/understudied targets from senescence subnetwork shown in panel C), but of special interest to the current study is interaction with regulators up- and downstream from mitogen-activated protein kinase (MAPK)6, one of the studied regulators in senescence processes also upregulated in the Senescome. MAPK6, activated downstream of oxidative signal inducible 1 (OXI1) and through other mechanisms, has been shown to activate WRKY6 in senescent *A.thaliana* (reviewed in Kim et al. 2018). All 7 WRKY TFs in the senescence subnetwork contain ERF096 binding sites in their upstream regions (identified by TomTom analysis), indicating potential regulation via this TF in addition to MAPK6. ERF096 and ERF1B also potentially drive ACC oxidase and ACC synthase expression, as binding sites for both TFs are also present in their upstream regions. These gene products drive biosynthesis of ethylene, which in turn drives ERF096 and ERF1B expression, driving WRKY expression and thus regulation of the majority of genes within the senescence subnetwork. ACC synthase is additionally directly phosphorylated by MAPK6, leading to its activity in response to stress. Panel D shows some of the cellular death genes present in the Senescome, and demonstrates that the majority contain WRKY motifs in their upstream regions. Orange nodes represent nodes not present in the subnetwork but present in the ST-LRS supercluster. Acronyms: phospholipase D (PLD), 3-phosphoinositide-dependent protein kinase 1 (PDK), serine threonine kinase (STK), accelerated cell death (ACD), senescence associated gene (SAG), yellow leaf specific (YLS), wall-associated receptor kinase (WRK)

– their transcription could occur at any RWC between 35% and AD and were detected at AD in the present study. However, by 48h after rehydration, these senescence-encoding transcripts have served their purpose and are no longer synthesised in surviving cells of the ST and those that were present are presumably expunged by nucleases, their resulting free nucleotides apoplastically reclaimed by surviving cells. The remaining cells resemble air-dry tissue on the transcriptional level, confirming the hypothesis made in **chapter 2** that while most cells in the ST are lysed, some survive and contribute to the marginal RWC recovery of the tissue.

The present study found that, on the transcriptional level, protective mechanisms are being deployed in NST, PST and ST to the same degree: LEA, heat shock, sugar synthesis and anti-oxidant encoding genes are transcribed in all tissue types. Transcription below 35% RWC in the ST takes place in the context of a desiccated cell, as evidenced by the upregulation of desiccation tolerance genes. While there is evidence that these genes are transcribed in ST, there is no evidence as to whether they are translated and thus whether these gene products are performing their function in stabilising cells of the ST and ameliorating the stresses brought about by desiccation. Assuming these genes are translated and that their protein products are active, senescence is not the result of a deliberate switching off of desiccation tolerance processes (on the transcriptional level), rendering the tissue desiccation sensitive, but rather a parallel process engaging a relatively small number of tight regulators (WRKY, ERF and bHLH transcription factor families) to bring about macromolecular degradation, nutrient remobilisation and lysis in cells. The hypothesis that some of these desiccome genes are indeed translated in senescent tissue, despite the lack of confirmatory proteome analysis, is not unrealistic as it is not unreasonable to assume that stabilisation of the cellular constituents required for transcription of senescence genes below 35% RWC is presumably reliant on the presence of stabilising molecules such as LEA proteins, molecular chaperones, etc to maintain the correct conformation of transcriptional machinery below 35% RWC.

The question of how the overlapping osmotic, drought and oxidative stresses do not cause the same cellular death response in NST and PST during desiccation is an intriguing one. While there is some evidence that expression of the senescence subnetwork is triggered to a degree in these proximal tissues (expression of genes in cluster 3 and 6 do peak to a lesser degree in NST and PST than in ST, and there is increased log2 foldchange of the senescence subnetwork, as observed in **figures 3 and 4**), indicating that some cells may indeed succumb to the stress.

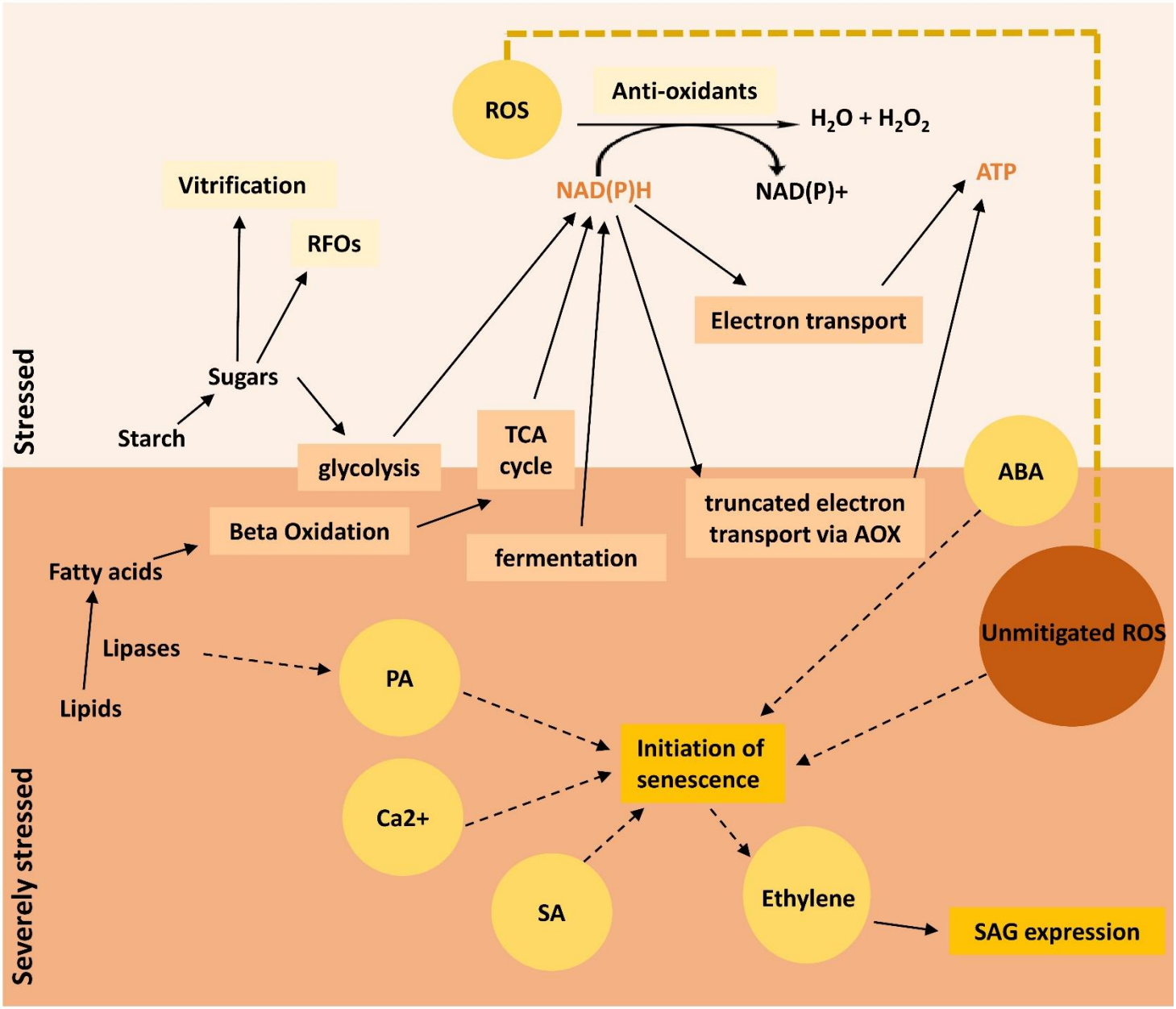

Figure 11: Proposed model coupling stress responses and energy requirements with senescence initiation in *X. schlechteri*. Stressed leaves shut down photosynthesis with the onset of water deficit. Glycolysis, the TCA cycle and electron transport in the mitochondria are presumably still active as transcripts encoding their enzymes do not diminish during desiccation, with some increasing in abundance (e.g. cytochrome C). These mechanisms drive production of ATP and NADH, required for a variety of intracellular protection mechanisms including production of vitrifying sugars and RFOs and mitigation of ROS via anti-oxidant enzymes (e.g. glutathione reductase) and for synthesis of non-enzymatic anti-oxidants (e.g. ascorbic acid). As the tissues become severely stressed (<20% RWC) available sources for the regeneration of NADH and ATP become fewer. Expression of enzymes involved with beta-oxidation and fermentation increase in order to produce NADH, as does expression of alternative oxidase (AOX), which truncates the electron transport chain, terminating it short of cytochrome C. This truncation of electron transport potentially prevents production of free radicals while still producing some ATP for cellular processes. However, as energy sources for production of NADH and ATP dwindle, as does the cell's ability to mount a defense against toxic intermediates and ROS. This accumulation of unmitigated ROS, coupled with phosphatidic acid build up (a result of the action of lipases required for entry of lipids into beta-oxidation), leads to triggering of senescence processes as described in figure 10, and expressions of senescence-associated genes (SAGs).

Why so many cells within ST succumb, leading to bulk tissue death, may be due to prolonged exposure to drought stress: these tissues are the first tissues to experience water deficit (leaves fold from the apex towards the base and presumably experience water deficit in the same direction, as is reflected in the lower RWC phenomenon discussed in chapter 2). These tissues have also endured prolonged exposure to UV radiation compared to their NST counterparts (due to their being the oldest part of the leaf). Therefore, the level of photoreactive damage they incur is presumably greater. They express similar levels of protectant (anti-oxidant, LEA, heat shock, secondary metabolite) transcripts, but perhaps this is not enough to mitigate the great level of damage they incur during drying and senescence processes are initiated in response to the many overlapping stress signals.

There is a parallel argument to be made regarding the energy balance within cells: NADH and ATP are required by enzymatic anti-oxidants, such as glutathione reductase, and for synthesis of non-enzymatic anti-oxidants for dealing with ROS and free radicals generated during water deficit stress. As proposed by Kranner *et al.,*(2002), the anti-oxidant status of a resurrection plant is the ultimate determinant of its viability. **Figure 11** illustrates the following proposal: to keep up with the demands for NADH and ATP, while limiting ROS formation, stressed cells shut down photosynthesis but keep glycolysis, the TCA cycle and electron transport active. As ST cells enter a severely stressed state, below 35% RWC, genes encoding lipases and beta-oxidation enzymes are transcribed to drive the TCA cycle for regeneration of NADH. The electron transport chain is truncated by AOX to limit high energy electron transitions and thus further unstable intermediate formation. Fermentation is additionally employed to meet energy demands. When a tipping point is reached, wherein the energy required to mitigate ROS and toxic intermediates is not produced rapidly enough to prevent their build-up, senescence processes are initiated via activation of ERF and WRKY genes as described in **Figure 10**. Additionally, the action of lipases to produce substrate for beta-oxidation, especially phospholipase C and D, drives production of phosphatidic acid, yet another driver for senescence initiation as outlined in **Figure 10**.

It is proposed here that intermediates apoplastically transported from senescent cells towards NST and PST enables these tissues to drive production of NADH and ATP and therefore conquer the mounting ROS within their own cells, as well as to provide substrate for full metabolic recovery upon water availability. The subject of nutrient remobilisation is precarious: while there are several transport-associated transcripts upregulated in ST, the presence of a transporter transcript says nothing about whether the transporter is present or whether it is active or, assuming it is, in which direction the nutrient or building block is being transported. However, the evidence of certain uptake transporters only differentially expressed in NST and PST and other bidirectional transporters highly expressed in AD ST suggests a directional flow of nutrient from ST to NST/PST and presents an

opportunity for further investigation of nutrient mobilisation via the apoplast in near-desiccated and rehydrated tissues.

According to this model, PST and NST will also eventually succumb to desiccation if left in the dry state for long enough, which is yet to be demonstrated. There is also some evidence suggesting older tissues are more susceptible to ethylene than younger tissues (Jing *et al.*, 2002, 2005), but it is yet to be determined how and indeed whether resurrection plants experience typical hallmarks of aging in the dry state. It is proposed here that survival of cells is dependent on a delicate balance between ROS homeostasis, meeting energy requirements and developmental susceptibility to ethylene and other hormones.

Supplementary

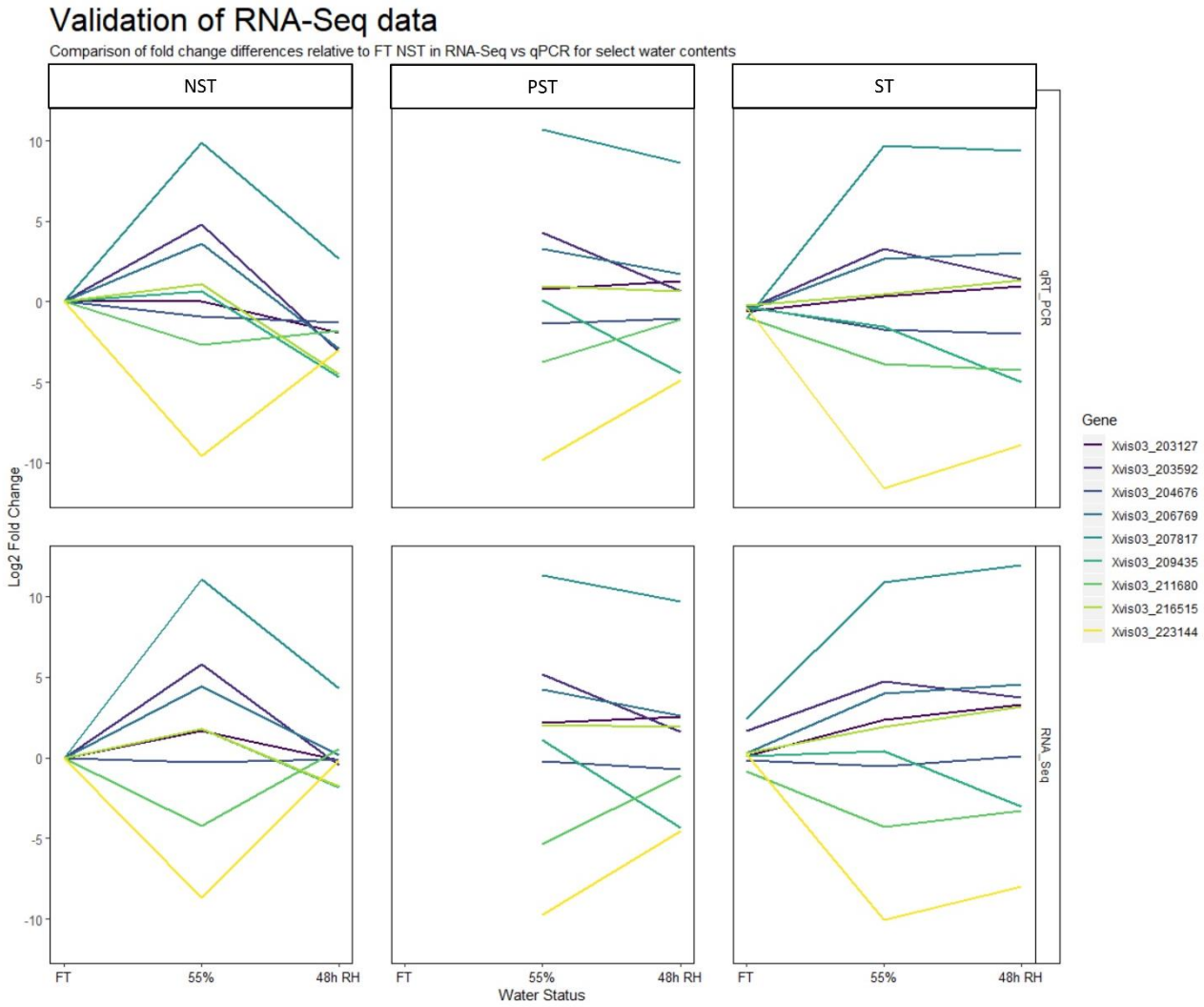

Supplementary figure 1: qPCR validation of trends in the transcriptome. RNA isolated from FT, 55% RWC (NST) and rehydrated samples was subjected to qPCR amplification to confirm consistency of the RNA Seq results.

Supplementary Table 1: An average of 87% of transcripts measured aligned to the reference genome.

Sample	Number of reads	Read Length				Mapping rate	Multiple alignment rate
		min	max	mean	stdev		
FT NST 1	25792292	35	75	74,4301	1,6678	22792996 (88.4% of input)	of these: 2589168 (11.4%) have multiple alignments (10 have >20)
FT NST 2	19229153	35	75	74,3772	2,21	16490111 (85.8% of input)	of these: 1861108 (11.3%) have multiple alignments (14 have >20)
FT NST 3	23246554	35	75	74,4468	1,5673	20286232 (87.3% of input)	of these: 2235862 (11.0%) have multiple alignments (4 have >20)
FT ST 1	20560559	35	75	74,4269	1,6575	18220110 (88.6% of input)	of these: 2044021 (11.2%) have multiple alignments (12 have >20)
FT ST 2	21830413	35	75	74,4406	1,5568	19122390 (87.6% of input)	of these: 2201322 (11.5%) have multiple alignments (14 have >20)
FT ST 3	25924940	35	75	74,444	1,4666	22826991 (88.1% of input)	of these: 2559372 (11.2%) have multiple alignments (7 have >20)
75% NST 1	27451624	35	75	74,4101	1,7686	23700736 (86.3% of input)	of these: 2256265 (9.5%) have multiple alignments (12 have >20)
75% NST 2	22454488	35	75	74,4666	1,5185	20039211 (89.2% of input)	of these: 1922780 (9.6%) have multiple alignments (12 have >20)
75% NST 3	22234613	35	75	74,4268	1,8523	19585132 (88.1% of input)	of these: 1795170 (9.2%) have multiple alignments (7 have >20)
75% PST 1	22259193	35	75	74,3962	1,9974	19631720 (88.2% of input)	of these: 1778586 (9.1%) have multiple alignments (11 have >20)
75% PST 2	23713951	35	75	74,4593	1,5466	21445678 (90.4% of input)	of these: 2137733 (10.0%) have multiple alignments (32 have >20)
75% PST 3	22479787	35	75	74,4246	1,8269	19887330 (88.5% of input)	of these: 1834823 (9.2%) have multiple alignments (11 have >20)
75% ST 1	25773607	35	75	74,4277	1,8698	22077599 (85.7% of input)	of these: 2119665 (9.6%) have multiple alignments (12 have >20)
75% ST 2	24881059	35	75	74,4314	1,7301	22400875 (90.0% of input)	of these: 2268921 (10.1%) have multiple alignments (26 have >20)
75% ST 3	26381596	35	75	74,4014	1,9541	23837688 (90.4% of input)	of these: 2266243 (9.5%) have multiple alignments (10 have >20)
55% NST 1	21943220	35	75	74,3551	2,2274	18759474 (85.5% of input)	of these: 1659908 (8.8%) have multiple alignments (34 have >20)
55% NST 2	32274948	35	75	74,416	1,897	28004522 (86.8% of input)	of these: 2501615 (8.9%) have multiple alignments (3 have >20)
55% NST 3	28191999	35	75	74,4279	1,724	24225855 (85.9% of input)	of these: 2212225 (9.1%) have multiple alignments (20 have >20)
55% PST 1	33569421	35	75	74,3847	2,1435	29331628 (87.4% of input)	of these: 2425094 (8.3%) have multiple alignments (5 have >20)
55% PST 2	25629440	35	75	74,4318	1,7912	22456984 (87.6% of input)	of these: 2024248 (9.0%) have multiple alignments (6 have >20)
55% PST 3	23174815	35	75	74,4295	1,7199	19936729 (86.0% of input)	of these: 1818656 (9.1%) have multiple alignments (9 have >20)
55% ST 1	35013141	35	75	74,4106	1,9136	30705691 (87.7% of input)	of these: 2996944 (9.8%) have multiple alignments (4 have >20)
55% ST 2	30515418	35	75	74,4311	1,7416	26533698 (87.0% of input)	of these: 2532274 (9.5%) have multiple alignments (10 have >20)
55% ST 3	21886007	35	75	74,4378	1,7152	18989827 (86.8% of input)	of these: 1771702 (9.3%) have multiple alignments (20 have >20)
35% NST 1	25113875	35	75	74,4158	2,0119	21597201 (86.0% of input)	of these: 2066116 (9.6%) have multiple alignments (4 have >20)
35% NST 2	19433823	35	75	74,4527	1,6235	17318277 (89.1% of input)	of these: 1702520 (9.8%) have multiple alignments (0 have >20)
35% NST 3	33830382	35	75	74,4194	1,8928	29565424 (87.4% of input)	of these: 2701801 (9.1%) have multiple alignments (17 have >20)
35% PST 1	29128372	35	75	74,4325	1,8564	25542335 (87.7% of input)	of these: 2404067 (9.4%) have multiple alignments (5 have >20)
35% PST 2	16716566	35	75	74,459	1,6329	14705769 (88.0% of input)	of these: 1397250 (9.5%) have multiple alignments (4 have >20)
35% PST 3	26106457	35	75	74,4051	1,989	22664155 (86.8% of input)	of these: 1983405 (8.8%) have multiple alignments (21 have >20)
35% ST 1	21151107	35	75	74,4489	1,6332	18346257 (86.7% of input)	of these: 1771107 (9.7%) have multiple alignments (6 have >20)
35% ST 2	26335629	35	75	74,4592	1,5457	23356949 (88.7% of input)	of these: 2312281 (9.9%) have multiple alignments (6 have >20)
35% ST 3	16261674	35	75	74,3853	2,1077	14021673 (86.2% of input)	of these: 1304631 (9.3%) have multiple alignments (16 have >20)
AD NST 1	22562653	35	75	74,4476	1,8622	19822345 (87.9% of input)	of these: 1655023 (8.3%) have multiple alignments (2 have >20)
AD NST 2	19421848	35	75	74,3322	2,6554	17066065 (87.9% of input)	of these: 1631914 (9.6%) have multiple alignments (6 have >20)
AD NST 3	18896477	35	75	74,2694	2,6134	16303351 (86.3% of input)	of these: 1548786 (9.5%) have multiple alignments (7 have >20)
AD PST 1	14293821	35	75	74,4881	1,5791	12716043 (89.0% of input)	of these: 1087256 (8.6%) have multiple alignments (8 have >20)
AD PST 2	20495749	35	75	74,4009	2,2409	18017476 (87.9% of input)	of these: 1715124 (9.5%) have multiple alignments (2 have >20)
AD PST 3	21061362	35	75	74,3907	2,167	18308562 (86.9% of input)	of these: 1732961 (9.5%) have multiple alignments (8 have >20)
AD ST 1	14805716	35	75	74,4546	1,8104	12940374 (87.4% of input)	of these: 1250809 (9.7%) have multiple alignments (2 have >20)
AD ST 2	23104005	35	75	74,3128	2,6374	20233293 (87.6% of input)	of these: 1981199 (9.8%) have multiple alignments (3 have >20)
AD ST 3	22039689	35	75	74,4148	1,8883	19132713 (86.8% of input)	of these: 1916650 (10.0%) have multiple alignments (8 have >20)
RH NST 1	15581678	35	75	74,4552	1,7115	13510344 (86.7% of input)	of these: 1397972 (10.3%) have multiple alignments (10 have >20)
RH NST 2	16484555	35	75	74,1181	3,1214	14125852 (85.7% of input)	of these: 1473882 (10.4%) have multiple alignments (23 have >20)
RH NST 3	20584373	35	75	74,433	1,766	18088038 (87.9% of input)	of these: 1862108 (10.3%) have multiple alignments (9 have >20)
RH PST 1	25088555	35	75	74,4216	1,7355	21906335 (87.3% of input)	of these: 2137735 (9.8%) have multiple alignments (3 have >20)
RH PST 2	22688980	35	75	74,4011	1,8369	20086315 (88.5% of input)	of these: 2023444 (10.1%) have multiple alignments (94 have >20)
RH PST 3	25080269	35	75	74,4064	1,9345	22023335 (87.8% of input)	of these: 2077406 (9.4%) have multiple alignments (6 have >20)
RH ST 1	13035356	35	75	74,4283	2,0366	10818250 (83.0% of input)	of these: 999655 (9.2%) have multiple alignments (0 have >20)
RH ST 2	14854856	35	75	74,3698	2,3143	12985666 (87.4% of input)	of these: 1227446 (9.5%) have multiple alignments (7 have >20)
RH ST 3	22614287	35	75	74,372	2,0825	19140402 (84.6% of input)	of these: 1802659 (9.4%) have multiple alignments (3 have >20)
AVERAGE	**23003614,75**	**35**	**75**	**74,410**	**1,909**	**87,382**	

Supplementary table 2: Enriched gene ontologies in the Reduced and Recovered supercluster. Classes were determined using BINGO in Cytoscape , the output of which was subjected to redundancy removal in ReviGO. The extent to which the ontologies are enriched is given by the o/e ratio (ratio of observed to expected number of genes) and the Bonferroni-adjusted qvalue for each ontology.

Cluster	Description	o/e	qval	Significance	Number of categories	representative GO term
8	reproduction	0,4559	8,06E-13	***	1	3
	cell recognition	0,4559	8,06E-13	***	1	8037
	response to organic substance	0,3214	0,0214	*	2	10033
	reproductive process	0,4559	8,06E-13	***	4	22414
	multicellular organismal process	0,3605	1,15E-09	***	1	32501
	(obsolete) cellular process involved in reproduction	0,4559	8,06E-13	***	1	48610
	multi-organism process	0,4306	4,96E-12	***	1	51704
	post-translational protein modification	0,13218	0,000216	***	5	43687
	cell communication	0,4247	7E-12	***	1	7154
	phosphorus metabolic process	0,133	0,000105	***	1	6793
	macromolecule modification	0,1261	0,000473	***	1	43412
	response to endogenous stimulus	0,3214	0,0214	*	1	9719
10	(obsolete) GTP catabolic process	0,4483	0	***	1	6184
	photosynthesis	0,5484	0	***	1	15979
	protein polymerization	0,346533	0,003467	***	3	51258
	GTP metabolic process	0,262213	0,001663	***	8	46039
	lipid biosynthetic process	0,202333	0,011567	*	3	8610
	nucleobase-containing compound catabolic process	0,374217	0,000192	***	12	34655
	regulation of cyclin-dependent protein serine/threonine kinase a	0,5714	0,0316	*	1	79
12	glycine catabolic process	0,75	1,46%	*	2	6546

Supplementary table 3: Enriched gene ontologies in the early response supercluster. Classes were determined using BINGO in Cytoscape , the output of which was subjected to redundancy removal in ReviGO. The extent to which the ontologies are enriched is given by the o/e ratio (ratio of observed to expected number of genes) and the Bonferroni-adjusted qvalue for each ontology.

Cluster	Description	o/e	qval	Significance	Number of categories	representative GO term
1	translational elongation	0,253333	0,00001	***	6	6414
	biological_process	0,06	0,0257	*	1	8150
	metabolic process	0,07	1,6E-06	***	1	8152
	cellular process	0,08	7,27E-15	***	1	9987
	energy coupled proton transport, down electrochemical gradient	0,28	0,00827	***	1	15985
	biosynthetic process	0,16	3,4E-39	***	1	9058
	protein folding	0,13	0,0331	*	1	6457
	cellular metabolic process	0,09	7,96E-20	***	1	44237
	primary metabolic process	0,08	4,57E-14	***	1	44238
	gene expression	0,175	2,76E-25	***	2	10467
	macromolecule metabolic process	0,1	5,14E-21	***	1	43170
	heterocycle metabolic process	0,12	0,0398	*	1	46483
	protein metabolic process	0,11	2,9E-21	***	1	19538
	purine ribonucleotide biosynthetic process	0,29087	0,019375	***	23	9152
9	(obsolete) oxygen and reactive oxygen species metabolic process	0,4545	0,0172	*	1	6800
	superoxide metabolic process	0,4545	0,0172	*	1	6801
	biological_process	0,0653	0,002	***	1	8150
	monovalent inorganic cation transport	0,10755	0,0336	*	4	15672
	localization	0,0822	0,0213	*	1	51179
	regulation of biological quality	0,1304	0,0229	*	1	65008
	cellular homeostasis	0,1385	0,0345	*	3	19725

Supplementary table 4: Enriched gene ontologies in the late response supercluster. Classes were determined using BINGO in Cytoscape , the output of which was subjected to redundancy removal in ReviGO. The extent to which the ontologies are enriched is given by the o/e ratio (ratio of observed to expected number of genes) and the Bonferroni-adjusted qvalue for each ontology.

Cluster	Description	o/e	qval	Significance	Number of categories	representative GO term
4	cellular process	0,07	0,0199	*	1	9987
	ribonucleoprotein complex biogenesis	0,19	0,0219	*	1	22613
	tetrapyrrole biosynthetic process	0,416	0	***	5	33014
	biosynthetic process	0,11	0	***	1	9058
	lipoprotein metabolic process	0,26	0,0443	*	1	42157
	photosynthesis	0,16	0,0376	*	1	15979
	nitrogen compound metabolic process	0,1	0	***	1	6807
	cofactor metabolic process	0,18	0,0006	***	1	51186
	cellular metabolic process	0,07	0,0001	***	1	44237
	macromolecule metabolic process	0,07	0,0074	***	1	43170
	lipoprotein biosynthetic process	0,26	0,0443	*	2	42158
	heterocycle metabolic process	0,15	0,0002	***	1	46483
	cofactor biosynthetic process	0,25	0,0001	***	1	51188
	ncRNA metabolic process	0,23875	0,006919	***	16	34660
	gene expression	0,1	0,0034	***	2	10467
	cellular nitrogen compound metabolic process	0,11	0	***	1	34641
	cellular amine metabolic process	0,11	0,0443	*	1	44106
	tetrapyrrole metabolic process	0,63	0	***	1	33013
	amino acid activation	0,165	0,0208	***	2	43038
	cellular biosynthetic process	0,1975	0,00005	***	4	44249
5	protein catabolic process	0,27	0,000374	***	8	30163
	regulation of organelle organization	0,63	0,0287	*	1	33043
	cellular localization	0,24	5,73E-05	***	1	51641
	cofactor biosynthetic process	0,27	0,0451	*	1	51188
	RNA splicing	0,5	0,011	*	5	8380
	regulation of ARF protein signal transduction	0,38	0,0496	*	1	32012
	transcription from RNA polymerase II promoter	0,538462	0,013997	*	3	6366
	vesicle-mediated transport	0,203297	0,020892	*	1	16192
	mRNA metabolic process	0,297872	0,025266	*	1	16071
	intracellular transport	0,251497	0,000225	***	5	46907
	transcription initiation from RNA polymerase II promoter	0,6	0,017061	*	1	6367
	proteolysis	0,177177	0,026449	*	1	6508
	protein localization	0,229508	0,0012	***	3	8104
	macromolecule localization	0,220513	0,002372	***	1	33036
7	post-Golgi vesicle-mediated transport	1	0,00267	***	2	6892
	ncRNA metabolic process	0,194	0,005913	***	5	34660
	ribosome biogenesis	0,175	0,0313	*	2	42254
	nitrogen compound metabolic process	0,1	4,78E-08	***	1	6807
	macromolecule metabolic process	0,06	0,0193	*	1	43170
	amino acid activation	0,122	0,020845	***	5	43038
	microtubule-based movement	0,19	0,00362	***	1	7018
	microtubule-based process	0,18	0,000536	***	1	7017
	gene expression	0,08	0,0295	*	1	10467
	mismatch repair	0,254	6,83E-05	***	5	6298
	cellular amine metabolic process	0,11	0,00911	***	1	44106
	amine metabolic process	0,1	0,0196	*	1	9308
	cellular ketone metabolic process	0,09	0,0295	*	1	42180
	nucleic acid metabolic process	0,1175	0,010576	***	8	90304

Supplementary table 5: Enriched gene ontologies in the drought/desiccation elevation cluster supercluster. Classes were determined using BINGO in Cytoscape , the output of which was subjected to redundancy removal in ReviGO. The extent to which the ontologies are enriched is given by the o/e ratio (ratio of observed to expected number of genes) and the Bonferroni-adjusted qvalue for each ontology.

Cluster	Description	o/e	qval	Significance	Number of categories	representative GO term
2	embryo development	0,695	0,009878	***	2	9790
	developmental process	0,39	0,0197	*	1	32502
	ion transmembrane transport	0,23	0,037525	*	4	34220
	hydrogen transport	0,2	0,0308	*	1	6818

Supplementary table 6: Enriched gene ontologies in the ST late response supercluster. Classes were determined using BINGO in Cytoscape , the output of which was subjected to redundancy removal in ReviGO. The extent to which the ontologies are enriched is given by the o/e ratio (ratio of observed to expected number of genes) and the Bonferroni-adjusted qvalue for each ontology.

Cluster	Description	o/e	qval	Significance	Number of categories	representative GO term
6	transport	0,126667	0,0178	*	3	6810
	response to wounding	1	0,033	*	1	9611
	carbohydrate catabolic process	0,2	0,0184	*	6	16052
	localization	0,12	0,0277	*	1	51179
	catabolic process	0,14	0,0483	*	1	9056
	coenzyme A metabolic process	0,56	0,033	*	1	15936
	lipid oxidation	1	0,033	*	1	34440
11	reproduction	0,18	0,000359	***	1	3
	protein phosphorylation	0,391818	0,028725	***	11	6468
	biological_process	0,04	0,00932	***	1	8150
	metabolic process	0,05	0,00193	***	1	8152
	reproductive process	0,18	0,000359	***	4	22414
	multicellular organismal process	0,14	0,0029	***	1	32501
	(obsolete) cellular process involved in reproduction	0,18	0,000359	***	1	48610
	multi-organism process	0,17	0,000625	***	1	51704
	cell recognition	0,18	0,000359	***	1	8037
	cell communication	0,16	0,000685	***	1	7154
	monosaccharide metabolic process	0,112222	0,022487	***	9	5996
	generation of precursor metabolites and energy	0,11	0,0208	*	1	6091
	coenzyme metabolic process	0,12	0,0499	*	1	6732
	phosphorus metabolic process	0,06	0,000219	***	1	6793
	macromolecule modification	0,05	0,028	*	1	43412
	oxidation-reduction process	0,06	0,0175	*	1	55114
	alcohol metabolic process	0,385	0,039	*	4	6066

Supplementary table 6: Transcription factors with known binding sites to the GTCAAHS motif identified by TomTom.

TomTom ID	Gene ID	X. schlechteri ID	Optimal offset	p-value	E-value	Overlap	Query consensus	Target consensus	Orientation
MA1165.1	AT1G49560		0	0.01	7.01	7	GTCAAAG	ATCAAAGATTC	+
MA1390.1	AT1G68670		2	0.02	9.56	7	GTCAAAG	GAATCAAAGATTC	+
MA1306.1	**WRKY11**	Xvis03_201752; Xvis03_213823; **Xvis03_205846; Xvis03_205928; Xvis03_214066**	5	0.00	0.98	7	GTCAAAG	AAAAAGTCAACGCT	-
MA1075.1	WRKY12		1	0.00	0.30	7	GTCAAAG	GGTCAACG	-
MA1314.1	WRKY14		4	0.00	1.04	7	GTCAAAG	AAAAGTCAACGAT	+
MA1076.1	WRKY15		2	0.00	0.13	7	GTCAAAG	AGGTCAACGC	+
MA1299.1	WRKY17		5	0.00	1.42	7	GTCAAAG	AAAAAGTCAACGCC	+
MA1077.1	WRKY18		3	0.00	1.20	7	GTCAAAG	ATGGTCAACG	+
MA1078.1	WRKY2	Xvis03_212849	2	0.00	1.54	6	GTCAAAG	CGGTCAAC	+
MA1295.1	WRKY20	Xvis03_200083; Xvis03_218672	4	0.00	0.43	7	GTCAAAG	AATAGTCAACGTT	-
MA1079.1	WRKY21		3	0.00	0.33	7	GTCAAAG	AAGGTCAACG	+
MA1303.1	WRKY22		4	0.00	1.49	7	GTCAAAG	AAAAGTCAACGAT	+
MA1080.1	**WRKY23**	**Xvis03_221572; Xvis03_203616; Xvis03_203836; Xvis03_211583**	1	0.00	0.17	7	GTCAAAG	AGTCAACG	+
MA1315.1	WRKY24		6	0.00	1.19	7	GTCAAAG	AAAAAAGTCAACGA	-
MA1081.1	WRKY25		2	0.01	2.57	6	GTCAAAG	CGGTCAAC	+
MA1297.1	WRKY26	Xvis03_209784	4	0.00	0.95	7	GTCAAAG	AAAAGTCAACGGT	+
MA1318.1	WRKY27		4	0.00	1.62	7	GTCAAAG	AAAAGTCAACGAT	-
MA1311.1	WRKY28	Xvis03_211038	4	0.00	0.64	7	GTCAAAG	AAAAGTCAACGAT	-
MA1298.1	WRKY29		4	0.00	1.06	7	GTCAAAG	AAAAGTCAACG	+
MA1309.1	WRKY3	Xvis03_200369; Xvis03_208183; Xvis03_215320; Xvis03_206017; Xvis03_219578	4	0.00	0.34	7	GTCAAAG	AAAAGTCAACG	+
MA1083.1	WRKY30		1	0.00	0.37	7	GTCAAAG	GGTCAACGCT	+
MA1307.1	WRKY31		12	0.00	2.31	7	GTCAAAG	GGATAAAAAAAAGTCAACG	+
MA1301.1	WRKY33	Xvis03_210468; Xvis03_221299	4	0.00	0.34	7	GTCAAAG	AAAAGTCAACG	+
MA1084.1	WRKY38		1	0.00	0.36	7	GTCAAAG	GGTCAACG	-
MA1085.2	WRKY40	Xvis03_201790; Xvis03_219584; Xvis03_214127; Xvis03_205822	3	0.01	2.89	7	GTCAAAG	AAAGTCAAAA	+
MA1310.1	WRKY42	Xvis03_223134	4	0.01	2.91	7	GTCAAAG	AAAAGTCAACGCTAATTAAAA	-
MA1086.1	WRKY43		2	0.00	1.01	7	GTCAAAG	AAGTCAACAC	+
MA1087.1	WRKY45		1	0.00	0.27	7	GTCAAAG	GGTCAACG	-
MA1296.1	WRKY46	Xvis03_201984; Xvis03_209794	4	0.00	0.38	7	GTCAAAG	CAAAGTCAACG	-
MA1312.1	WRKY47		2	0.00	0.67	7	GTCAAAG	AAGTCAACGCCGGT	-
MA1088.1	WRKY48		3	0.00	0.24	7	GTCAAAG	GAGGTCAACG	+
MA1317.1	WRKY50	Xvis03_214509; Xvis03_220179	6	0.00	0.53	7	GTCAAAG	AAAAAAGTCAAAG	-
MA1305.1	WRKY55		3	0.00	0.89	7	GTCAAAG	AAAGTCAACGCT	-
MA1089.1	WRKY57	**Xvis03_200381**	3	0.00	0.22	7	GTCAAAG	AAAGTCAACG	+
MA1304.1	WRKY59		5	0.00	0.07	7	GTCAAAG	AAAAAGTCAAAG	+
MA1300.1	**WRKY6**	**Xvis03_215220**; Xvis03_201108; Xvis03_209315	12	0.00	2.11	7	GTCAAAG	ATGTTAAAAAAAGTCAACG	-
MA1090.1	WRKY60		3	0.00	0.16	7	GTCAAAG	CCGGTCAACGT	+
MA1091.1	WRKY62		2	0.00	1.71	6	GTCAAAG	TGGTCAAC	+
MA1092.1	WRKY63		2	0.01	7.18	6	GTCAAAG	CGGTCAAC	+
MA1302.1	WRKY65	Xvis03_204587; Xvis03_207150; Xvis03_211384; Xvis03_213501; Xvis03_211410	4	0.00	0.81	7	GTCAAAG	AAAAGTCAACG	+
MA1313.1	WRKY7		5	0.00	1.19	7	GTCAAAG	AAAAAGTCAACGCT	-
MA1308.1	**WRKY70**	Xvis03_210487; Xvis03_217167; **Xvis03_203971**	4	0.00	1.25	7	GTCAAAG	AAAAGTCAACGCT	-
MA1316.1	**WRKY71**	**Xvis03_215653; Xvis03_221542**	4	0.00	0.46	7	GTCAAAG	AAAAGTCAACG	+
MA1093.1	**WRKY75**	**Xvis03_200827; Xvis03_221600; Xvis03_223511**	2	0.00	1.40	6	GTCAAAG	AAGTCAAC	+
MA1094.1	WRKY8		2	0.00	0.16	7	GTCAAAG	AGGTCAACG	+
MA0589.1	ZAP1		6	0.01	5.81	5	GTCAAAG	GGCTCGGTCAA	-

Supplementary table 7: Transcription factors with known binding sites to the CRCGTWS motif identified by TomTom.

TomTom ID	Gene ID	X. schlechteri ID	Optimal offset	p-value	E-value	Overlap	Query consensus	Target consensus	Orientation
MA0930.1	ABF3		1	0.01	5.96	6	CACGTT	ACACGTGT	+
MA0931.1	ABI5	Xvis03_213691	3	0.02	8.19	6	CACGTT	TGACACGTGG	+
MA0959.1	AIB (BHLH)		1	0.01	5.43	6	CACGTT	GCACGTGC	+
MA0956.1	BEE2		2	0.02	8.99	6	CACGTT	AGCACGTGCT	+
MA0960.1	BHLH104		2	0.02	8.99	6	CACGTT	GGCACGTGCC	+
MA0958.1	**BHLH13**	**Xvis03_204378**; Xvis03_222948; Xvis03_211193	1	0.01	5.96	6	CACGTT	GCACGTGC	+
MA0957.1	BHLH3		1	0.01	5.96	6	CACGTT	GCACGTGC	+
MA0962.1	BHLH34		1	0.01	5.43	6	CACGTT	GCACGTGG	+
MA0963.1	BHLH78		1	0.01	5.96	6	CACGTT	GCACGTGC	+
MA0964.1	BIM1	Xvis03_223143	1	0.02	9.90	6	CACGTT	GCACGTGACC	+
MA0965.1	BIM2	Xvis03_203332; Xvis03_223142	2	0.02	8.19	6	CACGTT	GGCACGTGCC	+
MA0966.1	BIM3		2	0.02	7.49	6	CACGTT	AGCACGTGCT	+
MA0969.1	CMTA2		4	0.02	9.12	5	CACGTT	AAACCGCGT	+
MA0970.1	CMTA3		1	0.01	6.23	6	CACGTT	CCGCGTTAC	+
MA0566.1	MYC2	Xvis03_216854; Xvis03_218694; Xvis03_218787	1	0.01	6.57	6	CACGTT	GCACGTGC	+
MA0568.1	MYC3		1	0.01	7.27	6	CACGTT	GCACGTGC	+
MA0569.1	MYC4	Xvis03_216855; Xvis03_201608; Xvis03_218693	1	0.01	5.96	6	CACGTT	ACACGTGC	+
MA0935.1	NAC025		0	0.01	4.20	6	CACGTT	TACGTAAC	+
MA1045.1	NAC043		2	0.01	6.33	6	CACGTT	TTTACGTAAT	-
MA0937.1	NAC055		1	0.00	0.61	6	CACGTT	ACACGTAA	+
MA1033.1	OJ1058_F05.8		1	0.01	5.96	6	CACGTT	ACACGTGT	+
MA0988.1	PHYPADRAFT_143875		2	0.02	8.19	6	CACGTT	CGCACGTGCG	+
MA1021.1	PHYPADRAFT_48267		1	0.01	5.96	6	CACGTT	CCACGTGC	+
MA0561.1	PIF4		0	0.01	6.57	6	CACGTT	CACGTGGC	+
MA0562.1	PIF5		1	0.02	8.84	6	CACGTT	TCACGTGG	+
MA1061.1	SPT		2	0.02	8.24	6	CACGTT	CCCACGTGC	+
MA0129.1	TGA1A	Xvis03_217288	1	0.02	8.50	6	CACGTT	TGACGTA	-
MA1411.1	TSAR1		2	0.02	8.19	6	CACGTT	AGCACGTGCG	+
MA1412.1	TSAR2		2	0.02	8.99	6	CACGTT	TGCACGTGCG	+
MA1074.1	UNE10	Xvis03_220116	1	0.01	5.96	6	CACGTT	CCACGTGC	+

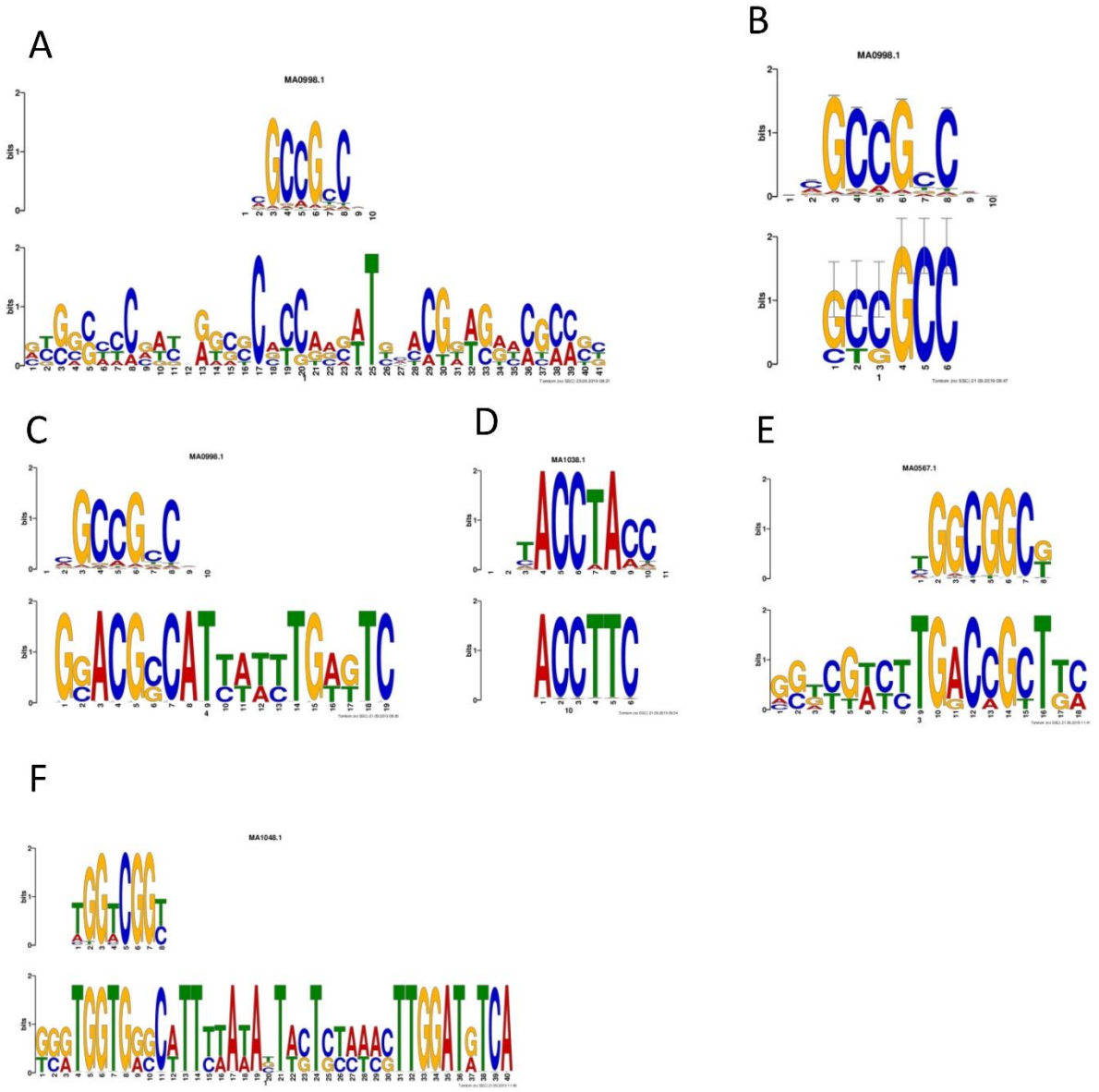

Supplementary Figure 2: Motifs upstream from key regulators in *X.schlechteri* senescence subnetwork. TomTom identification of motifs in enriched sites:
A ERF096 binding site with motif conserved in all upstream regions of the WRKY TFs identified in senescence subnetwork identified by DREME and TomTom.
B EF096 binding site in upstream regions of ethylene biosynthesis genes ACC oxidase and ACC synthase identified by DREME and TomTom.
C ERF096 binding site on ERF096 upstream region identified by MEME and TomTom.
D MYB3 binding site in ERF096 upstream region identified by MEME and TomTom.
E ERF01B binding site in all upstream regions of the WRKY TFs identified in senescence subnetwork identified by DREME and TomTom.
F ERF01B binding site in upstream regions of ethylene biosynthesis genes ACC oxidase and ACC synthase identified by DREME and TomTom.

Chapter 4

A model of senescence in *Xerophyta schlechteri*: integrating insights from the physiology, metabolome and transcriptome

Mitigation of desiccation-related stress in non-senescent tissues

Like other resurrection plants, non-senescent tissue (NST) of *Xerophyta schlechteri* enters the desiccated state with a suite of protectants intended to prevent cellular death, these being summarized in Figure 1. Prior to this, with initial decrease in relative water content (RWC) to 75% signaling via abscisic acid (ABA) is evident (**Chapter 2 Fig. 6**), driving transcription of genes within the ABI3 regulon, including oleosins, seed maturation proteins and 1-Cys peroxiredoxin (PER1) (confirming data from Costa *et al.,* 2017). These protectants, in addition to late embryogenesis abundant (LEA), heat shock proteins (HSPs), especially small HSPs, and other chaperone proteins, have been proposed to stabilize macromolecules within cells (Costa *et al.,* 2017). Stabilization of proteins is crucial for their functioning in catalyzing the reactions that bring about quiescence, as well as preventing programmed cell death (PCD) signaling via the unfolded protein response (UPR) (Griffiths*, et al.* 2014). It is proposed here that photosynthetic decline brought about by water deficit, as evidenced by dramatically decreased abundance of transcripts relating to photosynthesis (**Chapter 3, Fig. 5)** and dismantling of thylakoid membranes (**Chapter 2, Fig. 4**) and diminishment of chlorophyll by 50% RWC (**Chapter 2, supplementary Fig. 1**). This cessation of photosynthesis likely prevents formation of reactive oxygen species (ROS), which have been proposed to damage cellular constituents and activate PCD signalling (Petrov *et al.,*2015). ROS are likely further mitigated by both enzymatic (increased transcript abundance of PER1 and peroxygenase) (**Chapter 3, anti-oxidants tab – Desiccome app**) and non-enzymatic anti-oxidants (chlorogenic, quinic, caffeic and aminocaproic acid) (**Chapter 2, Fig. 5**), decreasing their likelihood of signalling for PCD. Mechanical stress and potential rupture of the plasmalemma is prevented by the observed vacuolation in desiccating cells, as well as limited cell wall folding (**Chapter 2, Fig. 4**). Vitrification likely plays a role in this stabilization, as water is replaced with increasing concentrations of sucrose and other compatible solutes (**Chapter 2, Fig. 5**). Until NST reaches ~35% RWC, senescent tissue (ST) follows this same desiccation tolerance programme, deviating only in the very final stages of drying.

Signaling Senescence in *X. schlechteri*

This study revealed that cellular death during water deficit in *X. schlechteri* occurs at low water contents - within the desiccation range (20% - <5% RWC). It is proposed here that senescence is initiated in response to mounting ROS levels in severely stressed cells of the ST (modelled in **Figs 2 and 3**). These unmitigated ROS are presumably the result of activity within mitochondria, as they maintain activity of the electron transport chain (ETC) to supply the energy demands of the cell as it undergoes major structural changes required for quiescence. Enzymatic and non-enzymatic anti-oxidants are deployed, however do not successfully mitigate the ROS built up thought this energy

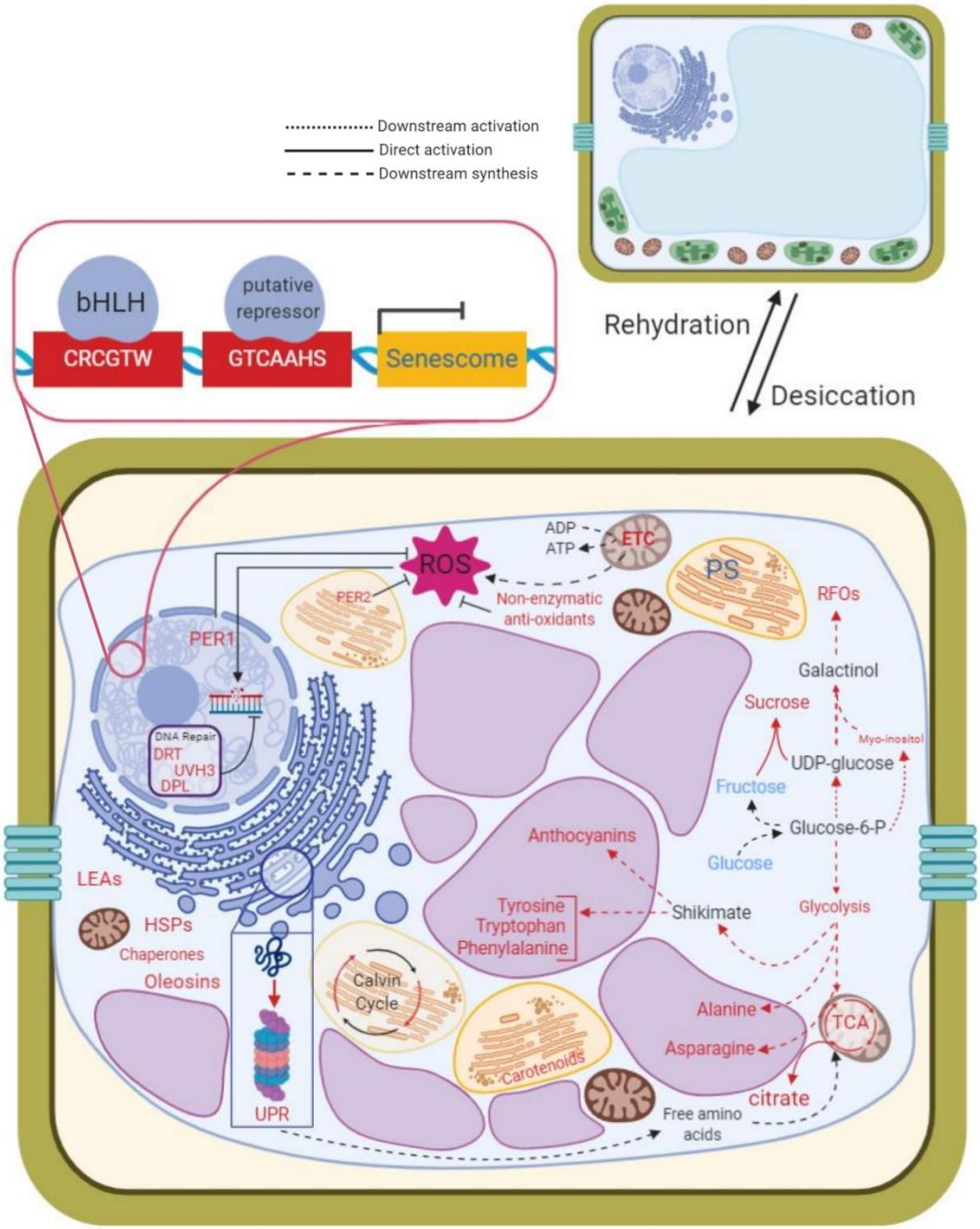

Figure 1: A model of desiccation tolerance in *X. schlechteri* leaf tissues during desiccation. Defining features of desiccation (below 35% RWC) in NST are presented here. Processes, gene products and compounds that are highly accumulated/triggered in NST relative to FT NST are shown in red; those lowly accumulated/triggered are shown in blue. The central vacuole is fragmented, and chloroplasts lose their chlorophyll, unstack their grana and accumulate plastoglobuli. Photosynthesis transcripts (PS) are diminished, and chloroplasts swell to aid in mechanical stabilization. As NST cells reach the desiccated state, they have accumulated protectants that prevent PCD on several fronts. ROS are mitigated by accumulation of enzymatic (PER1, PER2) and non-enzymatic anti-oxidants (not shown) Sugar metabolism is directed towards sucrose and RFO biosynthesis, probably in aid of vitrification. Compatible solutes (amino acids), LEAs, chaperones and sHSPs protect proteins against misfolding and overcrowding as the cell volume decreases. Oleosins accumulate to protect stored lipid bodies and DNA repair enzymes accumulate to repair UV and ROS-imposed DNA damage. Transcripts encoding enzymes of glycolysis and the TCA cycle are highly accumulated, implying that energy generation and amino acid biosynthesis proceed via these processes (further evidenced by the accumulation of asparagine, alanine and citrate). Tyrosine, phenylalanine and tryptophan are highly accumulated, as are the transcripts encoding their synthesis via the shikimate pathway. The UPR is triggered to prevent accumulation of proteins that are not essential for quiescence, and the resulting pool of free amino acids is presumably converted to asparagine for storage. Repression of Senescome genes is achieved by binding of repressors to the CRCGTW and GTCAAHS motifs in their promoter regions. Acronyms: PER1 (1-cys peroxiredoxin); PER2 (2-cys peroxiredoxin); DRT (DNA-damage-repair/toleration protein DRT111); UVH3 (ULTRAVIOLET HYPERSENSITIVE 3); DPL (Deoxyribodipyrimidine photo-lyase); PS (photosynthesis transcripts); HSP (heat shock proteins); UPR (unfolded protein response); RFO (raffinose family oligosaccharides).

generation (**Chapter 2, anti-oxidants tab – Desiccome**). ROS are known to signal PCD processes in a variety of scenarios (Petrov *et al.,* 2015). Here it is proposed that they trigger activation of MAPK6, leading to activation of WRKY6, MYB3 and ACC synthase, leading to enhanced biosynthesis of ethylene (**Chapter 3, Fig. 10**).

Considering the initiation-reorganisation-termination senescence paradigm, evidence for all three phases is present in the AD ST sampling point. Initiation (**Fig. 2**) is evidenced by the increased abundance of transcripts associated with hormone biosynthesis and transcriptional regulation (**Chapter 3, Hormones and RNA tabs – Senescome**). Signaling for this process may occur earlier in the timeline of imposed water deficit – increases in the phytohormone methyl-salicylic acid was observed from 35% RWC in this tissue (**Chapter 2, Fig. 5**), as were the transcripts encoding its biosynthesis in ST (**Chapter 3, Hormones tab – Senescome app**). Abscisic acid biosynthesis transcripts increased in abundance in the early response to drying (at 75% RWC in NST), tapering off at 55% RWC in NST. During the late stages of drying, however, they are observed to peak in AD ST (**Chapter 3, Hormones tab – Senescome app**), corresponding with an increase in abscisic acid abundance in AD ST (**Chapter 2, Fig. 6**). Similarly, ethylene biosynthesis transcripts increased in abundance in AD ST. These hormones, along with ROS, drive transcription of *Xs*SAGs (senescence-associated or Senescome genes), integrating signaling via kinases OXI1 and MAPK6 (**Chapter 3, Fig.2**).

Reorganisation (**Fig. 3**) is evidenced by an increase in transcripts to do with autophagy, correlating with an increase in trehalose abundance (**Chapter 2, Fig. 5**), a known intermediate in signalling for this process (Williams *et al.*, 2015). There is also increased expression of transporters responsible for transporting nitrogenous compounds (amino acids, peptides, nitrate) (modelled in **Figs 3 and 4**), sugars, sugar phosphates, fatty acids and ions (phosphate, potassium, sulphate, zinc) (**Fig. 3**). Termination is evidenced by the increased abundance transcripts encoding of mitochondrial uncoupling proteins, nucleases, proteases and decreased abundance of DNA repair transcripts (**Chapter 3, Senescome app**, **Fig 3**). The timeline between initiation and termination is unclear, however it is evident that this occurs between 20% RWC and AD in ST. These observations indicate that cells are undergoing this process beyond the threshold for desiccation tolerance – they employ the mechanisms for desiccation tolerance, but these are insufficient to prevent cellular death. There is evidence of controlled cellular death, however, in the observed accumulation of pro-senescence hormones and transcripts encoding their biosynthesis. This indicates that cellular death is not accidental but controlled and regulated in the near air-dry state and continues following rehydration.

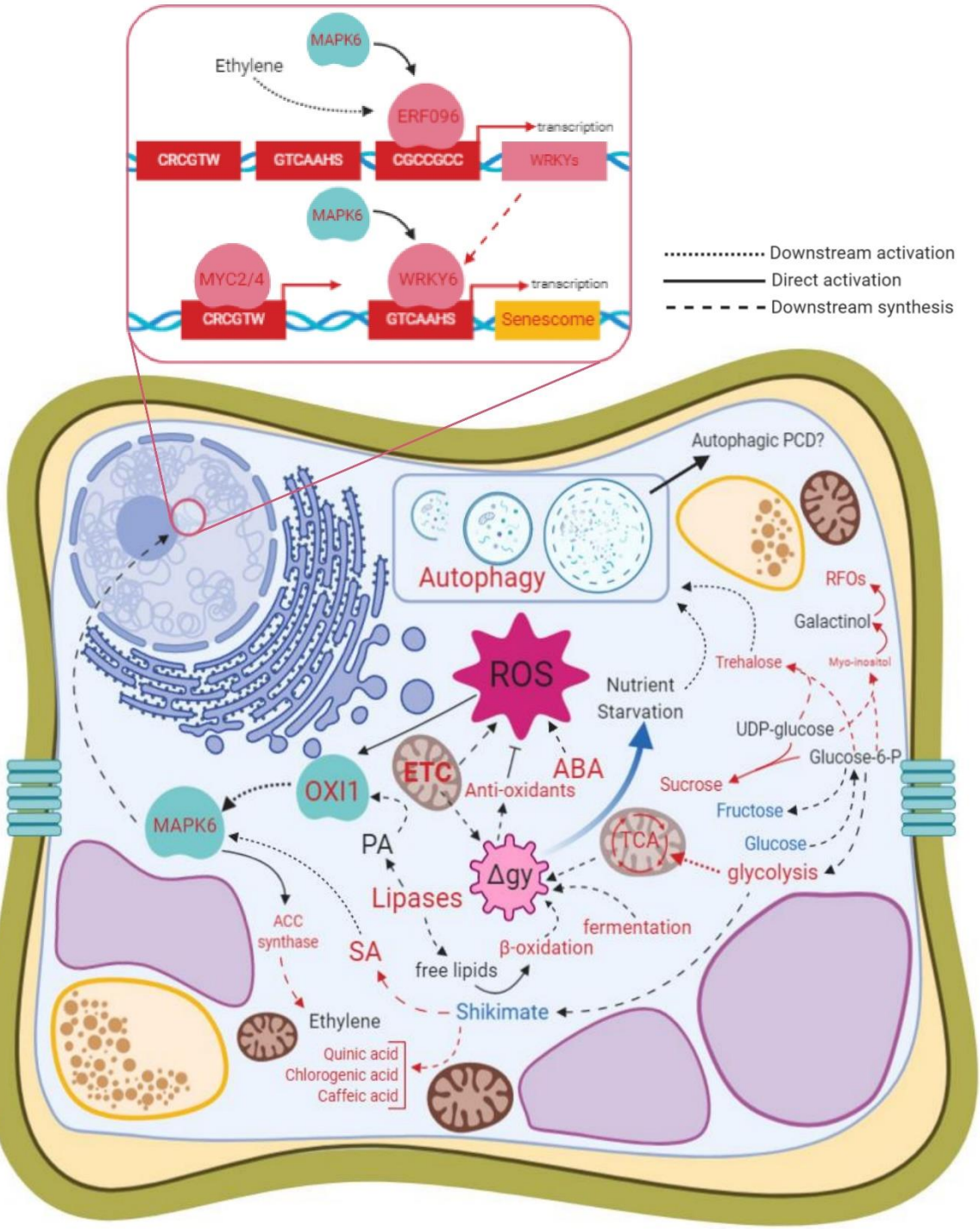

Figure 2: A model of senescence initiation in *X. schlechteri* apical leaf tissues approaching desiccation. Defining features of senescence initiation at ≤20% RWC in ST are presented here. Processes, gene products and compounds that are highly accumulated/triggered in AD ST relative to AD NST are shown in red; those lowly accumulated/triggered are shown in blue. Unmitigated ROS (dark pink star) are proposed here as a crucial signal for initiation of PCD processes. Energy in the form of NAD(P)H and ATP (pink cog) is required for synthesis of anti-oxidants (both enzymatic and non-enzymatic) to mitigate these ROS, as well as for functioning of other pro-life strategies, such as functioning of the UPR (not shown). Increases in transcripts encoding beta-oxidation and fermentation pathway enzymes indicate that cells are struggling to meet the energetic demands of the imposed stress. This increasingly insurmountable unmitigated ROS directly activates OXI1, triggering downstream activation of MAPK6. MAPK6 stimulates ethylene synthesis via activation of ACC synthase and transcription of WRKY TFs via ERF096, exacerbating expression of these pro-death regulators. MAPK6 is additionally responsive to salicylic acid (SA) and OXI1 to phosphatidic acid (PA) released as a by-product of the action of lipases. WRKY TFs, including WRKY6, drive expression of Senescome genes, including those encoding autophagosome components. Simultaneously, sugar metabolism is directed towards synthesis of protective compounds (RFOs and sucrose) but also towards trehalose, a proposed positive signal transducer for autophagy in resurrection plants. Acronyms: ACC (1-aminocyclopropane-1-carboxylate); OXI1 (OXIDATIVE SIGNAL-INDUCIBLE 1); TCA (tri-carboxylic acid cycle); ETC (electron transport chain); ABA (abscisic acid); MAPK6 (mitogen-activated protein kinase 6); RFOs (raffinose family oligosaccharides); Δgy (energy in the form of ATP and NAD(P)H)

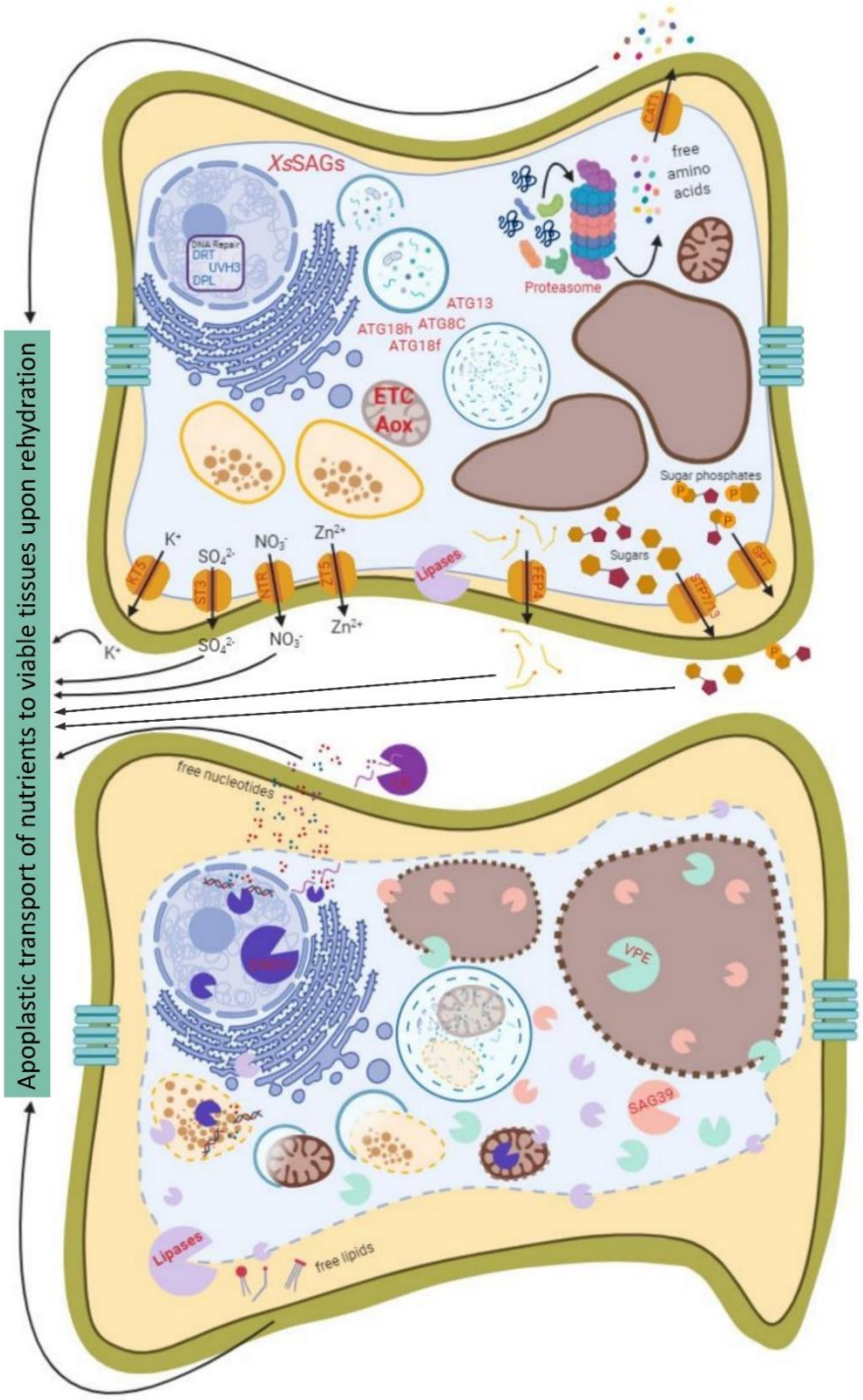

Figure 3: A model of reorganisation, termination and nutrient redistribution. In response to the action of WRKY TFs and ethylene, *Xs*SAGs (Senescome genes) increase in expression. Among these are a number of transporters including amino acid transporter (CAT1; cationic amino acid transporter 1), potassium transporter 5 (KT5), sulphate transporter 3 (ST3), nitrate transport proteins (NTP; NRT1/ PTR FAMILY 7.3 and 4.6), fatty acid export protein 4 (FEP4), sugar transfer protein (STP7 and 13) and sugar phosphate transporters (SPT; homologues of At3g11320 and At5g25400). Proteasome transcripts increase, indicating degradation of proteins for transport of free amino acids. Lipases (phospholipases A1, C1 and D) release free lipids and phosphatidic acid. It is proposed here that these nutrients are externalised from senesced cells until rehydration, whereupon they are transported to viable tissues apoplastically. With termination comes activity of endonuclease 1 (ENDO1), which cleaves both DNA and RNA non-specifically. Extracellular ribonuclease (LE) cleaves extracellular RNA that may leak from perished cells. These free nucleotides are transported apoplastically along with the other nutrients to viable tissues during rehydration. Vacuolar processing enzyme (VPE) and senescence-specific cystein protease (SAG39) lyse the vacuole and any remaining proteins in the cells. Autophagosome transcripts increase in abundance, concomitant with the appearance of macroautophagy visible in rehydrated ST, suggesting that autophagic PCD may play a role in senescence. Cell wall collapse, disruption of the plasmalemma and shrinkage of the cytoplasm herald the irredeemable demise of the cell. Acronyms: ATG (autophagy-related protein); Aox (alternative oxidase); ETC (electron transport chain).

How NST prevents senescence

As ethylene is synthesised and released as a volatile compound from senescent cells, this signal is perceived by neighbouring cells. In cells of a certain developmental age, this signal is perceived and transduced to induce gene expression of Senescome genes (or *Xs*SAGs). Because NST cells are developmentally younger than ST cells, it is likely this signal does not affect them. A potential mechanism for this repression of *Xs*SAG expression has been proposed here – the competitive binding of group IIId bHLH transcription factors to the CRCGTW motif upstream from most genes in the senescence subnetwork, or alternatively, binding of repressors to the GTCAAHS motif in NST cells (**Chapter 3, Fig. 8**). Additionally, it was reported here that cells of the NST repress synthesis of salicylic acid and ABA during late stages of drying (**Chapter 2, Fig. 5,6**), preventing expression of SAGs driven by these hormones (Woo *et al.,*2019). It is also possible that repressors act on the signal transduction level, through binding of repressors to signal transducers like MAPK6 or OXI1, or via small non-coding RNAs which act upon transcription factors to regulate their function (reviewed by Woo *et al.,*(2019)).

As mentioned in **Chapter 1**, the anti-oxidant status of resurrection plants is the main determinant in their revival after desiccation (Kranner *et al.,*2002). Younger cells may simply be more plastic in their ability to efficiently switch into desiccation tolerance programming than older cells, leading to more efficient mitigation of ROS as cells enter quiescence, as well as prevention of their accumulation altogether.

Nutrient remobilisation

As senescence was observed below RWC values of 20%, it is highly unlikely that nutrients are mobilised and taken up by viable tissues at the time of death. A number of nutrient transporters are highly expressed in AD ST (**Chapter 3, Transport tab – Senescome; Fig. 3, 4**), some exclusively at this sampling point, indicating that an attempt is indeed made to release nutrients for remobilisation. Some transporters responsible for the retrieval of nutrients were found to be only highly expressed in viable tissues at this sampling point, indicating directionality of nutrient flow from ST to NST/PST (**Fig. 4**). Because of the degree of water deficit experienced by the plant when this process is initiated, it is most likely that nutrients are exported into the apoplast and transported to viable tissues upon rehydration.

Implications of this research and future work

This is the first piece of work done to demonstrate how senescence may be regulated on the transcriptional level. Outstanding questions to be answered exist on multiple levels (see text box

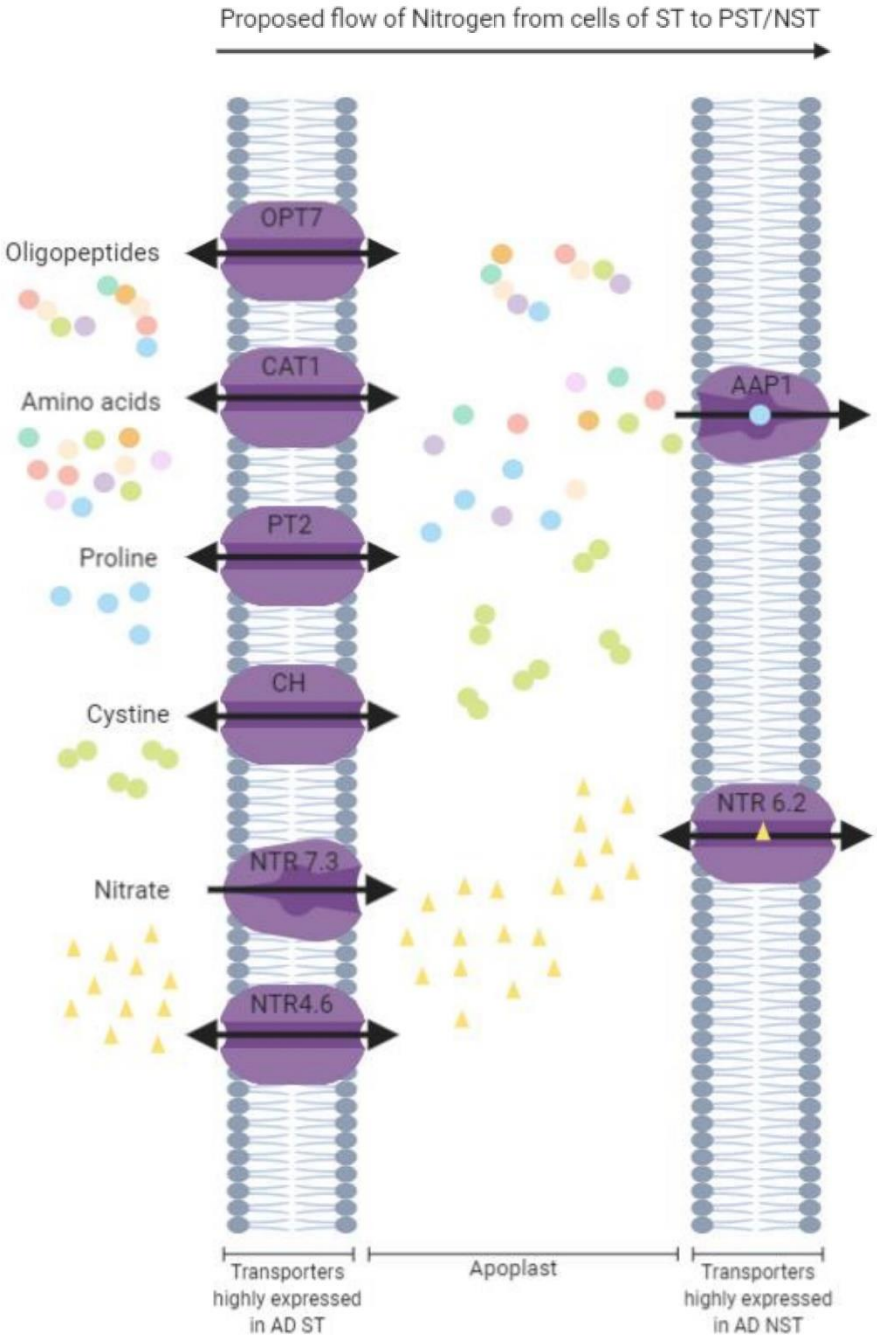

Figure 4: Proposed mechanism for transport of nitrogenous compounds to NST via the apoplast during senescence. Cells of the ST (represented by the membrane on the left) upregulate expression of oligopeptide transporter 7 (OPT7), cationic amino acid transferase 1 (CAT1), proline transporter 2 (PT2), cytinosin homologue (CH) and nitrate transporters (NTR 4.3 and 4.6), while cells of the NST upregulated expression of unidirectional amino acid permease 1 (AAP1) and nitrate transporter (NTR 6.2).

below). This work can be the point of departure for several projects. Of great interest to me is determining which transcriptional regulators are indeed binding to the identified GTCAAHS and CRCGTW motifs in both ST and NST. Binding assays such as yeast 1 hybrid screens can be utilised to determine binding, as well as promoter-reporter and functional assays in *A.thaliana* (due to the high degree of homology).Another alternative is to perform ChIP (chromatin immunoprecipitation) assays, targeting potential transcriptional regulators (e.g. bHLH13, MYC4, WRKY6 and ERF096) and sequencing the DNA they are bound to. It will also be interesting to investigate whether repression of signalling via MAPK6 plays a role in repression of these genes in NST. Co-immunoprecipitation with MAPK6 and OXI1 might provide insights into this regulation. It will also be interesting to research the role of microRNAs in the regulation of senescence in resurrection plants.

Outstanding Questions:

Physiological Level:

1. Are unmitigated ROS triggers for leaf senescence in *X. schlechteri*?
2. Does programmed cell death of root tissue occur during desiccation?
3. How does the water potential of the plant change during leaf senescence?

Molecular Level:

1. What factors influence repression of senescence gene expression in NST?
2. What factors influence signal transduction in NST to repress senescence?
3. Can autophagic cellular death be demonstrated in this species?

Answers to these questions will aid in design of system for prevention of senescence processes in response to water deficit in monocots. This theoretical senescence prevention mechanism (for example enhanced expression of the theoretical transcriptional repressor of the CRCGTW motif upstream of senescence genes) could be deployed in conjunction with a mechanism to prevent ROS accumulation (such as enhanced expression of anti-oxidants) and a strategy to stabilize macromolecules (such as enhanced expression of LEA and HSP proteins). Such a multi-pronged approach could be deployed or engineered in drought sensitive crops, through a transient or stable expression system (depending on the environmental conditions, regulations of the country, duration of the stress, etc.) for enhanced stress tolerance. A systems biology approach is essential to improve stress tolerance, integrating information on the molecular, physiological and ecological levels to meet the demands of unique food security challenges. How and when to deploy technologies for improved

stress tolerance in crops is context-specific: these technologies need to be tailored to meet the needs of specific communities.

References

Abreu, M. Elizabeth, and Sergi Munné-Bosch. 2008. “Salicylic Acid May Be Involved in the Regulation of Drought-Induced Leaf Senescence in Perennials: A Case Study in Field-Grown *Salvia Officinalis* L. Plants.” *Environmental and Experimental Botany* 64 (2): 105–12. https://doi.org/10.1016/j.envexpbot.2007.12.016.

Alden, Keith P., Sandrine Dhondt-Cordelier, Kerrie L. McDonald, Theresa J. Reape, Carl K.Y. Ng, Paul F. McCabe, and Christopher J. Leaver. 2011. “Sphingolipid Long Chain Base Phosphates Can Regulate Apoptotic-like Programmed Cell Death in Plants.” *Biochemical and Biophysical Research Communications* 410 (3): 574–80. https://doi.org/10.1016/j.bbrc.2011.06.028.

Artur, Mariana Aline Silva, Tao Zhao, Wilco Ligterink, Eric Schranz, and Henk W.M. Hilhorst. 2019. “Dissecting the Genomic Diversification of Late Embryogenesis Abundant (LEA) Protein Gene Families in Plants.” *Genome Biology and Evolution* 11 (2): 459–71. https://doi.org/10.1093/gbe/evy248.

Asami, Pauline, Thusitha Rupasinghe, Lalehvash Moghaddam, Isaac Njaci, Ute Roessner, Sagadevan Mundree, and Brett Williams. 2019. “Roots of the Resurrection Plant *Tripogon loliiformis* Survive Desiccation Without the Activation of Autophagy Pathways by Maintaining Energy Reserves.” *Frontiers in Plant Science* 10 (April). https://doi.org/10.3389/fpls.2019.00459.

Bailey, Timothy L. 2011. “DREME: Motif Discovery in Transcription Factor ChIP-Seq Data.” *Bioinformatics* 27 (12): 1653–59. https://doi.org/10.1093/bioinformatics/btr261.

Bailey, Timothy L., Mikael Boden, Fabian A. Buske, Martin Frith, Charles E. Grant, Luca Clementi, Jingyuan Ren, Wilfred W. Li, and William S. Noble. 2009. “MEME Suite: Tools for Motif Discovery and Searching.” *Nucleic Acids Research* 37 (SUPPL. 2): W202–8. https://doi.org/10.1093/nar/gkp335.

Balazadeh, S, D M Riaño-Pachón, and B Mueller-Roeber. 2008. “Transcription Factors Regulating Leaf Senescence in *Arabidopsis Thaliana*.” *Plant Biology* 10(S1) (September): 63–75. https://doi.org/10.1111/j.1438-8677.2008.00088.x.

Bannenberg, Gerard, Marta Martínez, Mats Hamberg, and Carmen Castresana. 2009. “Diversity of the Enzymatic Activity in the Lipoxygenase Gene Family of *Arabidopsis Thaliana*.” *Lipids* 44 (2): 85–95. https://doi.org/10.1007/s11745-008-3245-7.

Bartels, Dorothea, and Syed Sarfraz Hussain. 2011. “Resurrection Plants: Physiology and Molecular Biology.” In *Plant Desiccation Tolerance, Ecological Studies*, 215:339–64. https://doi.org/10.1007/978-3-642-19106-0.

Bartolozzi, Francesco, Gianpaolo Bertazza, Daniele Bassi, and Graziella Cristoferi. 1997. “Simultaneous Determination of Soluble Sugars and Organic Acids as Their Trimethylsilyl Derivatives in Apricot Fruits by Gas-Liquid Chromatography.” *Journal of Chromatography A* 758 (1): 99–107. https://doi.org/10.1016/S0021-9673(96)00709-1.

Berjak, Patricia. 2006. “Unifying Perspectives of Some Mechanisms Basic to Desiccation Tolerance across Life Forms.” *Seed Science Research* 16 (1): 1–15. https://doi.org/10.1079/ssr2005236.

Bibhuti Bhusan Mishra, Bibhuti x. 2016. “Polyphenol Oxidases: Biochemical and Molecular Characterization, Distribution, Role and Its Control.” *Enzyme Engineering* 05 (01): 1–9. https://doi.org/10.4172/2329-6674.1000141.

Bleecker, Anthony B., Mark A. Estelle, Chris Somerville, and Hans Kende. 1988. “Insensitivity to Ethylene Conferred by a Dominant Mutation in *Arabidopsis Thaliana*.” *Science* 241 (4869): 1086–

89. https://doi.org/10.1126/science.241.4869.1086.

Blum, Abraham, and Roberto Tuberosa. 2018. “Dehydration Survival of Crop Plants and Its Measurement.” *Journal of Experimental Botany* 69 (5): 975–81. https://doi.org/10.1093/jxb/erx445.

Bohner, Anne, Soichi Kojima, Mohammad Hajirezaei, Michael Melzer, and Nicolaus Von Wirén. 2015. “Urea Retranslocation from Senescing Arabidopsis Leaves Is Promoted by DUR3-Mediated Urea Retrieval from Leaf Apoplast.” *Plant Journal* 81 (3): 377–87. https://doi.org/10.1111/tpj.12740.

Bonawitz, Nicholas D., Whitney L. Soltau, Michael R. Blatchley, Brendan L. Powers, Anna K. Hurlock, Leslie A. Seals, Jing Ke Weng, Jake Stout, and Clint Chapple. 2012. “REF4 and RFR1, Subunits of the Transcriptional Coregulatory Complex Mediator, Are Required for Phenylpropanoid Homeostasis in Arabidopsis.” *Journal of Biological Chemistry* 287 (8): 5434–45. https://doi.org/10.1074/jbc.M111.312298.

Breeze, Emily, Elizabeth Harrison, Stuart McHattie, Linda Hughes, Richard Hickman, Claire Hill, Steven Kiddle, *et al.,*2011. “High-Resolution Temporal Profiling of Transcripts during Arabidopsis Leaf Senescence Reveals a Distinct Chronology of Processes and Regulation.” *The Plant Cell* 23 (3): 873–94. https://doi.org/10.1105/tpc.111.083345.

Bresson, Justine, Stefan Bieker, Lena Riester, Jasmin Doll, and Ulrike Zentgraf. 2018. “A Guideline for Leaf Senescence Analyses: From Quantification to Physiological and Molecular Investigations.” *Journal of Experimental Botany* 69 (4): 769–86. https://doi.org/10.1093/jxb/erx246.

Buchanan-Wollaston, Vicky, Tania Page, Elizabeth Harrison, Emily Breeze, Ok Lim Pyung, Gil Nam Hong, Ji Feng Lin, *et al.,*2005. “Comparative Transcriptome Analysis Reveals Significant Differences in Gene Expression and Signalling Pathways between Developmental and Dark/Starvation-Induced Senescence in Arabidopsis.” *Plant Journal* 42 (4): 567–85. https://doi.org/10.1111/j.1365-313X.2005.02399.x.

Chai, Jinyu, Jian Liu, Jun Zhou, and Da Xing. 2014. “Mitogen-Activated Protein Kinase 6 Regulates NPR1 Gene Expression and Activation during Leaf Senescence Induced by Salicylic Acid.” *Journal of Experimental Botany* 65 (22): 6513–28. https://doi.org/10.1093/jxb/eru369.

Challabathula, Dinakar, Jos T. Puthur, and Dorothea Bartels. 2016. “Surviving Metabolic Arrest: Photosynthesis during Desiccation and Rehydration in Resurrection Plants.” *Annals of the New York Academy of Sciences* 1365 (1): 89–99. https://doi.org/10.1111/nyas.12884.

Challabathula, Dinakar, Qingwei Zhang, and Dorothea Bartels. 2018. “Protection of Photosynthesis in Desiccation-Tolerant Resurrection Plants.” *Journal of Plant Physiology* 227 (April): 84–92. https://doi.org/10.1016/j.jplph.2018.05.002.

Chong, Jasmine, Othman Soufan, Carin Li, Iurie Caraus, Shuzhao Li, Guillaume Bourque, David S. Wishart, and Jianguo Xia. 2018. “MetaboAnalyst 4.0: Towards More Transparent and Integrative Metabolomics Analysis.” *Nucleic Acids Research* 46 (W1): W486–94. https://doi.org/10.1093/nar/gky310.

Christ, Bastien, Aurélie Egert, Iris Süssenbacher, Bernhard Kräutler, Dorothea Bartels, Shaun Peters, and Stefan Hörtensteiner. 2014. “Water Deficit Induces Chlorophyll Degradation via the ‘ PAO / Phyllobilin ’ Pathway in Leaves of Homoio- (*Craterostigma Pumilum*) and Poikilochlorophyllous (*Xerophyta viscosa*) Resurrection Plants.” *Plant, Cell & Environment* 37(11): 2521–31. https://doi.org/10.1111/pce.12308.

Cimini, Sara, Carla Gualtieri, Anca Macovei, Alma Balestrazzi, Laura De Gara, and Vittoria Locato. 2019. “Redox Balance-DDR-MiRNA Triangle: Relevance in Genome Stability and Stress Responses in

Plants." *Frontiers in Plant Science* 10 (August): 1–22. https://doi.org/10.3389/fpls.2019.00989.

Coll, Nuria S, Dominique Vercammen, Andrea Smidler, Charles Clover, Van Breusegem, Jeffery L Dangl, and Petra Epple. 2017. "Arabidopsis Type I Metacaspases Control Cell Death." *Science* 330 (6009): 1393–97. DOI: 10.1126/science.1194980

Corratgé-Faillie, Claire, and Benoît Lacombe. 2017. "Substrate (Un)Specificity of Arabidopsis NRT1/PTR FAMILY (NPF) Proteins." *Journal of Experimental Botany* 68 (12): 3107–13. https://doi.org/10.1093/jxb/erw499.

*Costa, Maria Cecília D., Mariana A.S. Artur, Julio Maia, Eef Jonkheer, Martijn F.L. Derks, Harm Nijveen, Brett Williams, *et al.,*2017. "A Footprint of Desiccation Tolerance in the Genome of *Xerophyta viscosa*." *Nature Plants* 3 (March). https://doi.org/10.1038/nplants.2017.38.

Costa, Maria Cecília D., Jill M. Farrant, Melvin J. Oliver, Wilco Ligterink, Julia Buitink, and Henk M.W. Hilhorst. 2016. "Key Genes Involved in Desiccation Tolerance and Dormancy across Life Forms." *Plant Science* 251: 162–68. https://doi.org/10.1016/j.plantsci.2016.02.001.

Cruz De Carvalho, Maria Helena. 2008. "Drought Stress and Reactive Oxygen Species: Production, Scavenging and Signaling." *Plant Signaling and Behavior* 3 (3): 156–65. https://doi.org/10.4161/psb.3.3.5536.

Dace, H., Heather W. Sherwin, N. Illing, and Jill M. Farrant. 1998. "Use of Metabolic Inhibitors to Elucidate Mechanisms of Recovery from Desiccation Stress in the Resurrection Plant *Xerophyta humilis*." *Plant Growth Regulation* 24 (3): 171–77. https://doi.org/10.1023/A:1005883907800.

Dai, Cheng, Yuree Lee, In C. Lee, Hong G. Nam, and June M. Kwak. 2018. "Calmodulin 1 Regulates Senescence and ABA Response in Arabidopsis." *Frontiers in Plant Science* 9 (July): 1–13. https://doi.org/10.3389/fpls.2018.00803.

Dai, Yuntao, Jaap van Spronsen, Geert Jan Witkamp, Robert Verpoorte, and Young Hae Choi. 2013. "Natural Deep Eutectic Solvents as New Potential Media for Green Technology." *Analytica Chimica Acta* 766: 61–68. https://doi.org/10.1016/j.aca.2012.12.019.

Davletova, Sholpan, Karen Schlauch, Jesse Coutu, and Ron Mittler. 2005. "The Zinc-Finger Protein Zat12 Plays a Central Role in Reactive Oxygen and Abiotic Stress Signaling in Arabidopsis" 139 (October): 847–56. https://doi.org/10.1104/pp.105.068254.1.

Dickman, Martin, Brett Williams, Yurong Li, Paul Figueiredo, and Thomas Wolpert. 2017. "Reassessing Apoptosis in Plants." *Nature Plants* 3 (10): 773–79. https://doi.org/10.1038/s41477-017-0020-x.

Dieryckx, Cindy, Vanessa Gaudin, Jean-William Dupuy, Marc Bonneu, Vincent Girard, and Dominique Job. 2015. "Beyond Plant Defense: Insights on the Potential of Salicylic and Methylsalicylic Acid to Contain Growth of the Phytopathogen *Botrytis Cinerea*." *Frontiers in Plant Science* 6 (October). https://doi.org/10.3389/fpls.2015.00859.

Dinakar, Challabathula, and Dorothea Bartels. 2013. "Desiccation Tolerance in Resurrection Plants: New Insights from Transcriptome, Proteome and Metabolome Analysis." *Frontiers in Plant Science* 4 (November): 1–14. https://doi.org/10.3389/fpls.2013.00482.

Dinkeloo, Kasia, Shelton Boyd, and Guillaume Pilot. 2018. "Update on Amino Acid Transporter Functions and on Possible Amino Acid Sensing Mechanisms in Plants." *Seminars in Cell and Developmental Biology* 74: 105–13. https://doi.org/10.1016/j.semcdb.2017.07.010.

Djilianov, D., T. Georgieva, D. Moyankova, A. Atanassov, K. Shinozaki, S. C.M. Smeeken, D. P.S. Verma, and N. Murata. 2005. "Improved Abiotic Stress Tolerance in Plants by Accumulation of Osmoprotectants—Gene Transfer Approach." *Biotechnology and Biotechnological Equipment*

19: 63–71. https://doi.org/10.1080/13102818.2005.10817287.

Do, Cao Trung, Brigitte Pollet, Johanne Thévenin, Richard Sibout, Dominique Denoue, Yves Barrière, Catherine Lapierre, and Lise Jouanin. 2007. "Both Caffeoyl Coenzyme A 3-O-Methyltransferase 1 and Caffeic Acid O-Methyltransferase 1 Are Involved in Redundant Functions for Lignin, Flavonoids and Sinapoyl Malate Biosynthesis in Arabidopsis." *Planta* 226 (5): 1117–29. https://doi.org/10.1007/s00425-007-0558-3.

Doorn, Wouter G. Van. 2011. "Classes of Programmed Cell Death in Plants, Compared to Those in Animals." *Journal of Experimental Botany* 62 (14): 4749–61. https://doi.org/10.1093/jxb/err196.

Duan, Yunfeng, Wensheng Zhang, Bao Li, Youning Wang, Kexue Li, T. Sodmergen, Chunyu Han, Yizhang Zhang, and Xia Li. 2010. "An Endoplasmic Reticulum Response Pathway Mediates Programmed Cell Death of Root Tip Induced by Water Stress in Arabidopsis." *New Phytologist* 186 (3): 681–95. https://doi.org/10.1111/j.1469-8137.2010.03207.x.

Farage-Barhom, Sarit, Shaul Burd, Lilian Sonego, Rafael Perl-Treves, and Amnon Lers. 2008. "Expression Analysis of the BFN1 Nuclease Gene Promoter during Senescence, Abscission, and Programmed Cell Death-Related Processes." *Journal of Experimental Botany* 59 (12): 3247–58. https://doi.org/10.1093/jxb/ern176.

*Farrant, Jill M, Wolf Brandt, and George G Lindsey. 2007. "An Overview of Mechanisms of Desiccation Tolerance in Selected Angiosperm Resurrection Plants." *Plant Stress*. https://www.semanticscholar.org/paper/An-overview-of-mechanisms-of-desiccation-tolerance-Farrant-Brandt/b812c9a1370d125b91af265dbd2f417b4329a9df

*Farrant, Jill M, Keren Cooper, Amelia Hilgart, Kamal O Abdalla, Sagadevan G Mundree, and Mohamed S Rafudeen. 2015. "A Molecular Physiological Review of Vegetative Desiccation Tolerance in the Resurrection Plant *Xerophyta viscosa* (Baker)." *Planta* 242 (2): 407–26. https://doi.org/10.1007/s00425-015-2320-6.

Floková, Kristýna, Danuše Tarkowská, Otto Miersch, Miroslav Strnad, Claus Wasternack, and Ondřej Novák. 2014. "UHPLC-MS/MS Based Target Profiling of Stress-Induced Phytohormones." *Phytochemistry* 105: 147–57. https://doi.org/10.1016/j.phytochem.2014.05.015.

Foyer, Christine H. 2018. "Reactive Oxygen Species, Oxidative Signaling and the Regulation of Photosynthesis." *Environmental and Experimental Botany* 154 (April): 134–42. https://doi.org/10.1016/j.envexpbot.2018.05.003.

Fujimoto, Susan Y., Masaru Ohta, Akemi Usui, Hideaki Shinshi, and Masaru Ohme-Takagi. 2000. "Arabidopsis Ethylene-Responsive Element Binding Factors Act as Transcriptional Activators or Repressors of GCC Box-Mediated Gene Expression." *Plant Cell* 12 (3): 393–404. https://doi.org/10.1105/tpc.12.3.393.

Gaff, Donald F., Cecilia K. Blomstedt, Alan D. Neale, Tuan N. Le, John D. Hamill, and Hamid R. Ghasempour. 2009. "Sporobolus Stapfianus, a Model Desiccation-Tolerant Grass." *Functional Plant Biology* 36 (7): 589–99. https://doi.org/10.1071/FP08166.

Gaff, Donald F. 1977. "Desiccation Tolerant Vascular Plants of Southern Africa." *Oecologia* 31 (1): 95–109.

Gasber, A., S. Klaumann, O. Trentmann, A. Trampczynska, S. Clemens, S. Schneider, N. Sauer, *et al.,*2011. "Identification of an Arabidopsis Solute Carrier Critical for Intracellular Transport and Inter-Organ Allocation of Molybdate." *Plant Biology* 13 (5): 710–18. https://doi.org/10.1111/j.1438-8677.2011.00448.x.

Gechev, Tsanko S., Challabathula Dinakar, Maria Benina, Valentina Toneva, and Dorothea Bartels.

2012. “Molecular Mechanisms of Desiccation Tolerance in Resurrection Plants.” *Cellular and Molecular Life Sciences* 69 (19): 3175–86. https://doi.org/10.1007/s00018-012-1088-0.

Giarola, Valentino, Stephanie Krey, Barbara von den Driesch, and Dorothea Bartels. 2016. “The *Craterostigma Plantagineum* Glycine-Rich Protein CpGRP1 Interacts with a Cell Wall-Associated Protein Kinase 1 (CpWAK1) and Accumulates in Leaf Cell Walls during Dehydration.” *New Phytologist* 210 (2): 535–50. https://doi.org/10.1111/nph.13766.

Golldack, Dortje, Olga V. Popova, and Karl Josef Dietz. 2002. “Mutation of the Matrix Metalloproteinase At2-MMP Inhibits Growth and Causes Late Flowering and Early Senescence in Arabidopsis.” *Journal of Biological Chemistry* 277 (7): 5541–47. https://doi.org/10.1074/jbc.M106197200.

Graaff, Eric Van Der, Rainer Schwacke, Anja Schneider, Marcelo Desimone, Ulf Ingo Flügge, and Reinhard Kunze. 2006. “Transcription Analysis of Arabidopsis Membrane Transporters and Hormone Pathways during Developmental and Induced Leaf Senescence.” *Plant Physiology* 141 (2): 776–92. https://doi.org/10.1104/pp.106.079293.

Graham, Laura E., Jos H M Schippers, Paul P. Dijkwel, and Carol Wagstaff. 2012. "Ethylene and Senescence Processes." *Annual Plant Reviews* 44. https://doi.org/10.1002/9781118223086.ch12.

Graindorge, Matthieu, Cécile Giustini, Anne Claire Jacomin, Alexandra Kraut, Gilles Curien, and Michel Matringe. 2010. “Identification of a Plant Gene Encoding Glutamate/Aspartate-Prephenate Aminotransferase: The Last Homeless Enzyme of Aromatic Amino Acids Biosynthesis.” *FEBS Letters* 584 (20): 4357–60. https://doi.org/10.1016/j.febslet.2010.09.037.

Griffiths, Cara a, Donald F Gaff, and Alan D Neale. 2014. “Drying without Senescence in Resurrection Plants.” *Frontiers in Plant Science* 5 (February): 36. https://doi.org/10.3389/fpls.2014.00036.

Guidetti, Roberto, Angela Maria Rizzo, Tiziana Altiero, and Lorena Rebecchi. 2012. “What Can We Learn from the Toughest Animals of the Earth? Water Bears (Tardigrades) as Multicellular Model Organisms in Order to Perform Scientific Preparations for Lunar Exploration.” *Planetary and Space Science* 74 (1): 97–102. https://doi.org/10.1016/j.pss.2012.05.021.

Guo, Woei Jiun, and Tuan Hua David Ho. 2008. “An Abscisic Acid-Induced Protein, HVA22, Inhibits Gibberellin-Mediated Programmed Cell Death in Cereal Aleurone Cells.” *Plant Physiology* 147 (4): 1710–22. https://doi.org/10.1104/pp.108.120238.

Gupta, Shobhit, John A. Stamatoyannopoulos, Timothy L. Bailey, and William Stafford Noble. 2007. “Quantifying Similarity between Motifs.” *Genome Biology* 8 (R24). https://doi.org/10.1186/gb-2007-8-2-r24.

Hatsugai, Noriyuki, Kenji Yamada, Shino Goto-Yamada, and Ikuko Hara-Nishimura. 2015. “Vacuolar Processing Enzyme in Plant Programmed Cell Death.” *Frontiers in Plant Science* 6 (Apr): 1–11. https://doi.org/10.3389/fpls.2015.00234.

Havé, Marien, Anne Marmagne, Fabien Chardon, and Céline Masclaux-Daubresse. 2017. “Nitrogen Remobilization during Leaf Senescence: Lessons from Arabidopsis to Crops.” *Journal of Experimental Botany* 68 (10): 2513–29. https://doi.org/10.1093/jxb/erw365.

Houben, Maarten, and Bram Van de Poel. 2019. “1-Aminocyclopropane-1-Carboxylic Acid Oxidase (ACO): The Enzyme That Makes the Plant Hormone Ethylene.” *Frontiers in Plant Science* 10 (May): 1–15. https://doi.org/10.3389/fpls.2019.00695.

Hsieh, En Jung, Mei Chun Cheng, and Tsan Piao Lin. 2013. “Functional Characterization of an Abiotic Stress-Inducible Transcription Factor AtERF53 in *Arabidopsis Thaliana*.” *Plant Molecular Biology*

82 (3): 223–37. https://doi.org/10.1007/s11103-013-0054-z.

Ingle, Robert, U.G. Schmidt, J.M. Farrant, J.A. Thomson, and S.G. Mundree. 2007. “Proteomic Analysis of Leaf Proteins during Dehydration Ofthe Resurrection Plant *Xerophyta viscosa*.” *Plant, Cell and Environment* 30: 435–46. doi: 10.1111/j.1365-3040.2006.01631.x

Jardine, A. 2019. “DataTables.” 2019. http://datatables.net.

Jiang, Guoqiang, Zhi Wang, Haihong Shang, Wenlong Yang, Zhiang Hu, Jonathan Phillips, and Xin Deng. 2007. “Proteome Analysis of Leaves from the Resurrection Plant *Boea Hygrometrica* in Response to Dehydration and Rehydration.” *Planta* 225 (6): 1405–20. https://doi.org/10.1007/s00425-006-0449-z.

Jing, Hai Chun, Jos H.M. Schippers, Jacques Hille, and Paul P. Dijkwel. 2005. “Ethylene-Induced Leaf Senescence Depends on Age-Related Changes and OLD Genes in Arabidopsis.” *Journal of Experimental Botany* 56 (421): 2915–23. https://doi.org/10.1093/jxb/eri287.

Jing, Hai Chun, Marcel J.G. Sturre, Jacques Hille, and Paul P. Dijkwel. 2002. “Arabidopsis Onset of Leaf Death Mutants Identify a Regulatory Pathway Controlling Leaf Senescence.” *Plant Journal* 32 (1): 51–63. https://doi.org/10.1046/j.1365-313X.2002.01400.x.

Jung, Niklas Udo, Valentino Giarola, Peilei Chen, J. Paul Knox, and Dorothea Bartels. 2019. “ *Craterostigma Plantagineum* Cell Wall Composition Is Remodelled during Desiccation and the Glycine-rich Protein Cp GRP 1 Interacts with Pectins through Clustered Arginines .” *The Plant Journal*, 1–16. https://doi.org/10.1111/tpj.14479.

Kalatzis, Vasiliki, Stéphanie Cherqui, Corinne Antignac, and Bruno Gasnier. 2001. “Cystinosin, the Protein Defective in Cystinosis, Is a H+-Driven Lysosomal Cystine Transporter.” *EMBO Journal* 20 (21): 5940–49. https://doi.org/10.1093/emboj/20.21.5940.

Karbaschi, Mohammad Reza, Brett Williams, Acram Taji, and Sagadevan G. Mundree. 2016. “*Tripogon loliiformis* Elicits a Rapid Physiological and Structural Response to Dehydration for Desiccation Tolerance.” *Functional Plant Biology* 43 (7): 643–55. https://doi.org/10.1071/FP15213.

Kim, Jeongsik, Jin Hee Kim, Jae Il Lyu, Hye Ryun Woo, and Pyung Ok Lim. 2018. “New Insights into the Regulation of Leaf Senescence in Arabidopsis.” *Journal of Experimental Botany* 69 (4): 787–99. https://doi.org/10.1093/jxb/erx287.

Kogan, Felix, Wei Guo, and Wenze Yang. 2019. “Drought and Food Security Prediction from NOAA New Generation of Operational Satellites.” *Geomatics, Natural Hazards and Risk* 10 (1): 651–66. https://doi.org/10.1080/19475705.2018.1541257.

Kranner, Ilse, Richard P. Beckett, Sabine Wornik, Margret Zorn, and Hartwig W. Pfeifhofer. 2002. “Revival of a Resurrection Plant Correlates with Its Antioxidant Status.” *Plant Journal* 31 (1): 13–24. https://doi.org/10.1046/j.1365-313X.2002.01329.x.

Kumar, Dhirendra, and Daniel F. Klessig. 2003. “High-Affinity Salicylic Acid-Binding Protein 2 Is Required for Plant Innate Immunity and Has Salicylic Acid-Stimulated Lipase Activity.” *Proceedings of the National Academy of Sciences of the United States of America* 100 (26): 16101–6. https://doi.org/10.1073/pnas.0307162100.

Lea, P. J., L. Sodek, M. A.J. Parry, P. R. Shewry, and N. G. Halford. 2007. “Asparagine in Plants.” *Annals of Applied Biology* 150 (1): 1–26. https://doi.org/10.1111/j.1744-7348.2006.00104.x.

Lehmann, Silke, Christophe Gumy, Eva Blatter, Silke Boeffel, Wieland Fricke, and Doris Rentsch. 2011. “In Planta Function of Compatible Solute Transporters of the AtProT Family.” *Journal of Experimental Botany* 62 (2): 787–96. https://doi.org/10.1093/jxb/erq320.

Lemonnier, Pauline, Cécile Gaillard, Florian Veillet, Jérémy Verbeke, Rémi Lemoine, Pierre Coutos-Thévenot, and Sylvain La Camera. 2014. “Expression of Arabidopsis Sugar Transport Protein STP13 Differentially Affects Glucose Transport Activity and Basal Resistance to *Botrytis Cinerea*.” *Plant Molecular Biology* 85 (4): 473–84. https://doi.org/10.1007/s11103-014-0198-5.

Lesniewicz, Krzysztof, Wojciech M. Karlowski, Joanna R. Pienkowska, Piotr Krzywkowski, and Elzbieta Poreba. 2013. “The Plant S1-like Nuclease Family Has Evolved a Highly Diverse Range of Catalytic Capabilities.” *Plant and Cell Physiology* 54 (7): 1064–78. https://doi.org/10.1093/pcp/pct061.

Li, Nannan, Irene Luise Gügel, Patrick Giavalisco, Viktoria Zeisler, Lukas Schreiber, Jürgen Soll, and Katrin Philippar. 2015. “FAX1, a Novel Membrane Protein Mediating Plastid Fatty Acid Export.” *PLoS Biology* 13 (2): 1–37. https://doi.org/10.1371/journal.pbio.1002053.

Li, Wei, and Martin B. Dickman. 2004. “Abiotic Stress Induces Apoptotic-like Features in Tobacco That Is Inhibited by Expression of Human Bcl-2.” *Biotechnology Letters* 26 (2): 87–95. https://doi.org/10.1023/B:BILE.0000012896.76432.ba.

Li, Zhonghai, Jinying Peng, Xing Wen, and Hongwei Guo. 2012. “Gene Network Analysis and Functional Studies of Senescence-Associated Genes Reveal Novel Regulators of Arabidopsis Leaf Senescence.” *Journal of Integrative Plant Biology* 54 (8): 526–39. https://doi.org/10.1111/j.1744-7909.2012.01136.x.

Liao, Chao Jan, Zhibing Lai, Sanghun Lee, Dae Jin Yun, and Tesfaye Mengiste. 2016. “Arabidopsis HOOKLESS1 Regulates Responses to Pathogens and Abscisic Acid through Interaction with MED18 and Acetylation of WRKY33 and ABI5 Chromatin.” *Plant Cell* 28 (7): 1662–81. https://doi.org/10.1105/tpc.16.00105.

Lim, Pyung Ok, Hyo Jung Kim, and Hong Gil Nam. 2007. “Leaf Senescence.” https://doi.org/10.1146/annurev.arplant.57.032905.105316.

Lin, Shan Hua, Hui Fen Kuo, Geneviève Canivenc, Choun Sea Lin, Marc Lepetit, Po Kai Hsu, Pascal Tillard, *et al.,*2008. “Mutation of the Arabidopsis NRT1.5 Nitrate Transporter Causes Defective Root-to-Shoot Nitrate Transport.” *Plant Cell* 20 (9): 2514–28. https://doi.org/10.1105/tpc.108.060244.

Lisec, Jan, Nicolas Schauer, Joachim Kopka, Lothar Willmitzer, and Alisdair R. Fernie. 2006. “Gas Chromatography Mass Spectrometry-Based Metabolite Profiling in Plants.” *Nature Protocols* 1 (1): 387–96. https://doi.org/10.1038/nprot.2006.59.

Liu, Yidong ;, and Shuqun Zhang. 2004. “Phosphorylation of 1-Aminocyclopropane-1-Carboxylic Acid Synthase by MPK6, a Stress-Responsive Mitogen-Activated Protein Kinase, Induces Ethylene Biosynthesis in Arabidopsis.” *The Plant Cell* 16 (iii): 3386–99. https://doi.org/10.1105/tpc.104.026609.1.

Lohse, Marc, Axel Nagel, Thomas Herter, Patrick May, Michael Schroda, Rita Zrenner, Takayuki Tohge, Alisdair R. Fernie, Mark Stitt, and Björn Usadel. 2014. “Mercator: A Fast and Simple Web Server for Genome Scale Functional Annotation of Plant Sequence Data.” *Plant, Cell and Environment* 37 (5): 1250–58. https://doi.org/10.1111/pce.12231.

Mazzucotelli, E., S. Belloni, D. Marone, A. De Leonardis, D. Guerra, N. Di Fonzo, L. Cattivelli, and A. Mastrangelo. 2006. “The E3 Ubiquitin Ligase Gene Family in Plants: Regulation by Degradation.” *Current Genomics* 7 (8): 509–22. https://doi.org/10.2174/138920206779315728.

Meyer, Andreas, Sepehr Eskandari, Silke Grallath, and Doris Rentsch. 2006. “AtGAT1, a High Affinity Transporter for γ-Aminobutyric Acid in *Arabidopsis Thaliana*.” *Journal of Biological Chemistry* 281 (11): 7197–7204. https://doi.org/10.1074/jbc.M510766200.

Miao, Ying, and Ulrike Zentgraf. 2007. “The Antagonist Function of Arabidopsis WRKY53 and ESR/ESP in Leaf Senescence Is Modulated by the Jasmonic and Salicylic Acid Equilibrium.” *Plant Cell* 19 (3): 819–30. https://doi.org/10.1105/tpc.106.042705.

Mittler, Ron, YongSig Kim, Luhua Song, Jesse Coutu, Alicia Coutu, Sultan Ciftci-Yilmaz, Hojoung Lee, Becky Stevenson, and Jian Kang Zhu. 2006. “Gain- and Loss-of-Function Mutations in Zat10 Enhance the Tolerance of Plants to Abiotic Stress.” *FEBS Letters* 580 (28–29): 6537–42. https://doi.org/10.1016/j.febslet.2006.11.002.

Moore, John P., Eric E. Nguema-Ona, Mäite Vicré-Gibouin, Iben Sørensen, William G T Willats, Azeddine Driouich, and Jill M. Farrant. 2013. “Arabinose-Rich Polymers as an Evolutionary Strategy to Plasticize Resurrection Plant Cell Walls against Desiccation.” *Planta* 237 (3): 739–54. https://doi.org/10.1007/s00425-012-1785-9.

Moore, John P, Ngoc Tuan Le, Wolf F Brandt, Azeddine Driouich, and Jill M Farrant. 2009. “Towards a Systems-Based Understanding of Plant Desiccation Tolerance.” *Trends in Plant Science* 14 (2): 110–17. https://doi.org/10.1016/j.tplants.2008.11.007.

Mortimer, Jennifer C., Godfrey P. Miles, David M. Brown, Zhinong Zhang, Marcelo P. Segura, Thilo Weimar, Xiaolan Yu, *et al.,*2010. “Absence of Branches from Xylan in Arabidopsis Gux Mutants Reveals Potential for Simplification of Lignocellulosic Biomass.” *Proceedings of the National Academy of Sciences of the United States of America* 107 (40): 17409–14. https://doi.org/10.1073/pnas.1005456107.

Moyankova, Daniela, Petko Mladenov, Strahil Berkov, Darin Peshev, Desislava Georgieva, and Dimitar Djilianov. 2014. “Metabolic Profiling of the Resurrection Plant *Haberlea Rhodopensis* during Desiccation and Recovery.” *Physiologia Plantarum* 152 (4): 675–87. https://doi.org/10.1111/ppl.12212.

*Mundree, Sagadevan G., Anne Whittaker, Jennifer A. Thomson, and Jill M. Farrant. 2000. “An Aldose Reductase Homolog from the Resurrection Plant *Xerophyta viscosa* Baker.” *Planta* 211 (5): 693–700. https://doi.org/10.1007/s004250000331.

Munné-Bosch, Sergi, and Leonor Alegre. 2004. “Die and Let Live: Leaf Senescence Contributes to Plant Survival under Drought Stress.” *Functional Plant Biology*. https://doi.org/10.1071/FP03236.

Oliver, Melvin J., Lining Guo, Danny C. Alexander, John A. Ryals, Bernard W.M. Wone, and John C. Cushman. 2011. “A Sister Group Contrast Using Untargeted Global Metabolomic Analysis Delineates the Biochemical Regulation Underlying Desiccation Tolerance in *Sporobolus Stapfianus*.” *The Plant Cell* 23 (4): 1231–48. https://doi.org/10.1105/tpc.110.082800.

Olvera-Carrillo, Yadira, Michiel Van Bel, Tom Van Hautegem, Matyáš Fendrych, Marlies Huysmans, Maria Simaskova, Matthias van Durme, *et al.,*2015. “A Conserved Core of Programmed Cell Death Indicator Genes Discriminates Developmentally and Environmentally Induced Programmed Cell Death in Plants.” *Plant Physiology* 169 (4): 2684–99. https://doi.org/10.1104/pp.15.00769.

Olvera-Carrillo, Yadira, José Luis Reyes, and Alejandra A. Covarrubias. 2011. “Late Embryogenesis Abundant Proteins: Versatile Players in the Plant Adaptation to Water Limiting Environments.” *Plant Signaling and Behavior* 6 (4): 586–89. https://doi.org/10.4161/psb.6.4.15042.

Oszvald, Maria, Lucia F. Primavesi, Cara A. Griffiths, Jonathan Cohn, Shib Sankar Basu, Michael L. Nuccio, and Matthew J. Paul. 2018. “Trehalose 6-Phosphate Regulates Photosynthesis and Assimilate Partitioning in Reproductive Tissue.” *Plant Physiology* 176 (4): 2623–38. https://doi.org/10.1104/pp.17.01673.

Ottensmann, Meinolf, Martin A. Stoffel, Hazel J. Nichols, and Joseph I. Hoffman. 2018. "GCalignR: An R Package for Aligning Gas-Chromatography Data for Ecological and Evolutionary Studies." *PLoS ONE* 13 (6): 1–20. https://doi.org/10.1371/journal.pone.0198311.

Parrott, David L., Kate McInnerney, Urs Feller, and Andreas M. Fischer. 2007. "Steam-Girdling of Barley (Hordeum Vulgare) Leaves Leads to Carbohydrate Accumulation and Accelerated Leaf Senescence, Facilitating Transcriptomic Analysis of Senescence-Associated Genes." *New Phytologist* 176 (1): 56–69. https://doi.org/10.1111/j.1469-8137.2007.02158.x.

Penfold, Christopher a., and Vicky Buchanan-Wollaston. 2014. "Modelling Transcriptional Networks in Leaf Senescence." *Journal of Experimental Botany* 65 (14): 3859–73. https://doi.org/10.1093/jxb/eru054.

Perez-Amador, M. A., M. L. Abler, E. J. De Rocher, D. M. Thompson, A. Van Hoof, N. D. LeBrasseur, A. Lers, and P. J. Green. 2000. "Identification of BFN1, a Bifunctional Nuclease Induced during Leaf and Stem Senescence in Arabidopsis." *Plant Physiology* 122 (1): 169–79.

Petrov, Veselin, Jacques Hille, Bernd Mueller-Roeber, and Tsanko S. Gechev. 2015. "ROS-Mediated Abiotic Stress-Induced Programmed Cell Death in Plants." *Frontiers in Plant Science* 6 (Feb): 1–16. https://doi.org/10.3389/fpls.2015.00069.

Qi, Tiancong, Jiaojiao Wang, Huang Huang, Bei Liu, Hua Gao, Yule Liu, Susheng Song, and Daoxin Xie. 2015. "Regulation of Jasmonate-Induced Leaf Senescence by Antagonism between BHLH Subgroup IIIe and IIId Factors in Arabidopsis." *Plant Cell* 27 (6): 1634–49. https://doi.org/10.1105/tpc.15.00110.

R Development Core Team, R. 2011. "R: A Language and Environment for Statistical Computing." Edited by R Development Core Team. *R Foundation for Statistical Computing*. R Foundation for Statistical Computing. R Foundation for Statistical Computing. https://doi.org/10.1007/978-3-540-74686-7.

Rentel, Malke C., David Lecourieux, Fatma Ouaked, Sarah L. Usher, Lindsay Petersen, Haruko Okamoto, Heather Knight, *et al.,*2004. "OXI1 Kinase Is Necessary for Oxidative Burst-Mediated Signalling in Arabidopsis." *Nature* 427 (6977): 858–61. https://doi.org/10.1038/nature02353.

Río, Luis A. Del. 2015. "ROS and RNS in Plant Physiology: An Overview." *Journal of Experimental Botany* 66 (10): 2827–37. https://doi.org/10.1093/jxb/erv099.

Robatzek, Silke, and Imre E. Somssich. 2002. "Targets Of AtWRKY6 regulation during plant senescence and pathogen defense". *Genes & Development* (16):1139–49. http://www.genesdev.org/cgi/doi/10.1101/ gad.222702.

RStudioTeam. 2015. "RStudio: Integrated Development for R." Boston, MA: RStudio, Inc. www.rstudio.com.

Schmid, Markus, Timothy S. Davison, Stefan R. Henz, Utz J. Pape, Monika Demar, Martin Vingron, Bernhard Schölkopf, Detlef Weigel, and Jan U. Lohmann. 2005. "A Gene Expression Map of *Arabidopsis Thaliana* Development." *Nature Genetics* 37 (5): 501–6. https://doi.org/10.1038/ng1543.

Shane, Michael W., Kyla Stigter, Eric T. Fedosejevs, and William C. Plaxton. 2014. "Senescence-Inducible Cell Wall and Intracellular Purple Acid Phosphatases: Implications for Phosphorus Remobilization in *Hakea Prostrata* (Proteaceae) and *Arabidopsis Thaliana* (Brassicaceae)." *Journal of Experimental Botany* 65 (20): 6097–6106. https://doi.org/10.1093/jxb/eru348.

*Sherwin, Heather W., and Jill M. Farrant. 1998. "Protection Mechanisms against Excess Light in the Resurrection Plants *Craterostigma Wilmsii* and *Xerophyta viscosa*." *Plant Growth Regulation* 24

(3): 203–10. https://doi.org/10.1023/A:1005801610891.

Shin, Kihye, Sumin Lee, Won Yong Song, Rin A. Lee, Inhye Lee, Kyungsun Ha, Ja Choon Koo, *et al.,*2015. "Genetic Identification of ACC-RESISTANT2 Reveals Involvement of Lysine Histidine TRANSPORTER1 in the Uptake of 1-Aminocyclopropane-1-Carboxylic Acid in *Arabidopsis Thaliana*." *Plant and Cell Physiology* 56 (3): 572–82. https://doi.org/10.1093/pcp/pcu201.

Shumbe, Leonard, Anne Chevalier, Bertrand Legeret, Ludivine Taconnat, Fabien Monnet, and Michel Havaux. 2016. "Singlet Oxygen-Induced Cell Death in Arabidopsis under High-Light Stress Is Controlled by OXI1 Kinase." *Plant Physiology* 170 (3): 1757–71. https://doi.org/10.1104/pp.15.01546.

Simpson, Paul J, Chonticha Tantitadapitak, Anna M Reed, Owen C Mather, Christopher M Bunce, Scott A White, and Jon P Ride. 2009. "Characterization of Two Novel Aldo–Keto Reductases from Arabidopsis: Expression Patterns, Broad Substrate Specificity, and an Open Active-Site Structure Suggest a Role in Toxicant Metabolism Following Stress." *Journal of Molecular Biology* 392 (2): 465–80. https://doi.org/https://doi.org/10.1016/j.jmb.2009.07.023.

Smékalová, Veronika, Anna Doskočilová, George Komis, and Jozef Šamaj. 2014. "Crosstalk between Secondary Messengers, Hormones and MAPK Modules during Abiotic Stress Signalling in Plants." *Biotechnology Advances* 32 (1): 2–11. https://doi.org/10.1016/j.biotechadv.2013.07.009.

Sturms, Ryan, Alan A. DiSpirito, D. Bruce Fulton, and Mark S. Hargrove. 2011. "Hydroxylamine Reduction to Ammonium by Plant and Cyanobacterial Hemoglobins." *Biochemistry* 50 (50): 10829–35. https://doi.org/10.1021/bi201425f.

Sturn, Alexander, John Quackenbush, and Zlatko Trajanoski. 2002. "Genesis: Cluster Analysis of Microarray Data." *Bioinformatics (Oxford, England)* 18 (1): 207–8. https://doi.org/10.1093/bioinformatics/18.1.207.

Su, Yan Hua, Wolf B. Frommer, and Uwe Ludewig. 2004. "Molecular and Functional Characterization of a Family of Amino Acid Transporters from Arabidopsis." *Plant Physiology* 136 (2): 3104–13. https://doi.org/10.1104/pp.104.045278.

Suguiyama, Vanessa F., Emerson A. Silva, Sergio T. Meirelles, Danilo C. Centeno, and Marcia R. Braga. 2014. "Leaf Metabolite Profile of the Brazilian Resurrection Plant *Barbacenia Purpurea* Hook. (Velloziaceae) Shows Two Time-Dependent Responses during Desiccation and Recovering." *Frontiers in Plant Science* 5 (March): 1–13. https://doi.org/10.3389/fpls.2014.00096.

Tan, Tinghong, Yanni Sun, Shishuai Luo, Chao Zhang, Huapeng Zhou, and Honghui Lin. 2017. "Efficient Modulation of Photosynthetic Apparatus Confers Desiccation Tolerance in the Resurrection Plant *Boea Hygrometrica*." *Plant and Cell Physiology* 58 (11): 1976–90. https://doi.org/10.1093/pcp/pcx140.

The UniProt Consortium. 2019. UniProt: a worldwide hub of protein knowledge. Nucleic Acids Res. 47: D506-515 https://www.uniprot.org/

Thomas, Stephen G., Andrew L. Phillips, and Peter Hedden. 1999. "Molecular Cloning and Functional Expression of Gibberellin 2-Oxidases, Multifunctional Enzymes Involved in Gibberellin Deactivation." *Proceedings of the National Academy of Sciences of the United States of America* 96 (8): 4698–4703. https://doi.org/10.1073/pnas.96.8.4698.

Torras-Claveria, Laura, Olga Jáuregui, Carles Codina, Antonio F. Tiburcio, Jaume Bastida, and Francesc Viladomat. 2012. "Analysis of Phenolic Compounds by High-Performance Liquid Chromatography Coupled to Electrospray Ionization Tandem Mass Spectrometry in Senescent and Water-Stressed Tobacco." *Plant Science* 182 (1): 71–78. https://doi.org/10.1016/j.plantsci.2011.02.009.

Trapnell, Cole, Adam Roberts, Loyal Goff, Geo Pertea, Daehwan Kim, David R Kelley, Harold Pimentel, Steven L Salzberg, John L Rinn, and Lior Pachter. 2014. "Differential Gene and Transcript Expression Analysis of RNA-Seq Experiments with TopHat and Cufflinks." *Nature Protocols* 9 (September): 2513. https://doi.org/10.1038/nprot1014-2513a.

Troncoso-Ponce, Manuel A., Xia Cao, Zhenle Yang, and John B. Ohlrogge. 2013. "Lipid Turnover during Senescence." *Plant Science* 205–206: 13–19. https://doi.org/10.1016/j.plantsci.2013.01.004.

Tshabuse, Freedom, Jill M. Farrant, Lydie Humbert, Deborah Moura, Dominique Rainteau, Christophe Espinasse, Abdelghani Idrissi, *et al.,*2018. "Glycerolipid Analysis during Desiccation and Recovery of the Resurrection Plant *Xerophyta humilis* (Bak) Dur and Schinz." *Plant Cell and Environment* 41 (3): 533–47. https://doi.org/10.1111/pce.13063.

Tuba, Z., H. K. Lichtenthaler, Zs Csintalan, Z. Nagy, and K. Szente. 1996. "Loss of Chlorophylls, Cessation of Photosynthetic CO2 Assimilation and Respiration in the Poikilochlorophyllous Plant *Xerophyta Scabrida* during Desiccation." *Physiologia Plantarum* 96 (3): 383–88. https://doi.org/10.1111/j.1399-3054.1996.tb00448.x.

Tuba, Zoltan, Michael C.F. Protor, and Zsolt Csintalan. 2002. "Ecophysiological Responses of Homoiochlorophyllous and Poikilochlorophyllous Desiccation Tolerant Plants: A Comparison and an Ecological Perspective." *Entomologia Experimentalis et Applicata* 103 (3): 239–48. https://doi.org/10.1023/A.

Vaidyanathan, Ramnath. 2016. "Sparkline 2.0." https://cran.r-project.org/package=sparkline.

Vanlerberghe, Greg C. 2013. "Alternative Oxidase: A Mitochondrial Respiratory Pathway to Maintain Metabolic and Signaling Homeostasis during Abiotic and Biotic Stress in Plants." *International Journal of Molecular Sciences* 14 (4): 6805–47. https://doi.org/10.3390/ijms14046805.

Veljovic-Jovanovic, Sonja, Biljana Kukavica, and Flavia Navari-Izzo. 2008. "Characterization of Polyphenol Oxidase Changes Induced by Desiccation of *Ramonda Serbica* Leaves." *Physiologia Plantarum* 132 (4): 407–16. https://doi.org/10.1111/j.1399-3054.2007.01040.x.

Waidmann, Sascha, Branislav Kusenda, Juliane Mayerhofer, Karl Mechtler, and Claudia Jonak. 2014. "A Dek Domain-Containing Protein Modulates Chromatin Structure and Function in Arabidopsis." *Plant Cell* 26 (11): 4328–44. https://doi.org/10.1105/tpc.114.129254.

Walley, Justin W., Heather C. Rowe, Yanmei Xiao, E. Wassim Chehab, Daniel J. Kliebenstein, Doris Wagner, and Katayoon Dehesh. 2008. "The Chromatin Remodeler SPLAYED Regulates Specific Stress Signaling Pathways." *PLoS Pathogens* 4 (12): 1–8. https://doi.org/10.1371/journal.ppat.1000237.

Watanabe, M., S. Balazadeh, T. Tohge, A. Erban, P. Giavalisco, J. Kopka, B. Mueller-Roeber, A. R. Fernie, and R. Hoefgen. 2013. "Comprehensive Dissection of Spatiotemporal Metabolic Shifts in Primary, Secondary, and Lipid Metabolism during Developmental Senescence in Arabidopsis." *Plant Physiology* 162 (3): 1290–1310. https://doi.org/10.1104/pp.113.217380.

Watanabe, Masahiko, Tetsuya Sakashita, Akihiko Fujita, Takahiro Kikawada, Daiki D Horikawa, Yuichi Nakahara, Seiichi Wada, *et al.,*2006. "Biological Effects of Anhydrobiosis in an African Chironomid, *Polypedilum Vanderplanki* on Radiation Tolerance." *International Journal of Radiation Biology* 82 (8): 587–92. https://doi.org/10.1080/09553000600876652.

Wickham, H. 2016. "Ggplot2: Elegant Graphics for Data Analysis." Springer-Verlag New York.

Williams, Brett, Isaac Njaci, Lalehvash Moghaddam, Hao Long, and Martin B Dickman. 2015. "Trehalose Accumulation Triggers Autophagy during Plant Desiccation." *PLOS Genetics* 11(12): e1005705. https://doi.org/10.1371/journal.pgen.1005705.

Willigen, Clare Vander, N.W. Pammenter, Sagadevan Mundree, and Jill Farrant. 2001. “Comparisons of the Resurrection Grass, *Eragrostis Nindensis*, with the Related Desiccation-Sensitive Species, *E. Curvula*.” *Plant Growth Regulation* 35(2):121-129. University of Cape Town. https://link.springer.com/article/10.1023/A:1014425619913.

Woo, Hye Ryun, Hyo Jung Kim, Pyung Ok Lim, and Hong Gil Nam. 2019. “Leaf Senescence: Systems and Dynamics Aspects.” *Annual Review of Plant Biology* 70 (1):347-376. https://doi.org/10.1146/annurev-arplant-050718-095859.

Wu, Anhui, Annapurna Devi Allu, Prashanth Garapati, Hamad Siddiqui, Hakan Dortay, Maria Inás Zanor, Maria Amparo Asensi-Fabado, *et al.,*2012. “JUNGBRUNNEN1, a Reactive Oxygen Species-Responsive NAC Transcription Factor, Regulates Longevity in Arabidopsis.” *Plant Cell* 24 (2): 482–506. https://doi.org/10.1105/tpc.111.090894.

Xu, Guoyong, Shanshan Wang, Shaojie Han, Ke Xie, Yan Wang, Jinlin Li, and Yule Liu. 2017. “Plant Bax Inhibitor-1 Interacts with ATG6 to Regulate Autophagy and Programmed Cell Death.” *Autophagy* 13 (7): 1161–75. https://doi.org/10.1080/15548627.2017.1320633.

Yadav, Umesh Prasad, Alexander Ivakov, Regina Feil, Guang You Duan, Dirk Walther, Patrick Giavalisco, Maria Piques, *et al.,*2014. “The Sucrose-Trehalose 6-Phosphate (Tre6P) Nexus: Specificity and Mechanisms of Sucrose Signalling.” *Journal of Experimental Botany* 65 (4): 1051–68. https://doi.org/10.1093/jxb/ert457.

Ye, Changming, Martin B. Dickman, Steven A. Whitham, Mark Payton, and Jeanmarie Verchot. 2011. “The Unfolded Protein Response Is Triggered by a Plant Viral Movement Protein.” *Plant Physiology* 156 (2): 741–55. https://doi.org/10.1104/pp.111.174110.

Yobi, Abou, Karen A. Schlauch, Richard L. Tillett, Won C. Yim, Catherine Espinoza, Bernard W.M. Wone, John C. Cushman, and Melvin J. Oliver. 2017. “*Sporobolus Stapfianus*: Insights into Desiccation Tolerance in the Resurrection Grasses from Linking Transcriptomics to Metabolomics.” *BMC Plant Biology* 17 (1): 1–30. https://doi.org/10.1186/s12870-017-1013-7.

Yobi, Abou, Bernard W.M. Wone, Wenxin Xu, Danny C. Alexander, Lining Guo, John A. Ryals, Melvin J. Oliver, and John C. Cushman. 2012. “Comparative Metabolic Profiling between Desiccation-Sensitive and Desiccation-Tolerant Species of *Selaginella* Reveals Insights into the Resurrection Trait.” *Plant Journal* 72 (6): 983–99. https://doi.org/10.1111/tpj.12008.

Yoshiyama, Kaoru Okamoto, Kengo Sakaguchi, and Seisuke Kimura. 2013. “DNA Damage Response in Plants: Conserved and Variable Response Compared to Animals.” *Biology* 2 (4): 1338–56. https://doi.org/10.3390/biology2041338.

Zhang, Qingwei, and Dorothea Bartels. 2016. “Physiological Factors Determine the Accumulation of D-Glycero-D-Ido-Octulose (D-g-D-i-Oct) in the Desiccation Tolerant Resurrection Plant *Craterostigma Plantagineum*.” *Functional Plant Biology* 43 (7): 684–94. https://doi.org/10.1071/FP15278.

Zhange, Qingwei, and Dorothea Bartels. 2018. “Molecular Responses to Dehydration and Desiccation in Desiccation-Tolerant Angiosperm Plants,” *Journal of Experimental Botany* 69(13):3211-3222. https://doi.org/10.1093/jxb/erx489.

Zhang, Z., C. J. Schofield, J. E. Baldwin, P. Thomas, and P. John. 1995. “Expression, Purification and Characterization of 1-Aminocyclopropane-1-Carboxylate Oxidase from Tomato in *Escherichia Coli*.” *Biochemical Journal* 307 (1): 77–85. https://doi.org/10.1042/bj3070077.

Zhao, Zhe, Yifan Li, Songchao Zhao, Jiawen Zhang, Hong Zhang, Bo Fu, Fan He, Mingqin Zhao, and Pengfei Liu. 2018. “Transcriptome Analysis of Gene Expression Patterns Potentially Associated

with Premature Senescence in *Nicotiana Tabacum* L." *Molecules* 23 (11):2856. https://doi.org/10.3390/molecules23112856.

Zhou, Xiaowei, Wenjun Li, Ross Mabon, and Linda J. Broadbelt. 2018. "A Mechanistic Model of Fast Pyrolysis of Hemicellulose." *Energy and Environmental Science* 11 (5): 1240–60. https://doi.org/10.1039/c7ee03208k.

Acknowledgements

I would like to acknowledge my mother before anyone else. We have been through so much together, but the greatest thread that you have woven into me is that I am *capable*. Throughout this process, and so many others, you believed in me and made me feel capable and worthy of achieving the things I wanted in this life. Thank you, Mommy, for this and for the innumerable sacrifices you made for me. I am eternally grateful.

Vikty, I am so thankful that I got to grow up alongside you. You directly shaped so much of how I see the world – how I interrogate and question the presumptions around me. You helped me become curious. Thank you for this, for being my big brother and for sharing your love of science with me.

Jill, you have given me so much. You have created opportunities for me. You have encouraged me endlessly. You have been my representation of a queer woman in science. You have become my friend. You also gave me space to explore the thoughts and concepts I wanted to explore and have let me fail gracefully. You have trusted me with the ideas I have and have helped me develop them. This trust is such a gift and has helped me develop my confidence in my own mind. Thank you for everything.

To my love, Simone. As I write this you are snoozing gently in the home we have made together. Your entry into my life has had the perfect timing – the most beautiful bookend to my PhD. Wrestling this thesis into something I am proud of has been made so much easier by being surrounded by your love. Your love has given me so much confidence. The respect we feel for one another has been incredible to experience. I feel completely capable of tackling anything life throws our way, with your paw in my paw. I love you. You spark joy.

I would like to say thank you to my step father Stephen and to my father Graham. Things have not been easy in our relationships, but I am grateful that you both believed in me and encouraged me to do great things with my life. I am very grateful for the sacrifices you made to get me a good education. Thank you to my family – Zolile, Helga, Ruby, Denise, Mandy, Granny Mamma, Julian, Suskia – you have all supported me and cheered me on, and I love you so much.

Chrissie, my comrade in arms. Thank you for becoming my sister in this PhD journey. It has been important to share the highlights and lowlights of this with someone going through a parallel process, who reeeeeeeeeeeeally gets it. You are amazing! Keren, thank you for help with the microscopy and for all of the salacious chats and skinners in your office. You have become a great friend. Jo, thank you for all the lols in the lab, and for the intellectual input. You're amazing. Francois, young grasshopper, thank you for help with the last bit of lab work and for your efforts in the microscopy and metabolomics experiment. You carried me through that last bit of work, more than you know. Thank

you. Arno, it has been so amazing to get to know you. Thank you for trusting me. Thank you also for help with the GC-MS work – I could literally not have done it without you. You taught me so much. Thank you. Thank you to Pei-Yin for help with the GC-MS and sorry for leaving the small molecules unit in disarray on occasion :P. To Suhail, thank you for the amazing intellectual input and the good-humoured chats – your pragmatic and relaxed approach to research has been very comforting. Mariam, thank you for reviewing part of this thesis and for being a lovely friend!

Thank you to Buffelskloof Private Nature Reserve for allowing me to collect plants. Thank you to Mishal for the lovely high res leaf scans, to Hayley for help with the microscopy and to Mo for help with the TEM. Thank you Arash for help with the transcriptome. Thank you to Madhu, Faezah, Shakiera and Bronwyn for help with equipment over the years. Thank you to Maureen, Unis and Priscilla for keeping our working spaces in shape. Thank you to Janet for influencing my thinking around signal transduction and for being a thoughtful HoD. Thank you to all of the postgrad committee members over the years for all of the *gees* they've promoted within the department.

Brett, thank you for being an amazing mentor and friend while hosting me at QUT – I have learnt so much from you both about research and about how to be a good colleague. Thank you for the intellectual input as well – I appreciate it so much. Saga, thank you for hosting me, making me feel included in your lab group and for making the transcriptomics possible. Hao, thank you for helping me with the qPCR robot and cloning! Jess and Bren, thank you for hosting me while I was working at QUT and for being great friends and lovely humans. Maria Cecilia, thank you for pointing me in the right direction in terms of the analysis of the transcriptome – your help was essential and came when I needed it most. Thank you. Henk, thank you for being an amazing friend and mentor throughout this process. I am very grateful for our deep chats and for all your intellectual input. Mariana, thank you for your friendship and sisterhood in science. Halford, thank you so much for technical assistance with the ABA quantification and for being a wonderful friend. You are the shiniest!

To my friends Mary and Adam, this PhD has kind of grown up alongside our friendship. There have been joyous moments and scary moments, and you have provided a refuge for me throughout all of it. Your love, support and acceptance of me as just Astrid has been invaluable. Love ya. Lauren, Kayo, Izelle, Tapiwa, Alex, Lara, Sarah, Jess, Josh, Naadirah – thank you all for being wonderful friends and fabulous distractions from this PhD. Thank you to Franie, who has been a second mother to me and an inspiration to me as a writer. Thank you to the RopeyThings squad for helping me create spaces for exploration. I have nothing but love for you all. There were times where I felt incredibly alone during this process but looking at this list of peeps who had my back makes me feel invincible going forward.

I would also like to thank Elre, the first friend with whom I felt safe to truly express myself as an intellectual person. Thank you for encouraging me to learn, to find value in learning and to never stop learning. I will always cherish the languid hours we spent in book stores as teenagers, figuring out who we were going to be. I love you.

I would also like to thank Mrs Mahood, my Biology teacher in high school, whose love for her subject was infectious. I can not describe how great an impact your passion for this subject and the joy you took in teaching it has had on my life. I did this because of the seed you planted in me. I would also like to thank Mrs Lehman, my English teacher, who imparted both her love of Shakespeare and of good, concise writing to me.

As they say, it takes a village. So many strong and capable women have played a role in getting me here – you all gave me so much of yourselves and I am humbled by how far I have been able to come. I am the first person in my family to attempt a postgraduate degree, and this is a big deal to us. This would also not have been possible without the support of the NRF and Harry Crossley foundation. Thank you so much for the support – I was able to spend this time doing basic research, thinking and writing without financial stress. This is nothing short of miraculous, and I am proud of what your support has yielded.

Appendix

Publication of Chapter 2:

Desiccation-Driven Senescence in the Resurrection Plant *Xerophyta schlechteri* (Baker) N.L. Menezes: Comparison of Anatomical, Ultrastructural, and Metabolic Responses Between Senescent and Non-Senescent Tissues

OPEN ACCESS

Edited by:
Dean E. Riechers, University of Illinois at Urbana-Champaign, United States

Reviewed by:
Dinakar Challabathula, Central University of Tamil Nadu, India
Dorothea Bartels, University of Bonn, Germany

****Correspondence:***
Jill M. Farrant
jill.farrant@uct.ac.za

Specialty section:
This article was submitted to Plant Abiotic Stress, a section of the journal Frontiers in Plant Science

Received: *25 June 2019*
Accepted: *09 October 2019*
Published: *30 October 2019*

Citation:
Radermacher AL, du Toit SF and Farrant JM (2019) Desiccation-Driven Senescence in the Resurrection Plant Xerophyta schlechteri (Baker) N.L. Menezes: Comparison of Anatomical, Ultrastructural, and Metabolic Responses Between Senescent and Non-Senescent Tissues. Front. Plant Sci. 10:1396. doi: 10.3389/fpls.2019.01396

Astrid Lillie Radermacher, Stephanus Francois du Toit and Jill M. Farrant*

Department of Molecular and Cell Biology, University of Cape Town, Cape Town, South Africa

Drought-induced senescence is a degenerative process that involves the degradation of cellular metabolites and photosynthetic pigments and uncontrolled dismantling of cellular membranes and organelles. Angiosperm resurrection plants display vegetative desiccation tolerance and avoid drought-induced senescence in most of their tissues. Developmentally older tissues, however, fail to recover during rehydration and ultimately senesce. Comparison of the desiccation-associated responses of older senescent tissues (ST) with non-ST (NST) will allow for understanding of mechanisms promoting senescence in the former and prevention of senescence in the latter. In the monocotyledonous resurrection plant *Xerophyta schlechteri* (Baker) N.L. Menezes*, leaf tips senesce following desiccation, whereas the rest of the leaf blade survives. We characterized structural and metabolic changes in ST and NST at varying water contents during desiccation and rehydration. Light and transmission electron microscopy was used to follow anatomical and subcellular responses, and metabolic differences were studied using gas chromatography-mass spectrometry and colorimetric metabolite assays. The results show that drying below 35% relative water content (0.7 gH_2O/g dry mass) in ST resulted in the initiation of age-related senescence hallmarks and that these tissues continue this process after rehydration. We propose that an age-related desiccation sensitivity occurs in older tissues, in a process metabolically similar to that observed during age-related senescence in *Arabidopsis thaliana*.

Keywords: age-related senescence, desiccation tolerance, resurrection plant, senescence prevention, *Xerophyta schlechteri*

Abbreviations: NST, Non-Senescent Tissue; ST, Senescent Tissue

Available online: https://www.frontiersin.org/articles/10.3389/fpls.2019.01396/full